Hygroscopic behavior of model respiratory droplets and implications for airborne disease transmission

Zur Erlangung des akademischen Grades einer

DOKTORIN DER NATURWISSENSCHAFTEN (Dr. rer. nat)

von der KIT-Fakultät für

Bauingenieur-, Geo- und Umweltwissenschaften

des Karlsruher Instituts für Technologie (KIT)

genehmigte

DISSERTATION

von

M. Sc. Yue Meng

Tag der mündlichen Prüfung: 28.11.2025

Referent: Prof. Dr. Jan Cermak

Korreferent: Prof. Dr. Thomas Leisner

Karlsruhe 2025

Erklärung

Hiermit erkläre ich, dass ich die vorliegende Dissertation, abgesehen von der Benutzung der angegebenen Hilfsmittel, selbstständig verfasst habe.

Alle Stellen, die gemäß Wortlaut oder Inhalt aus anderen Arbeiten entnommen sind, wurden durch Angabe der Quelle als Entlehnungen kenntlich gemacht.

Diese Dissertation liegt in gleicher oder ähnlicher Form keiner anderen Prüfungsbehörde vor.

Karlsruhe, im Oktober 2025
Yue Meng

Acknowledgments

To Prof. Dr. Thomas Leisner, for believing in me and supporting me throughout this journey. Our weekly meetings always provided timely feedback that kept me on the right path and research track.

To Dr. Alexei Kiselev, a reliable group leader with an intellectual kind of humor, for your patient guidance and endless support. From experiments to paper writing, from EDB to ESEM, our countless detailed discussions not only deepened my theoretical knowledge but also taught me how to face the challenges and questions as a scientist, which means a lot to me.

To Dr. Denis Duft, a troubleshooter with a magic touch for turning chaos into order, for introducing me every detail of EDB and helping me set up my own at the very beginning of my PhD journey, for developing LabView programs tailored to my needs, and for answering every stupid question from me with patience. “So!”

To Dr. Yanxia Li, my dearest friend on this PhD journey, a brave and hardworking woman with a passion like fire and a mind as clear as crystal, for filling my life with countless joy and unwavering support whenever I needed it. The treasured moments we shared in the green springs, burning red summers, golden autumns, and silver winters have become precious memories in the deepest part of my heart. Life may guide us down different paths, I hope our friendship will remain evergreen.

To Prof. Dr. Stephanie Jones and Johanna Seidel, my best colleagues and good friends, who inspired and empowered me with “You only live once”; with whom I shared countless coffees, funny stories, and culture-shock-breaking moments; and who colored my life in Karlsruhe far beyond work. In them, I see the strength of women, and I hope we all become the people we dream of being.

To Jun Jiang, my husband and beloved soulmate, for joining in my life, exploring the world together, and enlightening endless possibilities of me. Our love makes me soft, also makes me strong.

Finally, to my beloved grandma and grandpa, mom and dad, who are always on my side. I love you for giving me your shoulders, from which can I see the vastness beyond. You never sought to keep me caged, but instead set me free, letting me be myself, flying as far and as joyfully as I can. Because of you, I see a greater world; because of you, I see the meaning of love.

I’m free like a bird, soaring in the golden sky, wind in my hair, whispering the next stop, YAY!

Abstract

Airborne transmission is recognized as a major route for the spread of respiratory diseases. Respiratory aerosols and droplets, as the primary carriers of airborne pathogens, undergo physicochemical transformations after exhalation that directly influence their airborne lifetime and the survival of the pathogens they carry. While numerous studies have shown that environmental factors such as humidity and temperature significantly affect pathogen infectivity, limited research has focused on the underlying mechanisms: how the physicochemical properties of respiratory droplets changes under varying environmental conditions, and thereby impacts pathogen survival and transmission. Therefore, the aim of this thesis is to investigate the evaporation and hygroscopic growth behavior of respiratory droplets under varying environmental conditions, in order to gain a further insight into how these properties influence the airborne transmission and persistence of respiratory pathogens.

This thesis systematically investigates evaporation kinetics, equilibrium thermodynamics, and rehydration behavior of levitated model respiratory droplets using an electrodynamic balance, with an emphasis on the role of two key protein components: mucin and albumin, that dominate the protein composition of upper and lower respiratory tract fluids, respectively. Physicochemical parameters including droplet size, phase state, morphology, hygroscopicity, efflorescence, and deliquescence were characterized using light scattering patterns, scanning electron microscopy, and a high-speed video camera. Results show that artificial saliva droplets exhibit a complex morphology change behavior during evaporation at RH below 45%. Mucin forms a semi-permeable surface layer that retains water, slows evaporation, and suppresses full rehydration, thereby influencing droplet size, morphology, phase transitions, and structural stability. In contrast, albumin, relative to mucin, promotes faster water loss from NaCl droplets, displays pronounced surface activity, and induces strong morphological deformation, thereby altering deliquescence behavior while maintaining overall hygroscopic capacity.

These findings indicate that respiratory droplets originating from different regions of the respiratory tract behave distinctly under varying environmental conditions. By establishing the role of key proteins in droplet physicochemical transformations, this study contributes to a deeper understanding of droplet-mediated pathogen transmission and provides insights for improving public health strategies and pandemic preparedness.

Zusammenfassung

Die Tröpfchenübertragung durch die Luft gilt als ein wesentlicher Übertragungsweg für respiratorische Erkrankungen. Respiratorische Aerosole und Tröpfchen, die als Hauptträger luftübertragener Krankheitserreger fungieren, unterliegen nach der Exhalation physikochemischen Veränderungen, die ihre Verweildauer in der Luft sowie das Überleben der darin enthaltenen Pathogene maßgeblich beeinflussen. Zahlreiche Studien belegen, dass Umweltfaktoren wie Luftfeuchtigkeit und Temperatur einen erheblichen Einfluss auf die Infektiosität von Pathogenen haben. Dennoch ist bisher wenig darüber bekannt, wie genau sich die physikochemischen Eigenschaften respiratorischer Tröpfchen unter unterschiedlichen Umweltbedingungen verändern und wie sich dies auf das Überleben und die Übertragbarkeit von Krankheitserregern auswirkt. Daher besteht das Ziel dieser Arbeit darin, das Verdampfungs- und hygroskopische Wachstumsverhalten respiratorischer Tröpfchen unter verschiedenen Umweltbedingungen zu untersuchen, um ein tieferes Verständnis dafür zu gewinnen, wie diese Eigenschaften die luftgetragene Übertragung und Persistenz respiratorischer Pathogene beeinflussen.

Im Rahmen dieser Arbeit wurden die Verdampfungskinetik, das thermodynamische Gleichgewichtsverhalten sowie das Rehydrationsverhalten levitierter Modelltröpfchen mithilfe einer elektrodynamischer Falle (Paul-Falle) systematisch untersucht. Der Fokus liegt dabei auf dem Einfluss zweier zentraler Proteinkomponenten: Mucin und Albumin, die jeweils in den Flüssigkeiten der oberen bzw. unteren Atemwege dominieren. Wichtige physikochemische Parameter, einschließlich Tröpfchengröße, Phasenzustand, Morphologie, Hygroskopizität, Effloreszenz- und Deliqueszenzverhalten, wurden mithilfe von Lichtstreumusteranalyse, Rasterelektronenmikroskopie und Hochgeschwindigkeitskamera charakterisiert. Die Ergebnisse zeigen, dass künstliche Speicheltröpfchen bei relativen Luftfeuchtigkeiten unterhalb von 45 % ein komplexes morphologisches Veränderungsverhalten aufweisen. Mucin bildet dabei eine semipermeable Oberflächenschicht, die Wasser zurückhält, die Verdunstung verlangsamt und eine vollständige Rehydratation hemmt. Dadurch beeinflusst es maßgeblich die Tröpfchengröße, Morphologie, Phasenübergänge und strukturelle Stabilität. Im Gegensatz zu Mucin fördert Albumin einen schnelleren Wasserverlust aus NaCl-Tröpfchen, zeigt eine ausgeprägte Oberflächenaktivität und ruft starke morphologische Deformationen hervor, wodurch das Deliqueszenzverhalten verändert wird, während die gesamte hygroskopische Kapazität erhalten bleibt.

Diese Ergebnisse verdeutlichen, dass Tröpfchen, die aus unterschiedlichen Regionen der Atemwege stammen, unter wechselnden Umweltbedingungen ein unterschiedliches Verhalten zeigen. Die Erkenntnisse über die Rolle spezifischer Proteine bei physikochemischen Transformationen leisten einen wichtigen Beitrag zu einem besseren Verständnis der tröpfchenbasierten Übertragung von Krankheitserregern und liefern relevante Impulse zur Optimierung von Strategien im Bereich des Infektionsschutzes und der Pandemievorbereitung.

Contents

List of Figures

List of tables

Abbreviations

Abbreviations	Definition
AC	Alternating current
AIOMFAC	Aerosol inorganic-organic mixtures functional groups activity coefficients
AOT	Dioctyl sodium sulfosuccinate
APD	Average peak distance
AS	Artificial saliva without mucin
ASM	Artificial saliva with mucin
ASU	Artificial saliva with high urea
BSA	Bovine serum albumin
CCD	Charge-coupled device
CK-EDB	Comparative kinetics electrodynamic balance
COVID-19	Coronavirus disease 2019
DC	Direct current
DMEM	Dulbecco's modified Eagle's medium
DRH	Deliquescence relative humidity
EDB	Electrodynamic balance
EDX	Energy dispersive X-ray spectroscopy
ERH	Efflorescence relative humidity
ESEM	Environmental scanning electron microscope
FDC	Falling droplet column
GF	Growth factor
HSA	Human serum albumin
HSV	High-speed video
ITR	Infectious virus to total virus ratio
MERS	Middle East respiratory syndrome
MFS	Mass fraction of solute
MUC	Mucin
OVA	Ovalbumin
R	Radius
RH	Relative humidity
RTLF	Respiratory tract lining fluid
SADKAT	Single aerosol drying kinetics and trajectories
SARS	Severe acute respiratory syndrome
SARS-CoV-2	Severe acute respiratory syndrome coronavirus 2
SD	Standard deviation
SDS	Sodium dodecyl sulfate
SEM	Scanning electron microscope
SLF	Simulated lung fluid
TEM	Transmission electron microscope

1. Introduction

Aerosol droplets play a critical role in a wide range of natural and engineered systems, including atmospheric processes, climate dynamics, and biomedical applications such as respiratory drug delivery and airborne disease transmission. The outbreak of coronavirus disease 2019 (COVID-19) at the end of 2019 rapidly escalated into a global pandemic in 2020, resulting in millions of deaths worldwide. Other infectious respiratory diseases such as severe acute respiratory syndrome (SARS), Middle East respiratory syndrome (MERS), influenza and measles, also pose a significant burden on global public health, resulting in millions of deaths annually (Kudo et al., 2019; Niazi et al., 2021a; Wang et al., 2021). These outbreaks have underscored the critical importance of improving our understanding of the transmission mechanisms and prevention strategies for respiratory diseases.

Airborne transmission is now widely recognized as one of the main routes for the spread of numerous respiratory viruses (Lewis, 2022; Morawska and Cao, 2020; Prather et al., 2020; Wang et al., 2021). When infected individuals breathe, cough, sneeze, talk, or laugh, they release respiratory aerosols (typically < 5 μm in diameter) and droplets (> 5-100 μm), which contain pathogenic microorganisms such as viruses and bacteria (Ahlawat et al., 2020; Liu et al., 2017; Morawska and Cao, 2020; Oswin et al., 2022; Tang et al., 2021; Wang et al., 2021). These particles can remain suspended in the air for extended periods of time and settle onto surface, where they can be touched or re-inhaled by susceptible individuals, which inevitably poses a risk to human health (Figure 1). However, a deeper understanding of how physicochemical properties of exhaled aerosols and droplets are related to the infectivity of pathogens under varying environmental conditions is still limited, despite its critical importance in mitigating the airborne transmission of diseases.

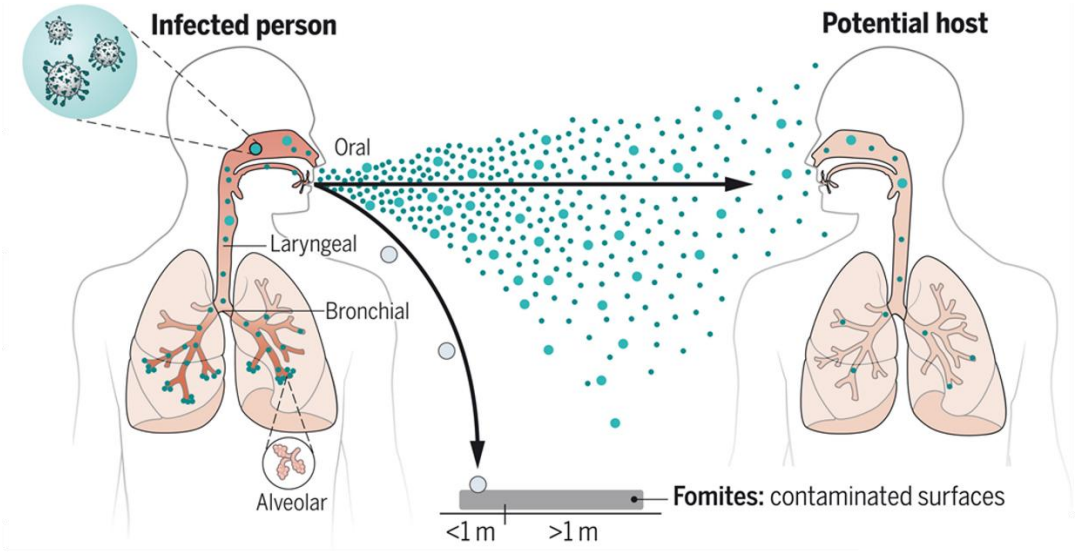

Figure 1. Airborne transmission of respiratory viruses. Figure reproduced from Wang et al., 2021.

This thesis combines single-droplet electrodynamic balance (EDB) trapping, scanning electron microscope (SEM), high-speed video (HSV) imaging and numerical modelling (SADKAT) to investigate the evaporation kinetics, hygroscopic behavior, phase transitions and morphology of artificial saliva droplets and model respiratory droplets. The aim is to better understand the role of different respiratory protein components, specifically mucin and albumin, in determining evaporation, water uptake behavior, phase transitions, and morphology of exhaled respiratory droplets under varying conditions, and thus enhance the understanding of how changes in the physicochemical properties of exhaled respiratory droplets, driven by environmental factors such as relative humidity (RH) and temperature, affect the stability and potential infectivity of loaded pathogenic microorganisms.

The structure of this thesis is organized as follows:

Chapter 1 provides an introduction to the research context and objectives, and presents the theoretical background relevant to the study. Topics covered include the transmission of infectious respiratory diseases, the impact of the environmental factors on the spread of respiratory pathogens, the complex composition of respiratory droplets, with a particular focus on mucin and albumin, and the processes of droplet evaporation and rehydration, as well as the associated efflorescence and deliquescence behaviors. Chapter 2 presents the detailed information about the experimental setup, methodology, and the modeling approach. Chapter 3 presents the results and discussion, organized into three main sections. Section 3.1 investigates the behavior of artificial saliva droplets under varying RH conditions. Section 3.2 focuses on

mucin, the most abundant protein in the upper respiratory tract, using a simplified NaCl-mucin system to support the findings presented in Section 3.1 and to further explore the effects of varying mucin concentrations on physicochemical properties of droplets under different RH conditions. Section 3.3 shifts the focus to albumin, a key protein in the lower respiratory tract, to investigate how protein components influence properties of respiratory droplets. Finally, Chapter 4 presents the overall conclusions and outlines future research directions.

1.1 Exhaled respiratory droplets

1.1.1 Generation processes and size distribution

Respiratory aerosols and droplets are primary carriers of infectious respiratory diseases, and their size provides critical insight into their formation processes and transmission potential. The size and generation mechanisms of these particles vary significantly depending on expiratory activities, such as breathing, talking, coughing, or sneezing (Ahlawat et al., 2020; Liu et al., 2017; Morawska and Cao, 2020; Oswin et al., 2022; Tang et al., 2021). These variations substantially influence their lifetime and propagation distance in the air. Traditionally, a particle size of 5 μm has been used as the critical size to distinguish aerosols from droplets. Infectious aerosols smaller than 5 μm have historically been considered as the primary agents of airborne transmission. However, recent studies have shown that all particles smaller than 100 μm exhibit comparable aerodynamic characteristics (Prather et al., 2020; Wang et al., 2021). Specifically, particles up to 100 μm in diameter can remain suspended in still air for more than 5 seconds when released from a height of 1.5 m, typically travel 1 to 2 m from the source, and are capable of being inhaled (Wang et al., 2021). In addition, such droplets undergo rapid evaporation, often shrinking into smaller residual particles, thereby extending their airborne lifetime and altering their deposition sites within the respiratory tract. This re-evaluation of the droplet size threshold for airborne transmission, extending it up to 100 μm, highlights a broader distribution of respiratory droplet sizes and their associated aerodynamic behavior. This shift challenges the long-standing assumption that only smaller aerosols pose a risk of airborne transmission.

Respiratory droplets can be classified based on their origin within the respiratory tract into oral, laryngeal, bronchial, and alveolar droplets, as illustrated in Figure 1 (Wang et al., 2021). Generally, the smaller the droplet, the deeper its origin within the respiratory tract. Morawska et al. (2022) reported that during normal breathing, droplets smaller than 1 μm are typically generated in the bronchi and alveoli. Droplets ranging from 1 to 5 μm are primarily produced in the larynx during vocalization and coughing. In contrast, larger droplets, approximately

100 µm in size, are mainly generated in the oral cavity during activities such as talking and coughing (Johnson et al., 2011; Morawska et al., 2022). Figure 2 illustrates the particle size distribution and their corresponding sites of generation.

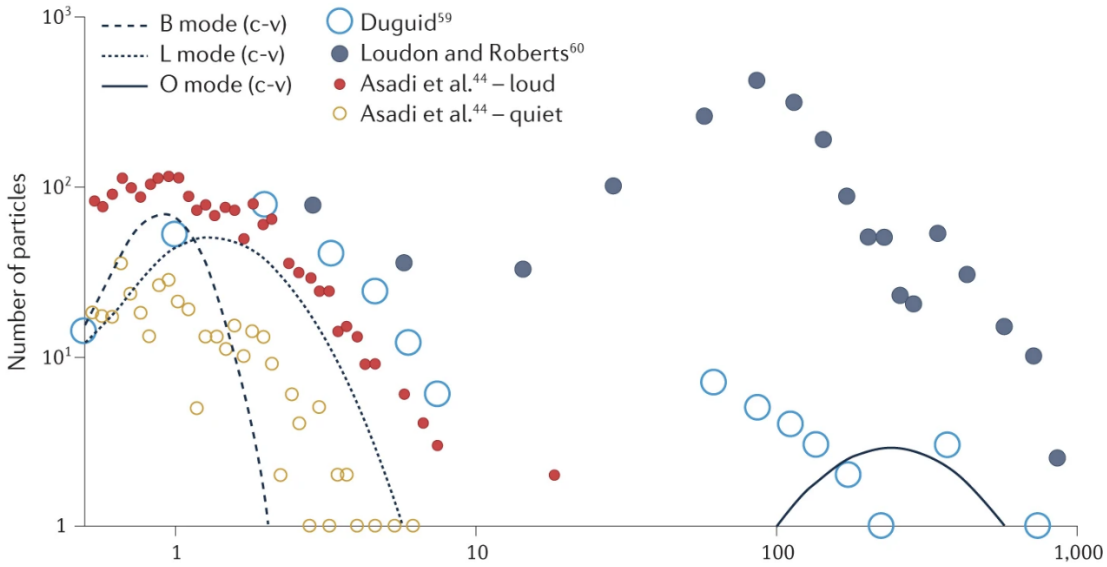

Figure 2. Size distribution of particles associated with different generation sites. B mode represents particles from bronchioles, L mode represents particles from Larynx, and O mode means particles from mouth. Figure reproduced from Morawska et al. (2022).

1.1.2 Respiratory droplet composition

Respiratory fluids are complex, multicomponent systems comprising both inorganic and organic constituents derived from various regions of the respiratory tract. They can be broadly categorized into saliva and lung fluid (Santarpia et al., 2024).

Saliva, representing secretions from the upper respiratory tract, is produced by the salivary glands located in the oral cavity. It consists primarily of water, up to 99.5%, along with inorganic compounds such as NaCl, KCl (0.2% to 0.9%) and organic components (0.4% to 0.6%) (Kubala et al., 2018; Liu and Duan, 2012). Saliva is rich in mucins, enzymes and antimicrobial peptides, and serves multiple functions including lubrication, digestion and oral defense. Among these components, mucins constitute a significant portion of the total protein content (Pöhlker et al., 2023; Santarpia et al., 2024). Although their concentrations can vary among individuals and are influenced by factors such as hydration status, overall health and oral diseases, mucins play a significant role in determining the physicochemical properties of

saliva droplets. Further details on the structure and function of mucins are provided in Section 1.1.3.

Lung fluid, representing secretions from the lower respiratory tract, plays a critical role in maintaining alveolar stability and protecting against inhaled pathogens (Garcia-Fojeda et al., 2019; Han et al., 2015). It consists predominantly of water (approximately 95% by weight), together with salts, surfactant lipids, and proteins (Boat and Cheng, 1980). Although lung fluid and saliva share common inorganic constituents, such as NaCl and KCl, the concentrations of these inorganics are generally higher in lung fluid (4.9-6.6 g/L) than in saliva (0.8-3.9 g/L) (Effros et al., 2005). Similarly, the total protein concentration in lung fluid (12-25 g/L) exceeds that in saliva (0.5-3 g/L) (Bicer, 2015; Pöhlker et al., 2023). Albumin is among the most abundant proteins in lung fluid, with concentrations ranging from 2.9 to 7.3 g/L, whereas its concentration in saliva is much lower (0.08-0.5 g/L) (Bicer, 2015; Pöhlker et al., 2023; Santarpia et al., 2024). In contrast, mucins, which dominate the protein mass fraction of salvia, are rarely detected in lung fluid (Pöhlker et al., 2023; Santarpia et al., 2024). Figure 3 compares the chemical composition of saliva and lung fluid on a mass concentration basis.

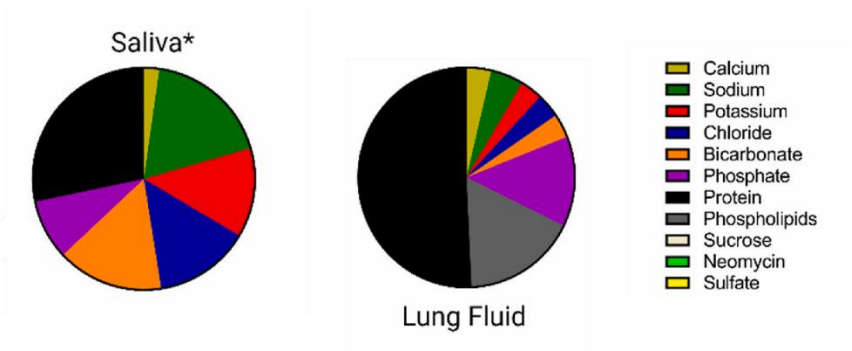

Figure 3. Comparison of the mass concentration of different components in saliva and lung fluid. Figure reproduced from Santarpia et al., 2024.

1.1.3 Mucin

Mucins (MUCs) are complex, high molecular weight glycoproteins, typically ranging from 2 to 50 megadalton (MDa), and contain up to 80% carbohydrate by weight (Ridley et al., 2014; Thornton et al., 2008). They are categorized into two classes based on chromosomal localization and amino acid sequence: secreted mucins and membrane bound mucins (Wagner et al., 2018). In biological secretions, mucins are the primary structural components of mucus (Song et al., 2020). Mucus is a viscoelastic gel composed mainly of water, salts, lipids, immune factors, and

mucins (McShane et al., 2021). It provides lubrication, traps pathogens, and forms a protective barrier over epithelial surfaces (Olsen, 2020).

Mucins are widely present in human saliva and play a crucial role in maintaining oral health and forming a protective barrier in the oral cavity (Ali et al., 2011; Corfield, 2015). Two major secreted mucins found in human saliva, produced from respiratory tract, are MUC5B and MUC7 (Takehara et al., 2013). MUC5B is a larger mucin protein compared to MUC7, classified as a secreted, polymeric, gel-forming mucin rich in cysteine residues. It is essential for mucus gel formation and therefore is responsible for the gel-like properties of saliva (Backstrom et al., 2013). MUC7 is a secreted, non-gel-forming mucin with no cysteine residues, existing primarily as monomers or dimers. MUC7 contributes to maintaining the fluidity and lubrication properties of saliva by preventing it from becoming too viscous, thereby supporting physiological functions such as speaking, chewing, and swallowing (Corfield, 2015). Figure 4 shows the schematic of secreted mucins in their monomeric form, gel network (stabilized by electrostatic interactions), and a transmission electron microscope (TEM) image of purified MUC5B.

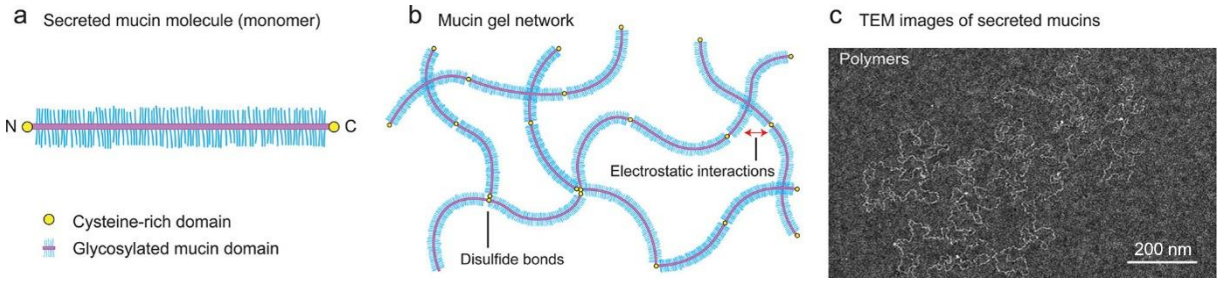

Figure 4. Schematic of secreted mucins: (a) mucin monomer, (b) mucin gel network, and (c) a TEM image of purified MUC5B. Scale bar: 200 nm. Figure reproduced from Song et al. 2020.

Respiratory droplets exhaled by infected individuals can carry viruses and bacteria. Because mucins are abundant and have distinct physicochemical properties, they likely influence the behavior of saliva droplets and, in turn, affect the activity of pathogens they contain. Alexander et al. (2022) reported that mucin in evaporating respiratory aerosols transiently sustains the coronavirus infectivity at 40% RH by enhancing the formation of "protective inclusions", which appear to protect viruses from inactivation. Pan et al. (2025) investigated the stability of influenza virus in respiratory droplets and found that the presence of mucin helps preserve virus integrity and protect the virus from environmental stressors, thereby enhancing its stability.

Mucin is also thought to influence evaporation and hygroscopic growth of exhaled respiratory droplets. Tian et al. (2024) compared the evaporation of artificial saliva droplets containing mucin and droplets containing all other solutes except mucin and found only a marginal difference in the evaporation rate at 40% RH. In their study, they observed a slight delay in the crystallization times of mucin-containing droplets. Based on this observation, they hypothesized that mucin may form a viscous surface film that affects mass transport and crystallization dynamics, resulting in a different amount of residual water that may be kinetically limited in release (Tian et al., 2024). Therefore, a clear and detailed understanding of the role of mucin in the evaporation of respiratory droplets is essential for elucidating RH-dependent virus activity.

1.1.4 Albumin

Albumin is a highly water-soluble protein consisting of a single polypeptide chain composed of more than 500 amino acids. It exhibits a globular, heart-shape structure, as shown in Figure 5 (Hutapea et al., 2023; Mishra and Heath, 2021). There are several types of albumins, such as human serum albumin (HSA, ~67 kDa), bovine serum albumin (BSA, ~69 kDa), and ovalbumin (OVA, found in egg white, ~47k Da) (Elzoghby et al., 2012). At a sequence level, serum albumins from different sources share over 62% identity, with HSA and BSA sharing 76% (Huang et al., 2004; Majorek et al., 2012). The structure of BSA closely resembles that of HSA, and this similarity is one of the main reasons BSA is frequently used as a substitute for HAS (Mishra and Heath, 2021). Additionally, BSA is commonly used in labs also due to its biomedical relevance, high availability, low cost, ease of purification, and its wide acceptance in the pharmaceutical industry (Tantra et al., 2010).

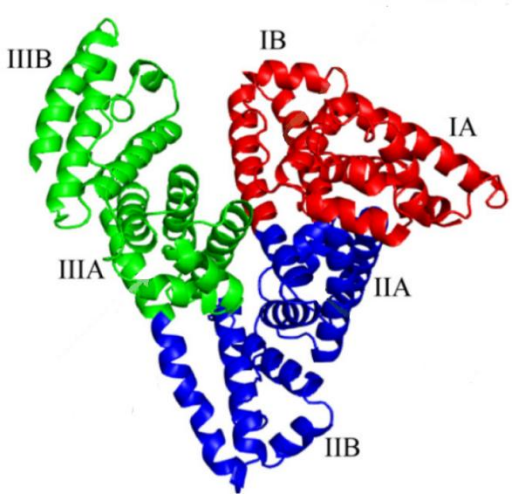

Figure 5. Structure of human serum albumin (HSA) with three predominant domains: domain I (red), domain II (blue), and domain III (green). Each domain is subdivided into two subdomains, A and B. Figure reproduced from Mishra and Heath, 2021.

Albumin is primarily synthesized in the liver and released into the bloodstream. Although it is the most abundant protein in blood plasma, its presence and functional roles in the respiratory tract, particularly within the respiratory tract lining fluid (RTLF), are also significant (Larsson et al., 2012). Albumin in the RTLF originates mainly from plasma leakage into the airways (Khor et al., 2009; Larsson et al., 2012). In this context, it contributes to the maintenance of osmotic pressure in the lung lining fluid, which is essential for the fluid balance (Campos Munoz et al., 2024). Albumin concentration in RTLF has been correlated with lung health conditions (Zhang et al., 2016). Clinical studies show that lower albumin levels are often associated with poorer lung function and an increased risk of respiratory complications (Delliere et al., 2018; Li et al., 2020; Liu et al., 2024; Wang et al., 2016). Albumin also serves as a carrier protein for various substances in the respiratory tract, including drugs and other molecules (Elzoghby et al., 2012). A detectable amount of albumin is also present in saliva. Selby et al. (1988) suggested that albumin found in saliva likely originates from contamination by trace amounts of blood or gingival fluid. Notably, the salivary concentration of albumin is significantly higher in frail elderly individuals (Meurman et al., 2002).

Beyond its structural and transport functions, albumin also plays an important role in host defense. Albumin can play a role in the immune response by binding to pathogens. For example, Varricchio et al. (2024) reported that HSA can bind to the SARS-CoV-2 spike protein and protects cells from infection. Conversely, albumin has also been shown to promote bacterial growth and virulence. Many bacterial species, especially streptococci, have surface proteins that can bind to albumin, this binding can lead to various effects, including the inactivation of

antibacterial peptides and the facilitation of bacterial adherence to host cells (Egesten et al., 2011; Quinn et al., 2018). In addition, Lin et al. (2020) investigated the effect of BSA on the viability of two bacteriophages, MS2 and Phi-6 in an environmental chamber maintained at room temperature (22 ± 1) °C, under low, intermediate, and high RH levels of 20%, 50%, and 80%. Their results showed that the presence of BSA can preserve the viability of both MS2 and phi-6 in droplets at intermediate and high RH. These findings highlight the multifunctional nature of albumin, which not only fulfills systemic physiological roles but also exerts important functions within the respiratory tract. Given its abundance, amphiphilic nature, and binding capabilities, albumin may influence the physicochemical properties of respiratory droplets under different conditions, which may alter the airborne lifetime and dispersal patterns of pathogen-laden respiratory droplets.

1.2 Environmental factors

Keeping pathogenic microorganisms viable is a crucial prerequisite for initiating infection (Huynh et al., 2022). The viability of pathogens is linked to various environmental factors such as temperature, humidity, sunlight, and CO_2 (Guo et al., 2021; Lin et al., 2020; Luo et al., 2023; Niazi et al., 2021b; Schuit et al., 2020; Smither et al., 2020). Among these, temperature and humidity have been identified as key determinants of influenza transmission (Gustin et al., 2015; Lowen et al., 2007). Further studies evaluating the effects of temperature, absolute humidity, and relative humidity on influenza virus activity and transmission have consistently highlighted the prominent role of RH (Marr et al., 2019; Prussin et al., 2018). Furthermore, recent studies have shown that the pH of respiratory droplets can significantly influence virus activity, opening up new avenues for the control of respiratory diseases (Haddrell et al., 2024; Luo et al., 2023). In the following subsections, the effects of RH and pH on pathogen activity are discussed in detail.

1.2.1 Relative humidity (RH)

Numerous studies have demonstrated that RH plays a multifaceted role in determining the survival of viruses in droplets (Lin and Marr, 2020; Niazi et al., 2021a; Prussin et al., 2018). Lin and Marr (2020) reported that viruses preserve their activity in both suspended aerosols and stationary droplets at environmental RH below 40% and near 100%, but become less active at intermediate RH, showing a distinctive U-shaped, RH-dependent infectivity pattern. This unique U-shaped pattern has been observed in many airborne viruses, including SARS-CoV-2 and influenza A (Lin et al., 2020; Niazi et al., 2021b; Yang et al., 2012). Similarly, Smither et

al. (2020) found that the persistence of SARS-CoV-2 in aerosolized artificial saliva is highly influenced by RH, with greater viral stability observed at RH levels between 68-88% compared to a medium RH range of 40-60%. Although the mechanisms underlying this RH-dependent infectivity pattern remain unclear, several contributing factors have been suggested. On the one hand, low RH negatively affects the immune system's ability to respond to pathogenic microorganisms, leading to a higher risk of infection (Ahlawat et al., 2020; Kudo et al., 2019); on the other hand, RH-induced changes in the physicochemical properties of exhaled respiratory droplets may also be responsible (Huynh et al., 2022; Lin and Marr, 2020).

1.2.2 pH

The pH of respiratory fluid is typically close to neutral, around 6.2-7.6 (Baliga et al., 2013). Upon exhalation, however, the pH of respiratory droplets can increase markedly, reaching strongly alkaline values of around 10 (Haddrell et al., 2023). This rise in pH is driven by the loss of bicarbonate (HCO_3^-) from the exhaled droplets, as dissolved $CO_{2(g)}$ evaporates into the surrounding air (Tian et al., 2025). In the human lung, the $CO_{2(g)}$ concentration is approximately 50,000 ppmV (5% atm), whereas in ambient air it typically ranges from about 400 ppmV (0.04% atm) to several thousand ppmV in crowded or poorly ventilated spaces (Bardow et al., 2000; Tillett, 2012). The steep concentration gradient facilitates the rapid escape of $CO_{2(g)}$ from exhaled droplets into the environment, a process that can be described by the following reaction (Haddrell et al., 2023):

$$CO_{2\,(g)} + H_2O_{\,(l)} \rightleftharpoons H_2CO_{3\,(aq)} \rightleftharpoons HCO_3^-{}_{(aq)} + H^+{}_{(aq)}$$

The increase in pH observed in exhaled respiratory droplets is distinct from that in most ambient aerosols, due to their origin in the CO_2-rich environment of the respiratory tract. These pH changes play a critical role in pathogen inactivation. Ahlawat et al. (2022) demonstrated that the enveloped bacteriophage Phi6 remains stable at neutral pH, with optimal inactivation occurring at both low pH (< 5) and high pH (> 10). Other studies have shown that high alkalinity (pH > 10) in droplets contributes significantly to the loss of viral infectivity (Oswin et al., 2022; Haddrell et al., 2023). However, the exact maximum pH value achievable in exhaled respiratory droplets and the time taken to reach, remain unclear.

Gaseous species in ambient air, such as CO_2, HNO_3, and NH_3, can influence aerosol pH and may also affect viral stability and infectivity. For example, increasing ambient CO_2 concentrations has been shown to buffer the alkalinity of exhaled droplets and enhance viral stability (Oswin et al., 2022; Tian et al., 2025). Haddrell et al. (2024) reported that increasing

environmental $CO_{2(g)}$ levels to 800 ppm significantly improved SARS-CoV-2 stability in droplets compared to typical atmospheric $CO_{2(g)}$ concentrations (~500 ppm), and this effect was consistent across all tested variants. Notably, in crowded, poorly ventilated indoor environments, $CO_{2(g)}$ levels can exceed 2000 ppm (Bogdanovica et al., 2020), potentially promoting viral persistence and increasing the risk of disease transmission. However, the pH change of exhaled respiratory droplets remains controversial. Luo et al. (2023) investigated expiratory droplet pH using a biophysical droplet model that accounted for common volatile acids such as HNO_3 and CH_3COOH. They reported that droplet pH decreased from neutral to approximately 4 within 2 minutes and gradually approached pH 3.7 due to further uptake of HNO_3 from indoor air. In addition, they also tested the inactivation of SARS-CoV-2 in suspended droplets under these conditions and reported that SARS-CoV-2 maintained its infectivity down to a pH of 3. A notably shorter inactivation time for SARS-CoV-2 was predicted in the acidified indoor air with pH < 3. The study further suggested that the presence of mucus provided partial protection against inactivation below a pH of 3.

1.2.3 Virus stability on surfaces of fomites

Although airborne transmission is the main route for the spread of respiratory pathogens, touching contaminated surfaces and objects may also contribute to transmission. SARS-CoV-2 has been shown to persist on materials such as plastic, stainless steel, ceramics, wood, and glass for 2 to 4 days at room temperature (Liu et al., 2021; van Doremalen et al., 2020). Pastorino et al. (2020) investigated the stability and infectivity of SARS-CoV-2 deposited on polystyrene plastic, aluminum, and glass surfaces. They found that virus exhibited the highest stability on polystyrene plastic, and its infectivity was significantly preserved in the presence of albumin under conditions of 45%-55% RH and temperature between 19-21°C, regardless of surface types. Notably, droplets as large as 200 μm have been reported to resuspend from partially wettable surfaces due to normal human activities (Nikfar et al., 2021). On non-wettable surfaces or in the case of semi-dry residual particles, smaller droplets can be resuspended at lower detachment velocities. These findings suggest that even when virus-laden respiratory droplets settle on surfaces, they may still pose a transmission risk, either through human contact with contaminated surfaces or via resuspension into the air.

1.3 Evaporation and hygroscopic growth

1.3.1 Evaporation

Evaporation is a surface phenomenon in which molecules at the liquid interface gain enough kinetic energy to escape into the gaseous phase (Rahimi and Ward, 2005). Respiratory droplets experience physicochemical changes during the evaporation as being exhaled from the respiratory tract (close to 100% RH) into the ambient environment (typically ranging from 30% to 60% RH). Evaporation leads to water loss, resulting in droplet shrinkage, increased solute concentrations, and changes in phase, morphology, viscosity and pH (Luo et al., 2023; Oswin et al., 2022; Walker et al., 2021). The evaporation of respiratory droplets is governed by dynamic processes that determine both the rate of water loss and the final droplet size and phase state at equilibrium. Key influencing factors include droplet size, RH, temperature, and composition, which together shape the residual droplet properties at equilibrium.

Equilibrium is reached when the rate of evaporation equals the rate of condensation, which means there is no net exchange of water molecules between the droplet and the surrounding air. This occurs when the vapor pressure of water at the droplet surface equals the ambient partial pressure of water vapor. Once equilibrium is achieved, droplets maintain their size without any further changes, making equilibrium size a critical determinant of droplet lifetime in the air. Smaller equilibrium sizes are associated with longer suspension times, thereby enhancing the potential for airborne transmission (Hinds, 1999; Marr et al., 2019; Wang et al., 2021). For example, in still air, a 100-µm droplet takes 5 seconds to fall to the ground from a height of 1.5 m, a 5-µm droplet takes approximately 33 minutes, and a 1-µm droplet can remain suspended in air for more than 12 hours (Hinds, 1999).

Several studies have shown that proteins significantly influence the equilibrium size of respiratory droplets (Lieber et al., 2021; Marr et al., 2019; Nicas et al., 2005). Marr et al. (2019) predicted that droplets composed of NaCl and varying protein concentrations exhibit different final size at RH ranging from 20% to 100%. For example, at 50% RH, droplets containing low protein concentrations (3 mg/mL) were predicted to stabilize at 0.19 of their initial size, whereas those with high protein concentrations (76 mg/mL) stabilized at 0.41. Thus, both the presence and concentration of proteins should be considered when evaluating evaporation of respiratory droplets.

1.3.2 Hygroscopic growth

When dried saliva particles enter a region of high RH, they can undergo hygroscopic growth: a process in which aerosol particles absorb water vapor from the surrounding environment, leading to an increase in particle size. This process significantly influences droplet properties such as size, density, morphology, phase state, chemical composition and residence time in a suspended state. These changes have important implications for airborne virus transmission and infectivity, as well as for determining the depth of lung penetration upon inhalation. The primary factors governing hygroscopic growth are droplet composition and size, along with the ambient RH (Chen et al., 2021; Vu et al., 2021). Particles exhibiting higher hygroscopicity may grow to larger sizes and settle more rapidly, while less hygroscopic particles may stay suspended in the surrounding air for longer periods, thereby increasing the potential for airborne transmission.

The growth factor (GF) is a key parameter used to characterize the extent of hygroscopic growth. It is defined as the ratio of the particle size under high RH conditions (r_{wet}) to the dry particle size under low RH conditions (r_{dry}, RH < 10%), expressed as:

$$GF = \frac{r_{wet}}{r_{dry}}$$

Studies on the hygroscopicity of respiratory droplets are limited, and the reported values vary across the few that exist (Davies et al., 2021; Groth et al., 2021; Tian et al., 2024; Walker et al., 2021). Groth et al. (2021) investigated the hygroscopicity of human cough aerosols produced by healthy individuals and reported an average GF of 1.31 at 90% RH. In contrast, comparable GF values are achieved at lower RH in other studies using surrogate respiratory fluids: Walker et al. (2021) reported a GF of 1.3 for deep lung fluid (DLF) droplets at ~85% RH, and Davies et al. (2021) found GF ≈ 1.3 for simulated lung fluid (SLF) droplets at ~70% RH. Despite the differences in fluid sources and RH levels, a consistent observation is that respiratory fluid exhibit significantly lower hygroscopicity compared to salt solutions. These findings underscore the influence of respiratory fluid composition on droplet hygroscopicity, with proteins such as mucin and albumin potentially playing critical roles.

1.3.3 Efflorescence and deliquescence

Efflorescence refers to a phase transition of an aqueous droplet to a crystalline solid. As water evaporates, the concentration of dissolved salts in the droplet increases. Once the salt concentration reaches a certain saturation level, the salts begin to precipitate out of solution,

forming crystals within the droplet. Continued evaporation and salt precipitation lead to the complete transformation of the droplet from a liquid to a solid state.

Efflorescence typically occurs at a specific range of RH, which is called the efflorescence relative humidity (ERH). For example, the ERH of a pure NaCl droplet is typically in the range of 45%-48% (Ahn et al., 2010; Li et al., 2014). This ERH can vary in the presence of other solutes, such as different salts, organics, and proteins (Mikhailov et al., 2004; Peng et al., 2022). For example, Li et al. (2014) investigated the efflorescence behavior of individual NaCl and KCl mixture aerosol particles, and reported that droplets at all mixing ratios exhibited a single efflorescence transition at their ERHs, resulting in a phase diagram composed of two different phases, as shown in Figure 6. Mikhailov et al. (2004) studied the dehydration behavior of mixed NaCl-BSA particles with varying BSA dry mass fractions and found that BSA apparently inhibited salt crystallization, leading to a reduction in ERH with increasing BSA mass fraction. Similarly, Gao et al. (2008) reported that water-soluble organics appeared to suppress the ERH of salt particles. A decrease in ERH of more than 30% RH was observed when the mole fraction of water-soluble organic compounds exceeded 0.5. Previous research has suggested that when saliva droplets are exposed to low RH, rapid salt crystallization may protect viruses from prolonged exposure to a highly concentrated saline solution (Niazi et al., 2021b). However, other studies have proposed that efflorescence is suppressed due to the formation of an organic shell, formed by proteins and lipids at the later stage of respiratory droplet drying (Huynh et al., 2022; Stewart et al., 2015). Such competing mechanisms highlight the complex interplay between inorganic and organic components in determining droplet behavior and ultimately pathogen survival.

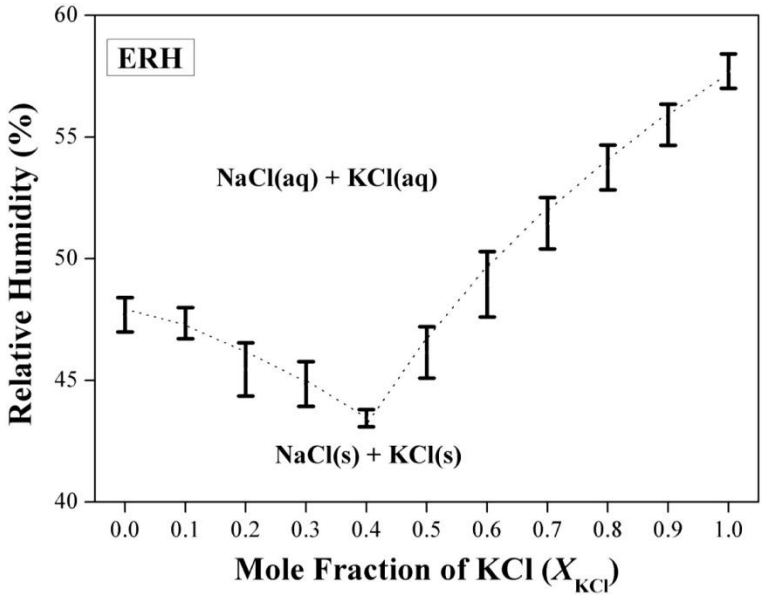

Figure 6. Measured ERH values as a function of the mole fraction of KCl in the NaCl-KCl mixture. "s" refers to the solid state, "aq" refers to the aqueous state. Figure reproduced from Li et al., 2014.

Deliquescence is the phase transition whereby a soluble solid particle takes up water vapor from the air and dissolves, forming an aqueous solution. DRH is defined as the RH on humidification at which the solid spontaneously converts to an aqueous phase. For pure NaCl particles, the DRH is reported to be approximately 75-76% (Li et al., 2014; Tang and Munkelwitz, 1993), which is significantly higher than the ERH of pure NaCl droplets. The difference between ERH and DRH is referred to as hysteresis, which means a substance does not absorb and lose water at the same RH. This phenomenon reflects the kinetic barrier involved in phase transitions (Peng et al., 2022). Figure 7 shows the radial growth factor of pure NaCl particles as a function of RH during rehydration and dehydration processes, clearly showing the hysteresis behavior between efflorescence and deliquescence points. Details of the measurement are given in Section 3.2.3.

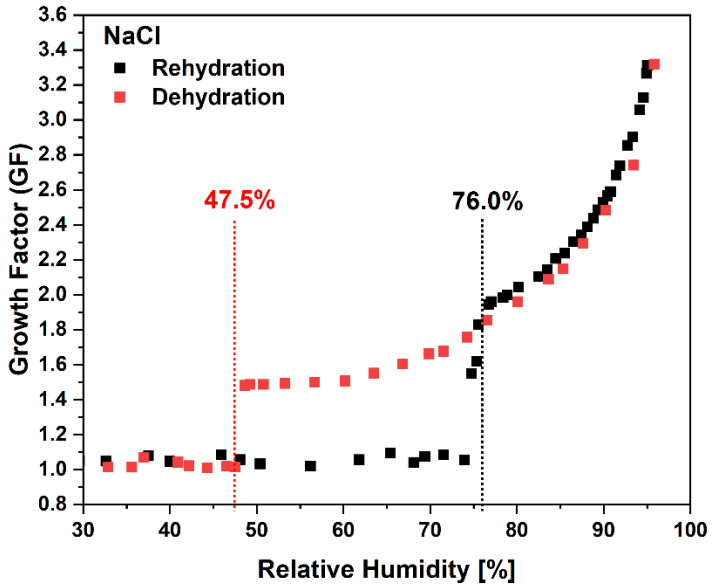

Figure 7. The growth factor (GF) of NaCl droplets as a function of RH. The dehydration process is shown in red, and the rehydration is shown in black. Dashed lines indicate the onset of efflorescence and deliquescence of NaCl droplets, corresponding to ERH (red) and DRH (black), respectively.

The effect of organic compounds on the hygroscopic behaviors of inorganic salts is complex. Choi and Chan (2002) studied the influence of five different organic species on the water uptake of NaCl and $(NH_4)_2SO_4$, and reported varied impacts. Glycerol and succinic acid did not affect the deliquescence properties of NaCl and $(NH_4)_2SO_4$. In contrast, malonic acid and citric acid, which behave as non-deliquescent species in single-particle studies, caused NaCl and $(NH_4)_2SO_4$ particles to absorb a significant amount of water before deliquescence. Glutaric acid caused these salts to deliquesce gradually over a broad RH range. Alshawa et al. (2009) demonstrated that the addition of surfactant AOT into aerosolized NaCl solution reduced the DRH and suppressed the hygroscopic growth of NaCl core. Given the complex composition of respiratory droplets which include various proteins and organic compounds, it is important to study their efflorescence and deliquescence behavior.

Both ERH and DRH are key parameters that describe the phase state and hygroscopicity of aerosol droplets. The physical state of respiratory particles (liquid, semi-solid or solid) may influence their resuspension from surfaces after initial sedimentation (see Section 1.2.3, Nikfar et al. 2021). Clearly, knowledge of the respiratory particle phase state at the moment of sedimentation would allow accessing the probability of the particle resuspension and would thus lead to better understanding of air-transmitted infectious diseases.

1.4 Research objectives

Exhaled respiratory droplets containing pathogens play a crucial role in the transmission of respiratory diseases. While environmental factors do not directly affect pathogens within these droplets, they influence the physicochemical properties of the droplets themselves, which in turn can affect pathogen infectivity. However, how does the physicochemical properties of respiratory droplets change under different RH conditions remain unclear.

The objective of this thesis is to investigate the evaporation and hygroscopic growth behavior of respiratory droplets under varying RH conditions, and to characterize key physicochemical properties of the droplets, including droplet size, phase state, morphology, ERH, DRH, and hygroscopic growth. Given the abundance and biological relevance of mucin and albumin in the human respiratory system, and the potential for complex interactions between inorganic salts and proteins within the respiratory droplets, these two components may critically influence droplet physicochemical behavior. This thesis provides a detailed examination of the effects of mucin and albumin, at varying concentrations, on the properties of respiratory droplets. These findings offer new insight into how RH conditions and different respiratory protein components influence the droplet behavior, and how these changes may, in turn, impact pathogen survival and transmission potential.

To investigate these properties, three types of artificial saliva and two simplified model respiratory systems were studied (see Section 2.1 and Section 2.2). An EDB was used to levitate single droplets at well-defined RH ranging from < 5% to 97%, enabling the examination of droplet evaporation and rehydration behavior. Droplet size was determined using two-dimensional light scattering patterns, recorded by a CCD camera at one-second intervals (see Section 2.3.5), and compared with simulated results from the SADKAT model. The droplet phase state and morphology were analyzed using SEM by collecting droplet samples from the trap onto silicon wafers (see Section 2.5.2). The chemical composition of collected droplets was mapped using EDX coupled with SEM. Droplet shape changes during evaporation in the trap were analyzed using a HSV camera (see Section 2.6).

2. Methods

2.1 Artificial saliva formulation and preparation

Three types of artificial saliva were investigated: artificial saliva with mucin (ASM), artificial saliva without mucin (AS), and artificial saliva without mucin but with a high urea content

(ASU). Because the inorganic composition of ASU differs from that of ASM and AS, the results obtained for ASU are not directly compared and discussed with those for ASM and AS in this thesis. Selected results for the ASU are presented in the Appendix where relevant.

The ASM was purchased from Pickering Laboratories (pH = 7.0, catalog No. 1700-0316, USA), containing type II mucin (from porcine stomach). The AS was prepared using the same components as in the ready-to-use ASM, excluding the mucin, and had a pH of 7.1. The detailed compositions of both artificial saliva solutions are shown in Table 1, together with the ASU. To ensure consistency, the laboratory-prepared AS also included the same amount of Pro-clean, a preservative present in the commercial ASM formulation to inhibit bacterial growth. The composition of Pro-clean is listed in Appendix Table S1. Prior to use, stock solutions of both ASM and AS were diluted to 20% *v/v* with deionized water (NanoPure^{TM} Infinity Ultrapure water system, Barnstead-Thermolyne Corporation) to prevent clogging of the droplet-on-demand dispenser.

Table 1. Compositions of artificial saliva with mucin (ASM), artificial saliva without mucin (AS), and artificial saliva without mucin but high in urea (ASU).

Components	**ASM in [g/L]**	**AS in [g/L]**	**ASU in [g/L]**
NaCl	0.88	0.88	0.4
$NaHCO_3$	0.42	0.42	-
KH_2PO_4	0.2096	0.2096	-
K_2HPO_4	0.4285	0.4285	-
KCl	1.04	1.04	0.4
KSCN	0.19	0.19	-
$CaCl_2 \cdot H_2O$	0.13	0.13	-
$MgCl_2 \cdot 7H_2O$	0.04	-	-
$MgCl_2 \cdot 6H_2O$	-	0.0368	-
NH_4Cl	0.11	0.11	-
$NaH_2PO_4 \cdot 2H_2O$	-	-	0.69
$Na_2S \cdot 9H_2O$	-	-	0.005
$CaCl_2 \cdot 2H_2O$	-	-	0.906
Urea	0.12	0.12	1.0
Mucin	3.0	-	-
Pro-clean	0.3 mL/L	0.3 mL/L	0.3 mL/L

2.2 Simplified model respiratory systems

Laboratory-prepared simplified model respiratory systems, namely, NaCl-mucin and NaCl-albumin solutions, were used as surrogates for exhaled respiratory droplets to further investigate and parameterize the effects of different proteins on the evaporation and hydroscopic behavior of respiratory droplets. Although both NaCl and KCl are prominent salts in human respiratory droplets (Niazi et al., 2021), NaCl was selected in this thesis to represent the inorganic component. This choice was made not only because respiratory secretions are dominated by Na^+ and Cl^-, but also because NaCl's hygroscopic and phase behavior are extensively characterized, enabling direct comparison with previous studies (Huynh et al., 2021; Lin and Marr, 2020; Marr et al., 2019). For the experiments, NaCl (ACS reagent, ≥ 99.5%, Merck KGaA, Germany) was prepared in an amount equivalent to the total molar concentration of inorganic salts in artificial saliva droplets (as shown in Table 1, after 20% *v/v* dilution).

Mucin (type II, from porcine stomach, Sigma-Aldrich, UK) and albumin (Bovine Serum Albumin, BSA, pH = 7.0, ≥ 98%, Sigma-Aldrich, UK), two of the most abundant protein components in the upper and lower respiratory tracts, respectively, were chosen as model proteins (Pöhlker et al., 2023; Santarpia et al., 2024). Each was mixed with NaCl to achieve the following mass fractions: $X_{\text{mucin/albumin}} = \text{mass}_{\text{mucin or albumin}} / \text{mass}_{\text{solutes}} = 0.1, 0.2, 0.3, 0.362$ (equivalent to 0.3 g/L), 0.532 (equivalent to 0.6 g/L), 0.7, and 0.85. Notably, the 0.6 g/L concentration aligns with the mucin concentration previously reported in the artificial saliva droplet study. All solutions were prepared using deionized water. To ensure complete dissolution of the solutes, each solution was subjected to ultrasonic agitation in an ultrasonic bath (Emmi-40, EMAG Technologies, AG-Germany) for 15 minutes.

2.3 Electrodynamic balance (EDB) setup

2.3.1 Droplet generation

Droplets with an initial radius of (48 ± 2) µm were generated using a piezoelectric drop-on-demand dispenser (GeSIM model SPIP: A010-006, featuring a cylindrical housing), as shown in Figure 8. The dispenser comprises a silicon chip covered with glass on one side, with a piezo-ceramic actuator attached to the other side. When an electrical pulse is applied to the piezo-ceramic, it induces a deformation of the water reservoir, resulting in the ejection of a single droplet from the dispenser tip. Droplets were inductively charged to approximately - 0.8 pC by applying a + 300 V voltage to a ring electrode placed in front of the dispenser tip. All operational settings were constant for each experiment.

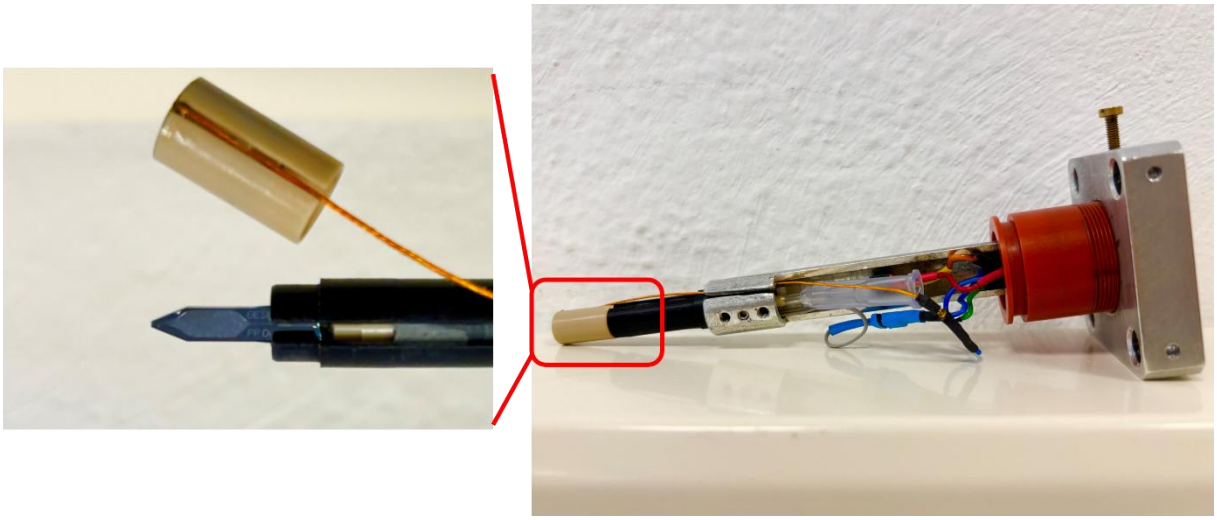

Figure 8. The piezoelectric drop-on-demand dispenser mounted on a holder. A closer view of the dispenser is shown on the left.

2.3.2 Working principles of EDB

EDB is the core part of the experimental setup, enabling the contact-free levitation of a single charged droplet using an oscillating electromagnetic field. The fundamental concept of using electromagnetic field to levitate particles initially comes from "Paul-trap", for which Wolfgang Paul was awarded the Nobel Prize in Physics in 1989. Building on this principle, the EDB has been adapted for the study of individual aerosol particles, allowing researchers to trap micron-sized droplets and investigate their behavior under controlled environmental conditions. The working principles of EDB have been comprehensively described in the study of Davis and Schweiger (2002). The theoretical basics specific to the EDB used in this study are detailed in the doctoral theses of Dr. Denis Duft (2011) and Dr. Nadine Hoffmann (2015). A brief overview of its working principle is provided below.

EDB levitates a single charged droplet in an upward-directed laminar flow inside the trap. Levitation is achieved by balancing three forces: the gravitational force F_g, the electric force F_e, and the drag force F_D, under controlled environmental conditions. The force balance is described by the following equation:

$$F_g - F_D - F_e = 0$$

where $F_g = mg$ (m: mass of the droplet, g: gravity acceleration), $F_D = 6\pi\eta rv$ (η: dynamic viscosity of gas, r: droplet radius, v: flow velocity), and $F_e = qE$ (q: droplet charge, E: electric field strength).

Vertically, a Direct Current (DC) electric field applied between the top and bottom electrodes generated an upward electric force that, together with an upward drag force generated by the laminar flow, counteracted the gravitational force acting on the droplet. Fine control over the laminar flow ensures stable droplet levitation and minimizes convective disturbances. The vertical position of the droplet can be precisely controlled by adjusting the DC voltage (U_{DC}). Horizontally, an Alternating Current (AC) potential was applied to the torus electrode to provide lateral confinement. This AC field creates a time-averaged restoring force that dynamically stabilizes the droplet and prevent lateral drift, ensuring that the droplet remains centered in the trap.

In this study, an EDB was located in a vacuum chamber for electrical and thermal isolation (as shown in the right part in Figure 9). The vacuum chamber was evacuated using a membrane pump and a turbo pump (MVP 015 and TMH 071P, Pfeiffer Vacuum), achieving a vacuum of $p = 1.7 \cdot 10^{-4}$ *mbar* in the chamber. The interior of EDB was maintained at atmospheric pressure. For droplet injection and initial trapping, an AC amplitude of $U_{AC} = 1600$ *V* and a frequency of $f = 150$ *Hz* were applied. Smaller droplets at equilibrium were levitated at higher frequencies (f = 800-1000 *Hz*, manually-controlled). A delay time of $t = 550$ μs was selected to synchronize droplet injection with the rising slope of the AC signal, optimizing trapping efficiency.

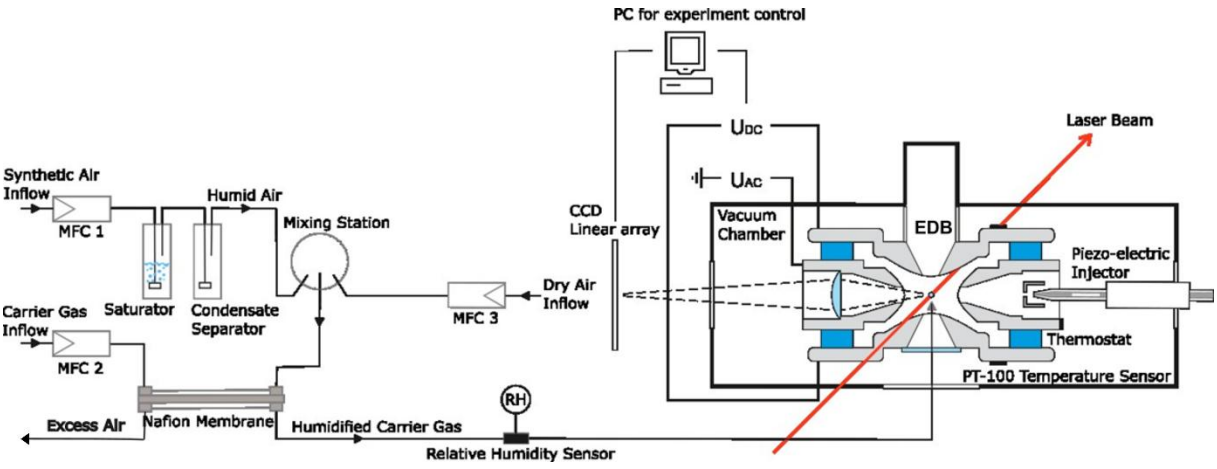

Figure 9. Schematic drawing of the experimental EDB setup equipped with humidity control system.

2.3.3 Relative humidity (RH) control system

Levitated droplets were exposed to a laminar flow of humidified synthetic air (N_2 + O_2). The flow diagram of the RH control system is shown in the left part in Figure 9. Synthetic air was

humidified to saturation at room temperature by passing through a water-filled saturator containing deionized water, following a condensate separator which removed entrained water droplets from the humid flow. Humidified synthetic air and dry synthetic air were mixed in different mixing ratio in the mixing station under the control of different mass flow controllers (MFC, Bronkhorst), and then entered the counterflow exchanger containing a permeable Nafion^{TM} membrane. Nafion^{TM} membrane worked as a selective membrane that facilitated the transfer of water vapor between two adjacent gas streams, without allowing the actual gases to mix. The mixed synthetic air was more humid than the carrier gas, and water molecules naturally diffused from the side with higher concentration to the side with lower concentration. By adjusting the flow rate of mixed air flow, the amount of water transferred can be regulated. This allows for precise control of the RH in the humidified carrier gas, which was monitored by a humidity sensor (Sensirion SHT41) positioned in the airflow, with an accuracy of ± 1.5% RH. The RH-defined airflow was directed through the EDB from below at the flow rate of 0.07 sL/min.

2.3.4 Other devices connected to EDB

Figure 10 shows the overall layout of the EDB bench. There were six ports available on the vacuum chamber, five of them were covered with glass windows or lenses, which provided optical access to the internal part of EDB; one port was open to the atmosphere, where the injector can be placed. A vertically polarized laser beam (HeNe laser, model 1136P, JDS Uniphase Corporation, wavelength λ = 632.8 nm, 25 mW) was directed into the center of the EDB through a calibrated system of mirrors to ensure that the beam accurately position on levitated droplets. To determine the droplet position, scattered light was detected by a vertically oriented linear Charge-Coupled Device (CCD) detector (Spectronics Devices). At the very beginning of the experiment, it is necessary to find and mark the center of the trap where droplets can be levitated stably. Once a droplet was levitated and locked in the center position of the trap while evaporating, the DC voltage was actively regulated to compensate the changing gravitational force and drag force. The frequency of the AC field can be automatically or manually controlled by the feedback mechanism in the LabView program. A CCD camera (model DMK21BF04, ImagingSource) was used to record two-dimensional light scattering patterns within the solid angle 18.8° centered around 45° scattering angle. The size of the droplet was determined based on Mie theory, see Section 2.3.5.

The temperature inside the trap was maintained at a constant (17.8 ± 0.3) °C using a thermostat (Julabo FP 50, model HE). Three PT-100 temperature sensors were placed on top, bottom and

ring electrodes (see Figure 9). The sensors were read out by a temperature monitor (model 218, LakeShore). The temperature difference measured from three electrodes was within 0.5 °C.

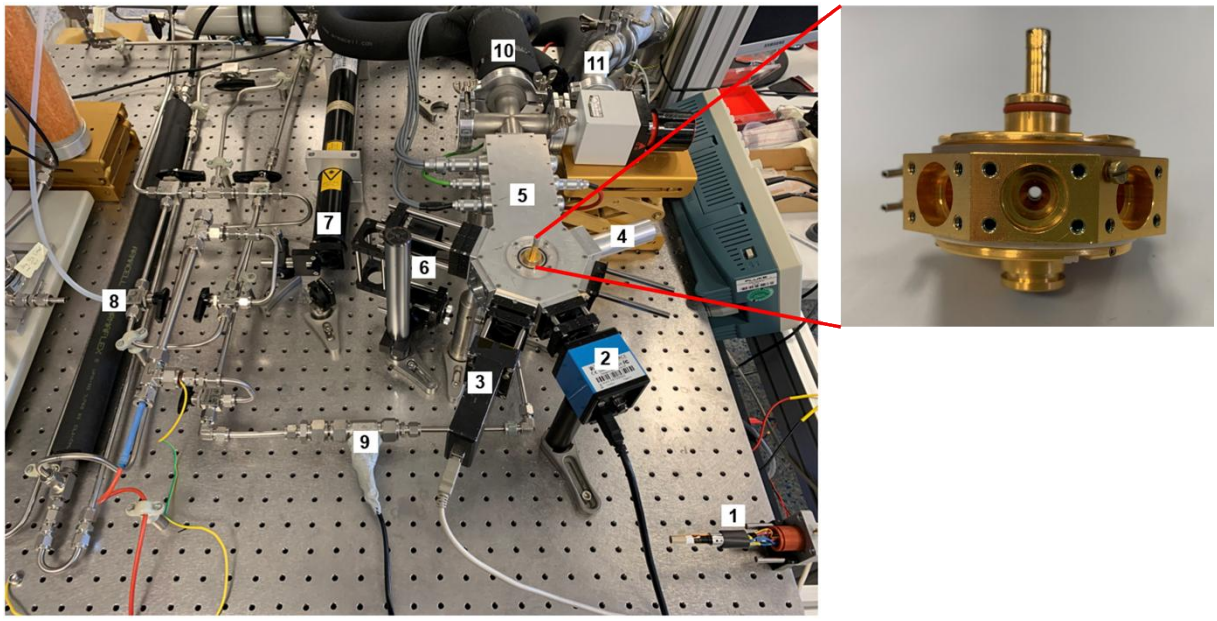

Figure 10. Image of the EDB setup with numbered components: (1) injector, (2) CCD-camera, (3) CCD array, (4) injector port, (5) vacuum chamber, (6) mirror system, (7) laser light, (8) humidity control system, (9) humidity sensor, (10) cooling system, and (11) vacuum pump connection. The inset (right) shows a detailed view of the EDB trap located inside the vacuum chamber.

2.3.5 Characterization of droplet size

Droplet size was characterized using Mie theory, which was developed by Gustav Mie in 1908. Mie theory provides a numerical solution to Maxwell's equations, describing the scattering of electromagnetic waves by a homogeneous, spherical particle of any size. A comprehensive description of Mie theory can be found in Bohren and Huffman (1998). Briefly, a key parameter in Mie theory is the size parameter x, defined as:

$$x = \frac{2\pi r}{\lambda}$$

where r is the droplet radius, and λ is the wavelength of the incident light. The size parameter is crucial in determining which scattering theory is applicable for particle analysis. It can be categorized into three regimes: (1) Rayleigh scattering ($x \ll 1$): the particle is much smaller than the wavelength. (2) Mie scattering ($x \sim 1$): the particle size is comparable to the wavelength. (3) Geometric optics ($x \gg 1$): the particle is much larger than the wavelength. In this study, the size parameter $x \approx 486$. Strictly speaking, this actually places droplets in the

geometric optics regime ($x \gg 1$). Nevertheless, because Mie theory provides the exact solution to Maxwell's equations for spherical particles, it was used to calculate scattering phase functions and droplet size in this thesis.

To determine the droplet radius, the angular distribution of scattered light was analyzed and compared with theoretical Mie scattering phase function. Figure 11 shows an example of droplet size determination from a recorded light scattering pattern using a LabView program. The two-dimensional scattering image was loaded into the LabView program and analyzed. The intensity profile within a solid angle of 18.8° centered around a scattering angle of 45° was extracted. The LabView program automatically identified the maxima and minima in the stripe pattern, and from their spacing calculated the average peak distance (APD), which is the key point used to infer droplet size. The droplet radius is obtained from the following equation:

$$R = (\frac{1}{APD} - B) \cdot \frac{1}{A(n)}$$

where *APD* is the average peak distance in degrees, *A(n)* is a scaling factor that relates droplet radius to stripe spacing, and *B* is a correction term. In this thesis, analysis was performed at 45° perpendicular polarization, for which A(n) is expressed as:

$$A(n) = \frac{1}{5.3830 \cdot n + 12.659}$$

with *n* represents the refractive index of the droplet. The correction factor is $B = 0.0013\ deg^{-1}$ for this geometry.

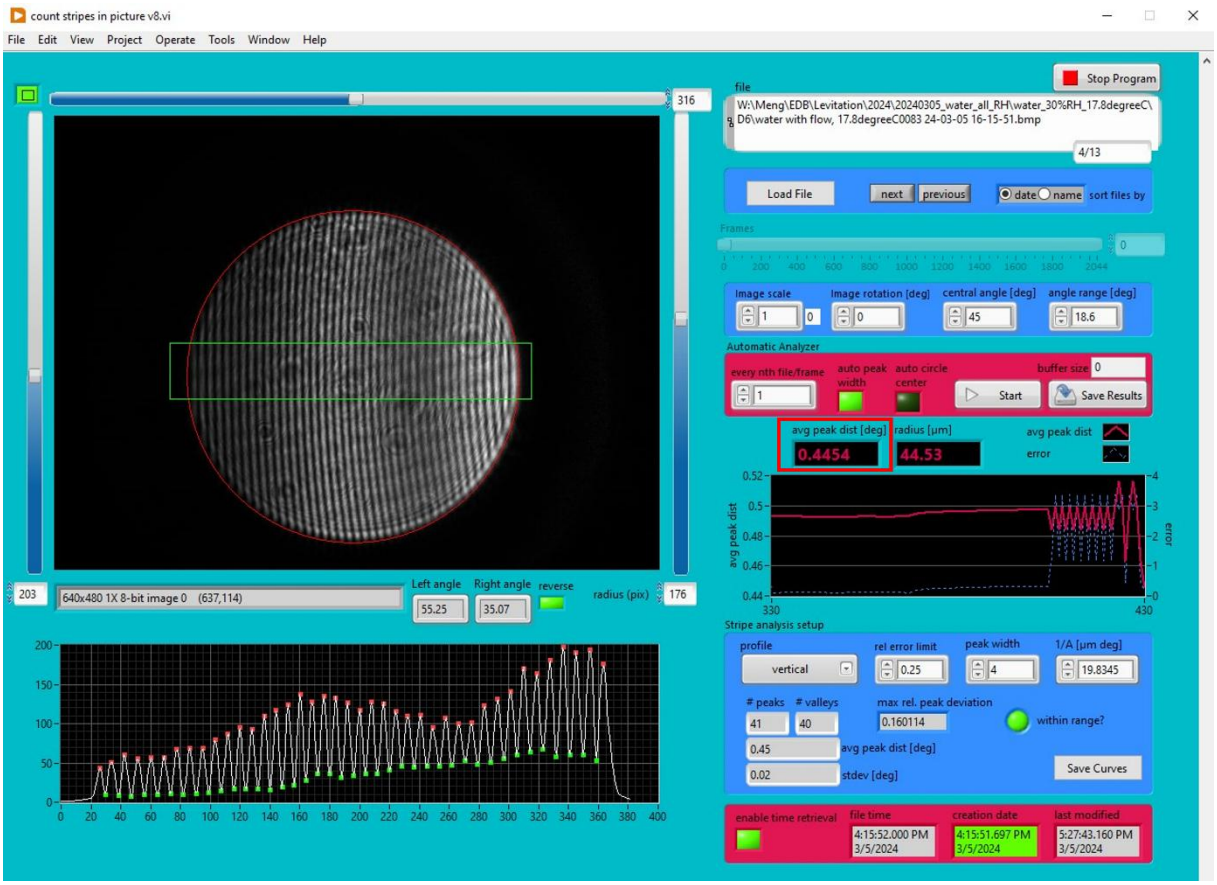

Figure 11. Example of droplet size determination from a light scattering pattern using a LabView program.

Because the refractive index is not fixed but evolves as droplets evaporate, it represents a key source of uncertainty in size determination. In this thesis, the refractive index was assumed changing from n = 1.333, which corresponds to the initial concentration of 20% *v/v* diluted artificial saliva (primarily water) and simplified model respiratory systems (NaCl-mucin and NaCl-albumin systems), to a maximum of n = 1.5 for dry residual particles. The refractive index of n = 1.5 was chosen based on commonly accepted refractive indexes of the organic and inorganic components typically found in saliva residues (Ebert et al., 2002). The relative uncertainty of measured radius was estimated to be 2.2%.

2.4 Evaporation and hygroscopic growth measurements

2.4.1 Evaporation and hygroscopic growth measurements

Droplets were introduced into the trap after both RH and temperature have been kept at set values for 30 minutes. Evaporation measurements were conducted by injecting droplets directly into the trap under specific RH conditions (< 5%, 15%, 30%, 45%, 60%, 75%, and 97% RH).

Droplets evaporated until reaching an equilibrium state, defined as no detectable change in size. All droplets were kept in an equilibrium state for a five-minute period.

The hygroscopic growth experiments were conducted by gradually increasing RH of the gas flow from low levels to 97%. Initially, droplets were injected and stably levitated under specific RH conditions (< 5%, 15%, 30%, 45%, 60%, and 75% RH) for a duration of 5 minutes. Subsequently, the RH in the trap was gradually raised to 97%, with no impact on the stable levitation of droplets. RH equilibration was defined as a fluctuation of RH within ±1.5% around 97%. The timescale for the trap to adjust to the new RH setting (97 ± 1.5%) varied depending on the initial RH, typically ranging from ten to twenty minutes. The droplets remained levitated for an additional hour after reaching and stabilizing at 97% RH. Light scattering images were continuously recorded from the beginning to the end of the experiments.

2.4.2 Efflorescence and deliquescence measurements

Droplet efflorescence and deliquescence were characterized by recording light scattering patterns with a CCD camera. Efflorescence measurements were conducted by initially trapping a droplet under 95% RH conditions. Once the droplet reached equilibrium, the RH was reduced to 20% over a period of approximately 25 minutes. During this process, the light scattering patterns evolved: the number of vertical stripes decreased, indicating a reduction in droplet size. At a distinct moment, the initially straight, regular vertical stripes became distorted and irregular, indicating the onset of efflorescence.

Figure 12(a) shows an example of an efflorescence event of a NaCl droplet, as characterized by recorded light scattering patterns. Before the onset of efflorescence, the droplet is spherical with a smooth surface, and interference between light refracted at the front and back interfaces produces well-defined light scattering patterns. When efflorescence occurs, the sudden crystallization destroys the homogeneous spherical morphology: the particle becomes irregular, its surface roughens, and multiple scattering directions emerge. As a result, the interference conditions required for clean scattering patterns break down, leading to an abrupt distortion of the scattering patterns. This distortion is taken as the optical signature of efflorescence, and the corresponding RH is reported as the ERH in this thesis.

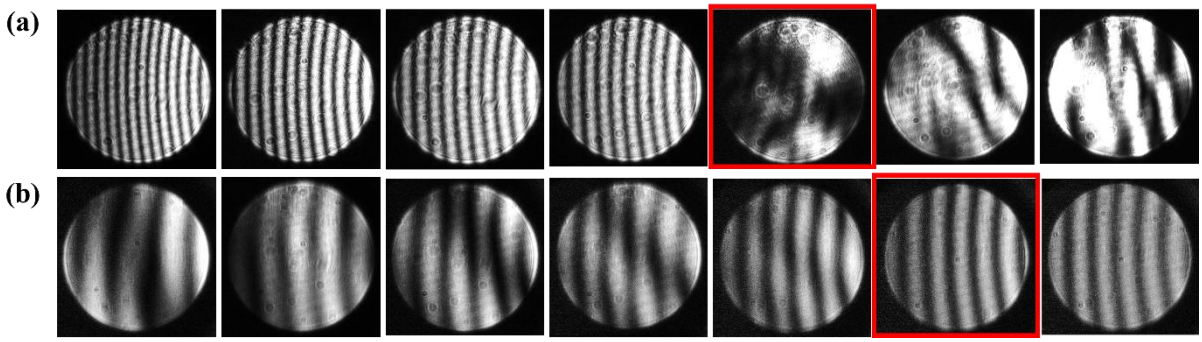

Figure 12. Phase transitions of NaCl droplets recorded by light scattering patterns. (a) Efflorescence process: the NaCl droplet evaporates at 47.5% RH, the onset of crystallization is highlighted in red. (b) Deliquescence process: the NaCl particle takes up water with increasing RH, and the moment of transition to the aqueous state is highlighted in red. All light scattering patterns were recorded at 1-second intervals.

Deliquescence measurements were performed by initially trapping a droplet under 30% RH conditions. After the droplet equilibrated at 30% RH, the RH was increased to 95% to induce rehydration. As RH increases and water is taken up, a liquid film forms on the particle surface, leading to dissolution of the NaCl crystal and recovery of a spherical liquid morphology. Consequently, the scattering pattern transitions back to regular interference patterns, visible as the reappearance of straight vertical stripes (Figure 12(b)). The number of stripes increases with further water uptake. The RH at which the regular patterns first reappeared is defined as the deliquescence point, and the corresponding RH is reported in this thesis as the DRH.

2.5 Scanning electron microscope (SEM) study

2.5.1 Droplet extraction

In order to analyze the physical state and morphology of droplets that have reached equilibrium under well-defined RH conditions, a custom-built droplet extraction device was used to extract droplets from the trap, as shown in Figure 13(a). The device consists of a plastic rod with a 2 mm × 2 mm silicon wafer (Si-wafer) attached to its end, which was introduced into the EDB through a T-junction. The top port of the T-junction was sealed to prevent leakage during the connection to the EDB, while the side and bottom ports remained open to ensure continuous airflow and stable pressure within the trap. As shown in Figure 13(b), the device was connected to the EDB, and the rod was moved downward and positioned such that the Si-wafer approached the center of the EDB closely enough to collect the droplet without disturbing the electric field or compromising the stability of the levitated droplet. Once the Si-wafer was properly positioned, the AC amplitude was set to zero and the DC voltage across the EDB was adjusted

to move the levitated droplet upward toward the Si-wafer. The plastic rod with Si-wafer was then moving up to the T-junction body, after which the bottom and side ports were closed to isolate the droplets from the surrounding air. The entire droplet extraction device was subsequently placed into an airtight container maintained at low RH conditions (< 5% RH at room temperature). Finally, the Si-wafer was transferred to a sample holder within the container in preparation for SEM analysis.

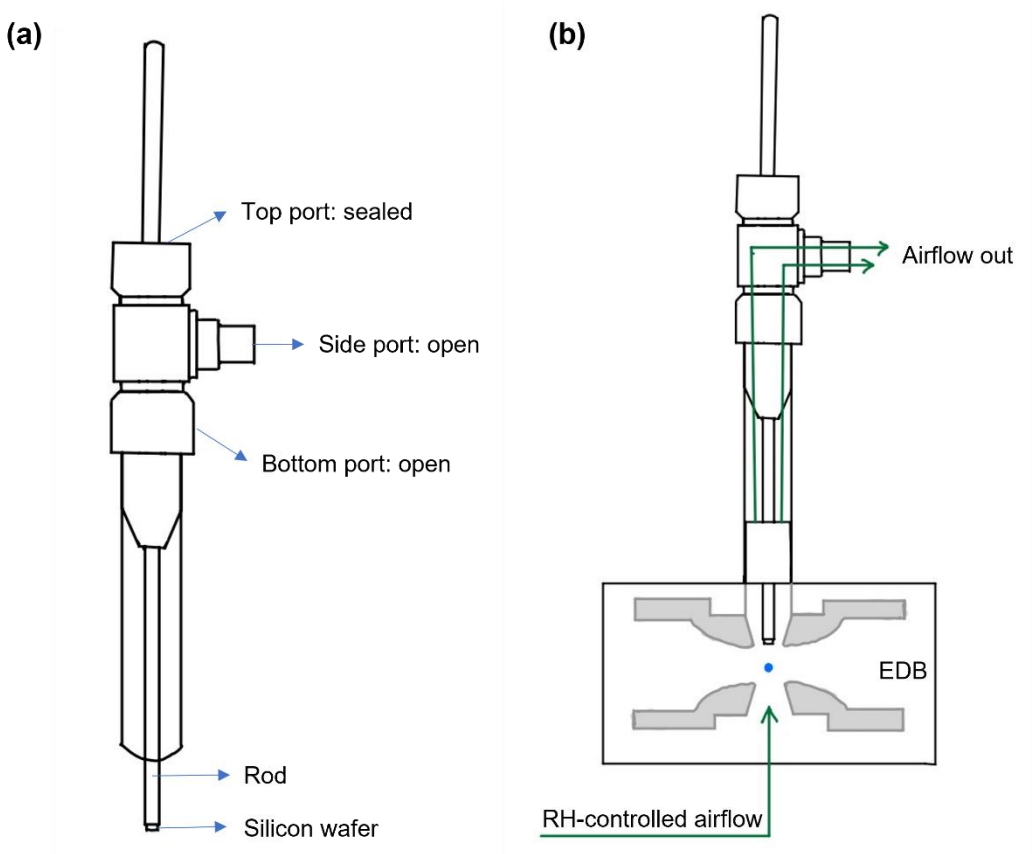

Figure 13. Schematic of (a) the droplet extraction device, and (b) the device connected to the EDB, with the airflow directions indicated by green arrows.

2.5.2 SEM analysis

The Si-wafers on which the droplets were collected were observed in the Environmental Scanning Electron Microscope (ESEM, FEI Thermo Fisher Quattro S) equipped with energy dispersive X-ray (EDX) spectrometer (Ametek EDAX Octane Elite). Prior to imaging, dry N_2 was introduced into the sample chamber of the ESEM to reduce the RH to approximately 10%, thereby minimizing the influence of ambient moisture on the droplet samples. During SEM

analysis, a background pressure of 50 Pa N_2 was maintained to avoid the need for sputter-coating under high vacuum, thus preserving the morphology of the samples.

2.6 High-speed video (HSV) camera study

Optical observation of droplets was conducted using another EDB equipped with a HSV camera (Phantom TMX 5010, Vision Research) and a long working distance objective lens (Mitutoyo, Japan). The temperature conditions in this EDB trap were maintained consistent with those used in the primary experimental setup, (17.8 ± 0.3) °C. The RH in the trap was maintained at approximately 30%. Video sequences capturing the deformation of droplets during evaporation were recorded at a frame rate of 30000 frames per second (fps) with an exposure time of 1 µs. The recorded videos were subsequently analyzed using Phantom Camera Control (PCC) software package.

2.7 Single Aerosol Drying Kinetics and Trajectories (SADKAT) model

The SADKAT model was used in this study to simulate the drying kinetics of artificial saliva droplets. SADKAT is an open-source numerical tool developed to simulate the evaporation profiles and transport dynamics of individual aerosol droplets. A detailed description of the model is provided by Hardy et al. (2023). Briefly, it is built upon the models initially developed by Xie et al. (2007), and later extended by Walker et al. (2021). The model from Xie et al. (2007) solved the coupled differential equations for droplet falling velocity, mass transfer, and heat transfer at discrete time steps, offering a robust representation of droplet behavior during evaporation. Walker et al. (2021) enhanced this model by incorporating thermodynamic treatments for complex, multicomponent solutions, such as simulated lung fluid and artificial saliva, enabling more accurate predictions of droplet evolution in scenarios relevant to respiratory emissions, such as coughing. Its accuracy has been validated through comparison with measurements from both Comparative Kinetics Electrodynamic Balance (CK-EDB) and Falling Droplet Column (FDC) experiments, as reported by Hardy et al. (2023).

The parameters of the physicochemical properties of the artificial saliva solution system are well-defined in the SADKAT model and are categorized into environmental, solvent, and solution properties. In this study, the input parameters for the SADKAT model include the mass fraction of solute (MFS), initial droplet radius, RH, and temperature. Here, the MFS is defined as $MFS = m_{solute} / (m_{solute} + m_{solvent})$. Solvent activity is parameterized as a function of MFS using a constrained polynomial, which is bounded between 0 and 1. $MFS = 0$ represents a pure solvent, while $MFS = 1$ corresponds to a theoretical state of pure solute (i.e., no solvent). For the initial

state (20% *v/v* diluted) of ASM droplets, the calculated MFS was 0.0013, and for AS droplets, the MFS was 0.0007.

3. Results and discussion

3.1 Measurements of artificial saliva droplets and implications for spreading of pathogens

This chapter investigates the behavior of artificial saliva droplets with and without mucin under varying RH conditions. The following sections present experimental investigations of:

1. Evaporation of artificial saliva droplets without and without mucin.
2. Morphology of artificial saliva droplets at equilibrium under varying RH conditions.
3. Rehydration behavior and phase transitions of artificial saliva droplets.

3.1.1 Evaporation behavior of levitated saliva droplets

The evaporation behavior of levitated artificial saliva droplets, both with and without mucin, was examined at a constant temperature of (17.8 ± 0.3) °C and under 7 different RH values ranging from < 5% to 97%, as shown in Figure 14. Single droplets of diluted artificial saliva solution with an initial radius of (48 ± 2) μm were injected into the EDB at fixed RH values. The droplets evaporated until reaching an equilibrium state. I observed that once in equilibrium, the droplets maintained their size without further changes. Here, the droplets were kept in an equilibrium state for a five-minute period. The process was repeated 10 times at each RH value to obtain the statistical average of the equilibrium size.

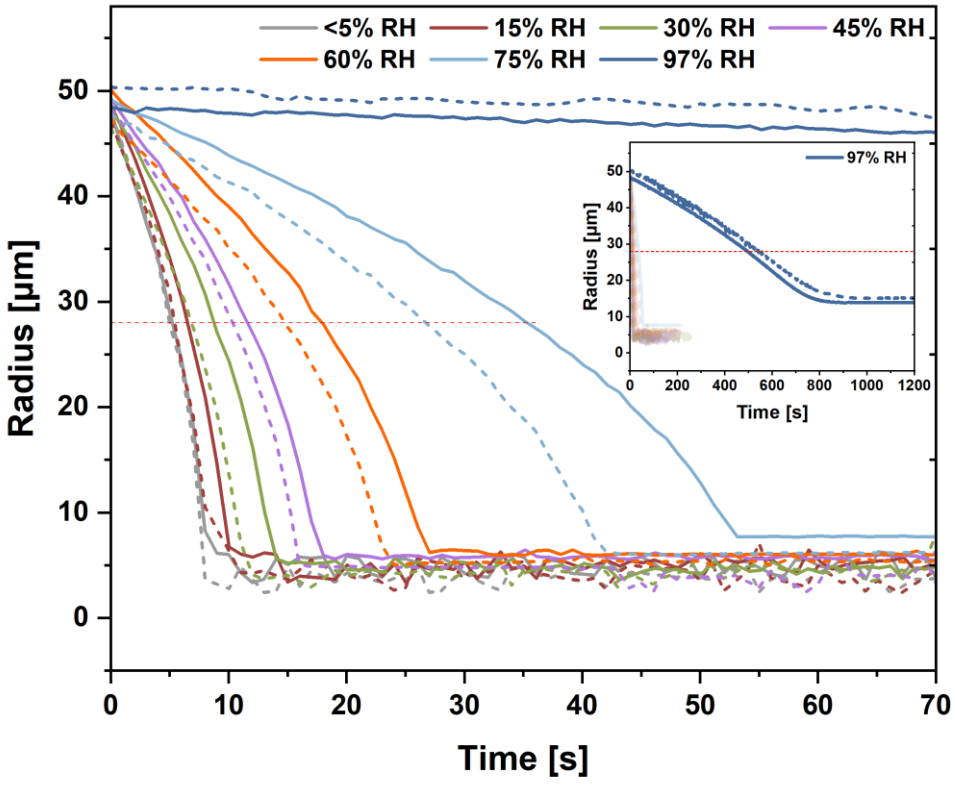

Figure 14. Comparison of the evaporation process of representative artificial saliva droplets containing mucin (ASM, solid lines) and artificial saliva droplets without mucin (AS, dashed lines) under different RH conditions. All measurements were carried out at a temperature of (17.8 ± 0.3) °C. The red dotted line indicates the size of saliva droplets when they reach the concentration of the original stock solution. The complete evaporation process of saliva droplets at 97% RH is shown by a zoom-out view in the inset.

At the initial stage, the evaporation of the diluted ASM and AS droplets follows a similar pattern. As evaporation continues, the loss of water leads to a reduction of droplet size and an increase of solute concentration. The red dotted line at radius of (28 ± 1) µm in Figure 14 marks the size, at which saliva droplets return to the concentration of the original stock solution, which corresponds to the composition of the representative natural human saliva fluid. Here, I speak of the radius of (28 ± 1) µm as the (stock solution) concentration-equivalent size (R_{ce}).

As expected, the evaporation rate of saliva droplets proceeds faster at lower RH. AS droplets evaporate faster and reach equilibrium more quickly than ASM droplets, as shown in Table 2. After the droplets have reached an equilibrium state, they can be levitated without exhibiting any detectable change of size.

Table 2. Time required for artificial saliva droplets to reach the equilibrium state and their equilibrium radius. Listed are average time and standard deviation for ten droplets measured at each setting.

Relative humidity [%]	Time to reach the equilibrium state [s]		Equilibrium radius [µm]	
	ASM	AS	ASM	AS
< 5	9.0 ± 0.3	8.1 ± 0.6	4.78 ± 0.15	3.84 ± 0.19
15	11.3 ± 0.5	8.8 ± 0.3	5.60 ± 0.76	4.17 ± 0.41
30	14.2 ± 0.4	11.1 ± 0.4	5.97 ± 0.56	4.40 ± 0.40
45	18.0 ± 0.7	16.4 ± 0.5	6.18 ± 0.69	4.45 ± 0.38
60	27.0 ± 1.1	24.1 ± 0.5	6.49 ± 0.32	5.42 ± 0.25
75	53.2 ± 0.4	43.5 ± 0.5	7.41 ± 0.21	6.10 ± 0.09
97	790 ± 4	780 ± 6	14.83 ± 0.79	14.53 ± 0.36

The equilibrium size of saliva droplets is a critical parameter in determining the transmissibility of pathogens (Marr et al., 2019; Parienta et al., 2011). It determines how long virus-laden droplets remain suspended in the air before settling on surfaces or the ground, and it also affects how deeply these droplets can penetrate into the respiratory system if inhaled. As shown in Figure 14, the radius of saliva droplets evaporating at humid conditions (RH ≥ 75%) stops at relatively larger equilibrium sizes, while the sizes of saliva droplets that evaporate at intermediate and dry conditions are smaller. Significant fluctuations in equilibrium size are observed in saliva droplets evaporating under dry conditions (RH ≤ 45%). This phenomenon is attributed to the distortion of the light scattering patterns at their equilibrium state, which may be a result of an inhomogeneity and a non-spherical shape of the saliva droplets. The equilibrium size is calculated as the average over all measurements of droplets size at these dry conditions.

Figure 15(a) shows the average equilibrium size of saliva droplets, obtained from measurements of ten droplets at each RH. The ASM droplets equilibrate at a larger size compared to AS droplets. This difference in equilibrium size can be attributed to two factors: (1) The ASM droplets have an additional 3 g/L of mucin, while the other components remain the same as in the mucin-free saliva droplets. This extra mass contributes directly to the droplet's size at equilibrium. (2) Mucin, a high-molecular-weight glycoprotein, potentially forms a viscous layer that limits water loss, thereby resulting in a larger equilibrium size (see discussion in Section 3.1.2). The ratio shown in Figure 15(b) applies for droplets of concentration-equivalent size (R_{ce} = (28 ± 1) µm), at which point the diluted saliva droplets have the concentration of the original stock solution. A slight trend towards larger equilibrium size with increasing RH is observable from RH < 5% to 60%, with a ratio R_{eq}/R_{ce} falling within the range of 0.17 - 0.23

for ASM droplets and within the range of 0.14 - 0.19 for AS droplets. Comparing with low RH measurements, a minor growth in size is evident at 75% RH, reaching 0.27 and 0.22 of their concentration-equivalent sizes for ASM and AS droplets, respectively. At 97% RH, substantially larger equilibrium sizes are observed, these ratios are 0.53 and 0.52, respectively. Marr et al. (2019) predicted that the droplets composed of NaCl and protein would be stable at 0.19 of the initial size for RH lower than 64%. Building upon this prediction, Lieber et al. (2021) investigated saliva droplets of various sizes in an acoustic levitator and observed reduction of 0.2 of the initial sizes, irrespective of temperature (ranging from 20 °C to 29 °C) and RH (between 6% and 65%). It is noteworthy that Walker et al. (2021) conducted measurements using the same compositions of artificial saliva solution as utilized in this study, and reported an equilibrium size of 0.29 of the initial size at 75% RH, which is in a good agreement with our results.

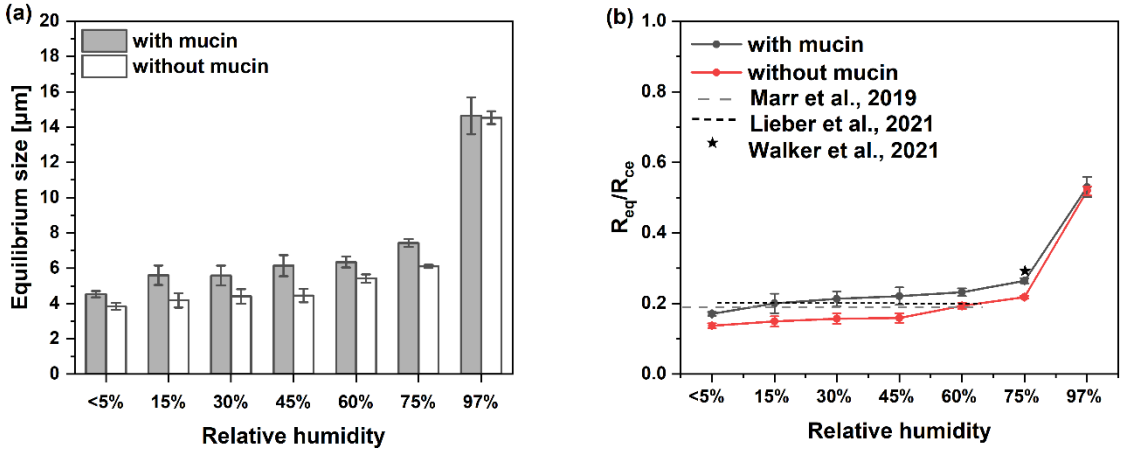

Figure 15. (a) Comparison of the equilibrium radius of saliva droplets with and without mucin at different RH levels. (b) Ratio of equilibrium radius to (stock solution) concentration-equivalent radius (R_{eq}/R_{ce}) as a function of RH for saliva droplets with and without mucin.

In the discussion of the effect of mucin on evaporation kinetics, the comparison of evaporation rates between ASM and AS droplets is of particular interest. For better comparability, I show the evolution of normalized squared droplet diameter (D^2/D_0^2) as a function of time at different RH (Figure 16). This normalization allows for an analysis independent of initial size and a direct phenomenological comparison to the D^2-law characteristic for evaporation of a dilute droplet as known since the beginning of the 20th century (Dalla Barba et al., 2021; Langmuir, 1918; Wells, 1934). As shown in Figure 16, the evaporation behavior of ASM and AS droplets

both show the linear decrease of surface area (the D^2-law) throughout the evaporation period, with only small deviations observed shortly before equilibrium is reached (Figure S1). A difference in the evaporation kinetics is clearly visible at RH ranging from 15% to 75%, with ASM droplets evaporating slower than AS droplets. This suggests that the presence of mucin hinders the diffusion of water molecules, leading to mass transfer limitations that slow down the evaporation process. However, the role of mucin in evaporation kinetics cannot be unambiguously specified under extremely dry (< 5% RH) or extremely humid (97% RH) conditions. I hypothesize that the slow evaporation of the ASM droplets at 97% RH does not result in surface enhancement of mucin concentration which stays evenly distributed across the volume of evaporating droplets, explaining similar evaporation rates of AS and ASM droplets at 97% RH. For the droplets evaporating at very low humidity (< 5% RH), the removal of water occurs so fast, that the mucin cannot accumulate at the surface; the whole droplet dries out almost instantaneously, preserving mucin homogeneously distributed across the droplet volume. In this case the evaporation rates are not affected by the mucin surface layer. This explains also the similar morphology for AS and ASM particles extracted from the EDB after drying at 5% RH (see Section 3.1.2, Figure 19).

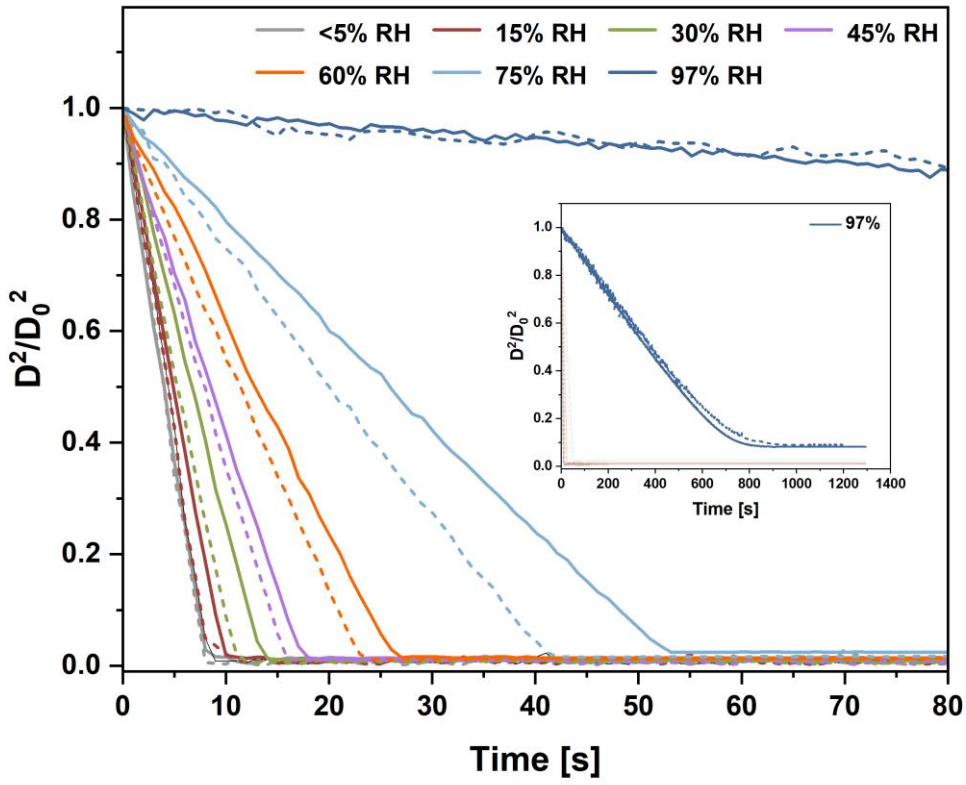

Figure 16. Evolution of normalized surface area of saliva droplets with mucin (solid lines) and without mucin (dashed lines) under different RH conditions. The complete evolution of saliva droplets at 97% RH is shown in the inset.

Tian et al. (2024) observed only marginal reduction of evaporation rate for artificial saliva droplets containing mucin at 40% RH, but noticed a statistically significant delay of crystallization onset as compared to mucin-free droplets. Based on these observations, they have suggested that mucin would form a viscous "mucin surface film" on evaporating droplets, which affects mass transport and crystallization dynamics.

For verification, the experimental results are compared with simulations generated by the SADKAT model, as shown in Figure 17. The model successfully reproduces the overall evaporation trends of artificial saliva without mucin across the RH range of < 5-75% (Figure 17(a)), showing good agreement between simulated and experimental results. In contrast, for artificial saliva containing mucin (Figure 17(b)), the discrepancies between model predictions and experimental results become increasingly pronounced with rising RH. The experimental data reveal that evaporation is markedly slower in the presence of mucin than predicted by the

model, particularly at high RH (e.g., 75%), indicating that mucin substantially prolongs water retention. Since the SADKAT model assumes thermal and compositional homogeneity within droplets (Hardy et al., 2023; Tian et al., 2024), the close agreement for mucin-free droplets and the significant mismatch for mucin-containing droplets suggest that mucin cannot be treated merely as an additional soluble component. Instead, its presence introduces physicochemical heterogeneity that becomes more pronounced during evaporation. These findings indicate that mucin's behavior in evaporating droplets is considerably more complex than the model currently accounts for.

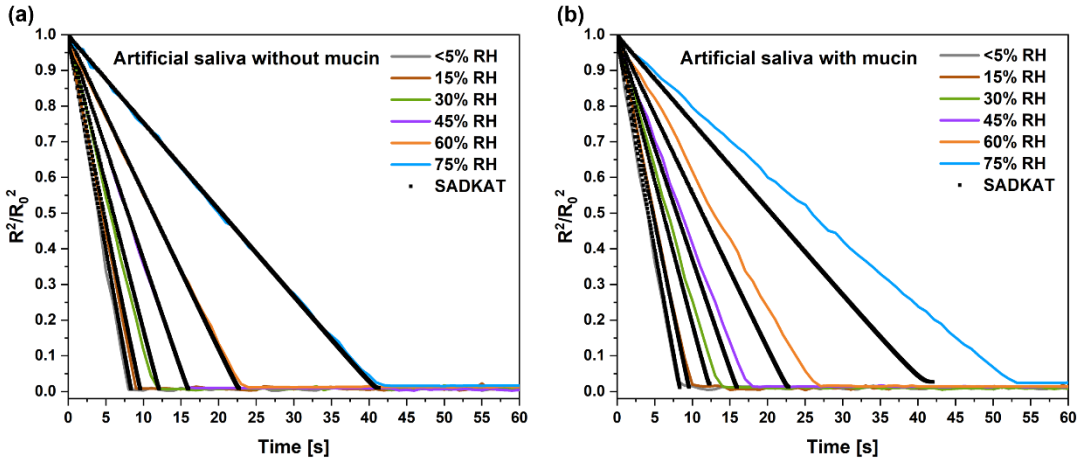

Figure 17. Comparison between SADKAT model simulations and experimental evaporation curves for (a) artificial saliva droplets without mucin, and (b) artificial saliva droplets with mucin. Solid lines in different colors represent results obtained from EDB, and black dashed lines represent SADKAT model predictions.

The experimental data on the content of residual water in evaporating saliva droplets is scarce (Lieber et al. 2021). In this study, I calculated the amount of retained water by subtracting the theoretical weight of dry material based on the initial concentration and saliva composition table (Table 1) from the final weight of saliva droplets which was calculated from recorded light scattering patterns. This calculation assumes a density of 1.002 g/cm^3 for saliva droplets in the original liquid state. However, information on the density of the solid part of human saliva is limited. Zhang (2011) calculated and experimentally measured density of the solid part of human saliva by considering four major salts (NaCl, KCl, $MgCl_2$, and NH_4HCO_3) and four proteins (amylase, albumin, secretory-IgA, and hystatin). The calculated density was 1.447 g/cm^3, and the mean of five experimental measurements from human saliva gave 1.402 g/cm^3. Here, I estimated the density of the solid part of ASM and AS droplets based on their compositions from Table 1, obtaining values of 1.38 g/cm^3 for ASM and 1.24 g/cm^3 for AS.

The density of partially evaporated droplets, prior to reaching equilibrium, is more difficult to determine. Here, the SADKAT was applied, assuming an initial MFS = 0.0007 for AS and MFS = 0.0013 for ASM droplets (see Appendix Table S2). This approach is appropriate for AS, where the solutes are primarily inorganic salts. For ASM, however, the presence of mucin complicates the system, as mucin cannot be treated simply as an additional soluble component in SADKAT. Nevertheless, the model was still applied here as an approximation to estimate the density of ASM droplets before reaching equilibrium. The values should be interpreted as approximate rather than exact.

Figure 18 summarizes the amount of water retained within saliva droplets at their equilibrium. Each result is based on the analysis of ten saliva droplets and shows the average as well as the range of values observed. At RH < 5%, less than 10 *w*% of water is retained within saliva droplets after evaporation. At 15% to 45% RH, there is a noticeable increase in the residual water content within ASM droplets. In contrast, AS droplets retain less residual water in this RH range. This results in a noticeable difference in the residual water content between the two types of droplets, particularly at 45% RH, where the difference in the residual weight fraction of water between droplets with and without mucin is on the order of 20 *w*%. This suggests that the presence of mucin within saliva droplets promotes water retention throughout the evaporation process at intermediate RH. This effect is primarily due to the mucin's hydrophilic nature, which allows it to form hydrogen bonds with water molecules (Ushida and Murata, 2013), and its ability to form a semi-permeable layer on the droplet surface (discussed in more detail in Section 3.1.2). At 60% RH, a significant increase in the residual water content is observed in AS droplets, with the residual weight fraction of water increasing from 15 *w*% (at 45% RH) to 50 *w*%, which is comparable to that of ASM droplets. The significant change of the residual water content within AS droplets between 45% RH and 60% RH indicates that saliva droplets without mucin undergo efflorescence during evaporation in this humidity range. When the RH is below 45%, most of the water in the droplets evaporates due to the absence of mucin. The substantial variability of the residual water fraction at low and intermediate RH below 60% (the observed data range is reflected by the error bars) can be attributed to the sensitivity of the calculated residual water to measurements, where even a slight difference in measured radius, as small as 0.1 µm, results in a 5.5% variation in the residual water fraction. The residual weight fraction of water within both types of saliva droplets is comparable under humid conditions, approximately 67 *w*% and 97 *w*% at 75% RH and 97% RH.

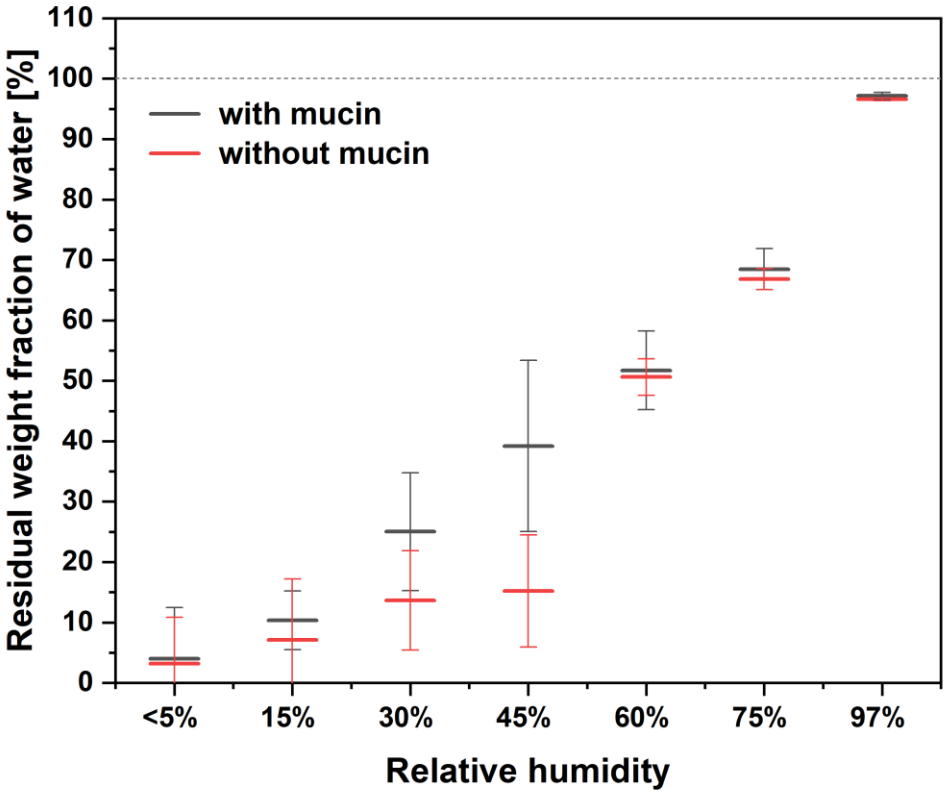

Figure 18. Residual weight fraction of water within saliva droplets at their equilibrium state under different RH conditions.

Regardless of the presence of mucin, elevated virus infectivity under humid conditions, a phenomenon reported in numerous studies (Lin et al., 2020; Lin and Marr, 2020; Prussin et al., 2018; Yang et al., 2012), can be attributed to the following two factors: (1) enhanced water retention within droplets at higher RH, and (2) the formation of virus aggregates during the slower evaporation process at humid conditions, which is expected to enhance virus protection against inactivation as reported by Lin et al. (2020). Our measurements show that for RH between 30% and 45% a virus would have lower chances to be deactivated due to dehydration in the ASM droplets compared to the mucin-free analogues, as these droplets retain more water in this RH range.

3.1.2 Morphology of saliva droplets extracted from the EDB

To study the morphology of artificial saliva droplets, droplets were collected from the EDB after they have reached equilibrium size and examined these droplets using SEM. The results are shown in Figure 19. It is important to note that during the transfer and investigation in the

SEM, the collected droplets are exposed to very dry conditions, which prevents them from being preserved in their equilibrium state. However, the morphology of collected droplets observed in the SEM reflects their phase state at the moment of deposition on the Si-substrate. The droplets deposited in a liquid state have a flat "pancake" shape and are surrounded by a dark area corresponding to the footprint of a liquid droplet upon deposition. Particles, deposited in a solid or semi-solid state have a compact shape. Example SEM images and details are provided in Appendix (Figure S2 to S4). This apparent difference allows us to deduce the humidity where the transition between the liquid and the semi-solid particle state is taking place while the droplet is suspended in the trap.

Figure 19(a) shows representative SEM images of AS droplets. The droplets transition to a solid or semi-solid state at RH $\leqslant$ 45%, whereas they remain in a liquid state at higher RH. This observation corroborates the findings on the residual weight fraction of water within AS droplets discussed in Section 3.1.1: (1) AS droplets remain in a liquid state at RH of 60% or higher. (2) At RH of 45% or lower, most of the water in AS droplets has evaporated, as evidenced by the formation of crystalline material in a compact solid or semi-solid state. This is close to the RH for efflorescence of NaCl of 45-48% (Ahn et al. 2010; Li et al. 2014). Similar SEM images are shown in Tian et al. (2024), who collected mucin-free saliva particles drying in a fall tube at 40% RH. Additional SEM images for AS droplets are shown in Appendix Figure S5.

Importantly, the presence of mucin leads to more pronounced morphological variations in artificial saliva droplet residues, as shown in Figure 19(b). ASM droplets assume an amorphous-like morphology already at RH $\leq$ 45% and do not exhibit a porous structure, unlike AS residues under dry conditions. Instead, the crystalline material appears to be covered by a layer of organic material (element quantification see Appendix Table S3). The distinct morphology differences observed at RH $\leq$ 45% between ASM and AS droplets are attributable to the presence of mucin, which is the sole difference in the formulation of the two saliva solutions. Our observations go in line with the previous study of Huynh et al. (2022), who reported that a higher protein content results in formation of a protein-enriched shell across a range of RH. More SEM images for ASM droplets are shown in Appendix Figure S6.

In addition, considering the various industrial applications of artificial saliva, I tested an additional type of artificial salvia solution that resembles the mineral composition of natural saliva, lacking mucin but high in urea, and find that urea behaves similarly to mucin during

droplet evaporation, creating a compact layer covering inorganic salt crystals (see Appendix Figure S7).

In Figure 19(b), RH demonstrates a notable effect on the extent of shape depression observed on the semi-solid organic layer at RH levels of 45% and below. Most semi-solid configurations showing pronounced depressions occur at RH levels of 30% or lower, where rapid increase in viscosity coincides with the development of surface depressions. The viscous layer remains permeable to water molecules, as shown by the decreasing residual water content at lower RH. Due to its viscous nature, this layer cannot readily adjust to the shrinking central part of the droplet, ultimately causing its collapse. The influence of mucin on the droplet shape will be further discussed in Section 3.1.4.

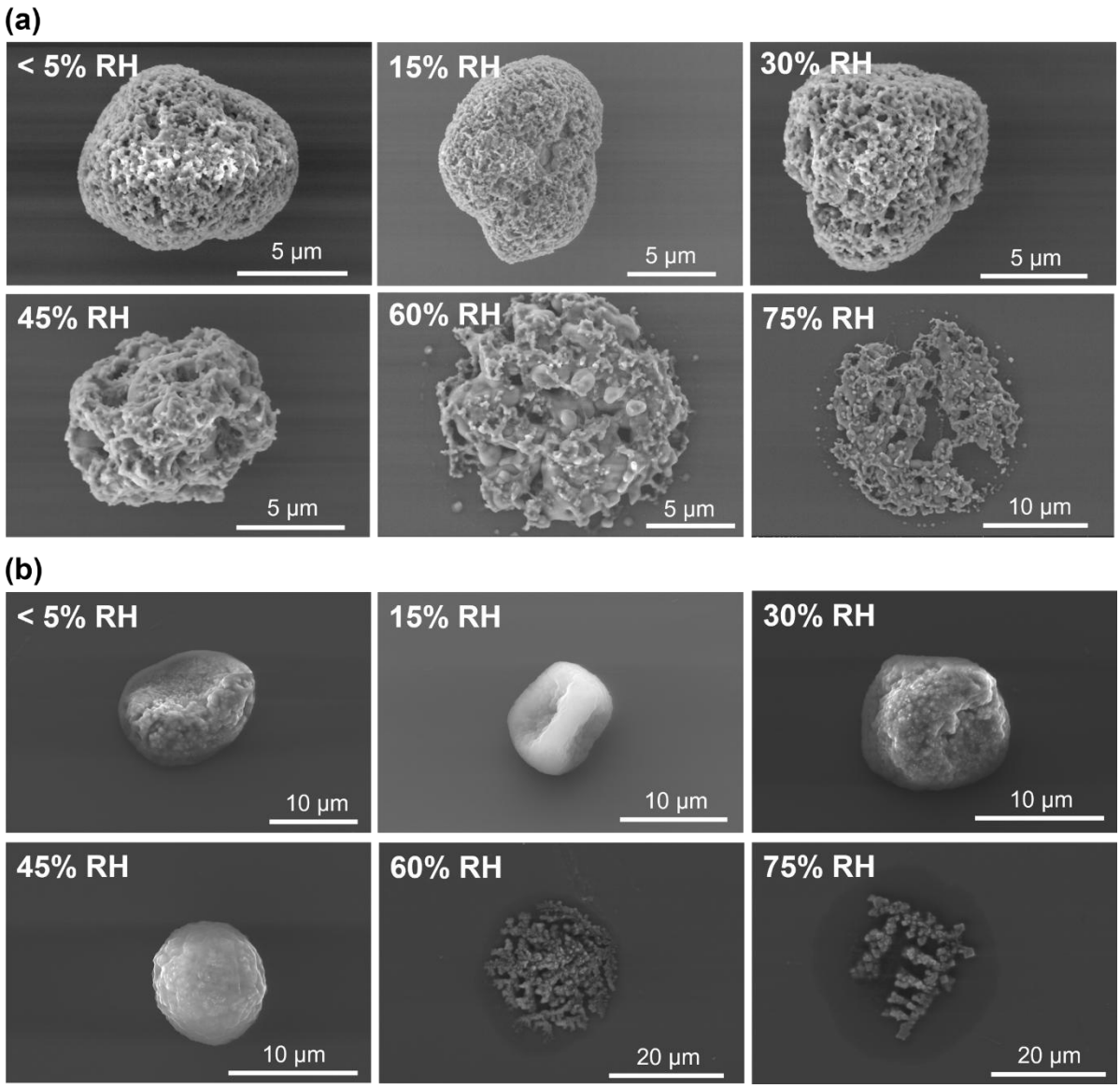

Figure 19. SEM images of saliva droplets collected from the EDB after they reached the equilibrium state under different RH conditions. (a) SEM images of saliva droplets without mucin (AS). (b) SEM images of saliva droplets with mucin (ASM).

Previous studies have suggested that the efflorescence of inorganic salts helps virus to survive in the droplets by reducing the concentration of electrolytes (Huynh et al. 2021; Niazi et al. 2021a; Tian et al. 2024). However, the presence of mucin in saliva droplets cannot be ignored. Alexander et al. (2022) investigated the infectivity of the virus in droplets with varying mucin concentrations at 40% RH, reporting that the mean infectivity of virus in droplets containing 0.1% *w/v* mucin is approximately 20% higher than that in droplets without mucin, and the infectivity become stronger with an increasing mucin content within droplets. Zuo et al. (2014) also observed a notable enhancement in the infectivity and survival of airborne MS2 bacteriophage in aerosolized ASM compared to AS, at a (45% ± 5%) RH and a temperature of

22 °C to 24 °C. The infectious virus to total virus ratio (ITR) is significantly higher, measuring 0.527 with mucin compared to 0.114 without mucin. Lin and Marr (2020) reported that viruses in suspended aerosols can keep their infectivity under extremely dry conditions, with little to no decay of infectivity at RH below 33%, but with reduced infectivity at intermediate RH (from 40% to 60%). Based on the observations, I propose an additional factor that may explain the survival of the viruses under extremely dry conditions: the surface layer of saliva droplets, enriched with mucin, protects viruses from inactivation by retaining water from evaporation. Enveloped viruses, such as coronaviruses, are more sensitive to environmental changes compared to non-enveloped viruses (Zeng et al., 2023). The hydrophobic nature of the viral envelope may cause them to remain within the droplet rather than go to the droplet surface (Huynh et al., 2022; Vejerano and Marr, 2018). Thus, the mucin-rich viscous layer can act as a physical barrier, potentially limiting the exposure of viruses to environmental conditions.

3.1.3 Hygroscopic growth of levitated saliva droplets

Water uptake controls the size, phase state, and chemical properties of saliva droplets (Jing et al., 2017). Respiratory aerosol particles exhibiting strong hygroscopic growth would be more rapidly removed by sedimentation, consequently contributing less to the transmission of pathogens. The highly hygroscopic compounds, such as KCl and NaCl, contribute almost 1/3 of the weight of the soluble material in artificial saliva. NaCl has a high degree of hygroscopicity, with a hygroscopic growth factor of 2.38 measured for 100 nm NaCl particles at 90% RH (Zieger et al., 2017) and the hygroscopic growth factor measured for 100 nm KCl particles is 2.05 at the same RH (Jing et al. 2017). However, organic aerosols are reported to have a low hygroscopic growth factor, with a value < 0.05 (Groth et al. 2021; Walker et al. 2021). Given the chemical complexity of saliva droplets, the hygroscopic behavior of concentrated saliva droplets cannot be predicted from hygroscopic behavior of individual components. Understanding how saliva droplets respond to the change of the ambient RH is crucial for predicting the airborne transmission of pathogens.

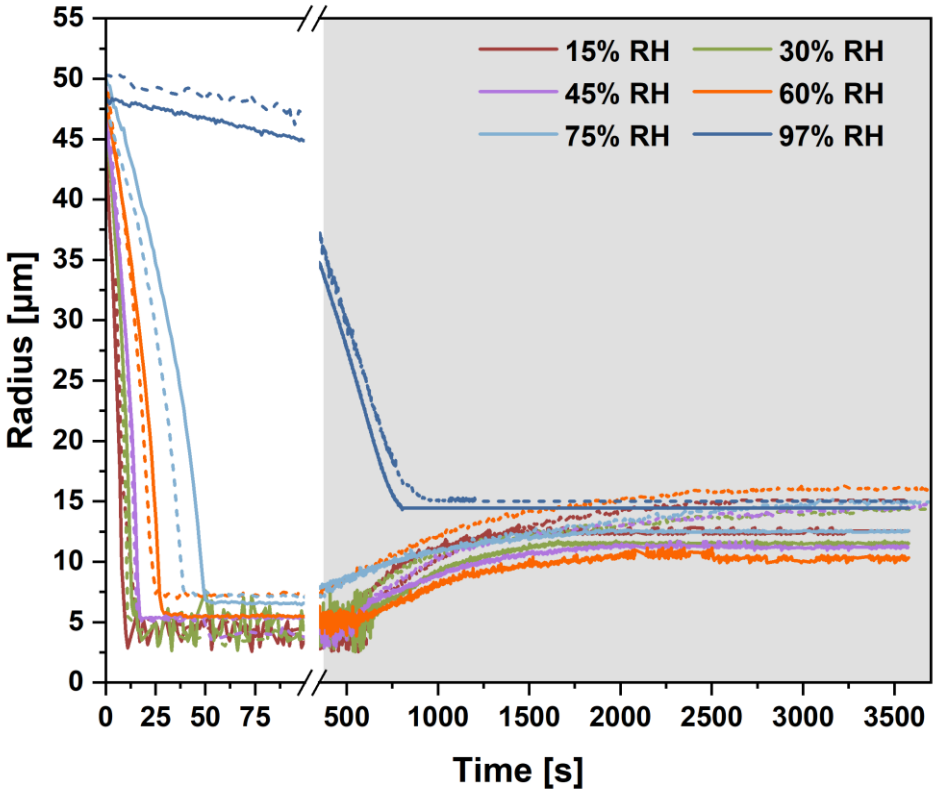

Figure 20. Evaporation and hygroscopic growth of representative saliva droplets with mucin (solid lines) and without mucin (dashed lines). The grey area in the figure indicates the rehydration stage at 97 % RH.

To assess the hygroscopicity of the saliva droplets dried at various RH, I have measured the hygroscopic growth of these droplets exposed to 97% RH. The results are presented in Figure 20 (Appendix Figure S8 shows the data of Figure 18 separately). For hygroscopic growth measurements, saliva droplets were levitated at equilibrium for 5 minutes at a specific constant RH. Then, the RH was increased in a single step to 97% RH. While the RH in the human mouth is typically assumed to be 99.5% (Morawska et al., 2009), it was set at a maximum of 97% RH in our study to ensure a proper operation of the EDB. After the humidity inside the EDB reached 97% RH, a process taking approximately 15 to 20 minutes depending on the initial RH, the droplets were kept suspended in the gas flow for one hour.

Figure 21(a) shows the ratio of droplet radius upon reaching equilibrium at rehydration and droplet initial radius. The weight fraction of water within saliva droplets after rehydration at 97% RH is shown in Figure 21(b). For comparison, the size and water fraction of ASM and AS

droplets injected into the EDB and kept at 97% RH are represented by grey and red bands in both figures.

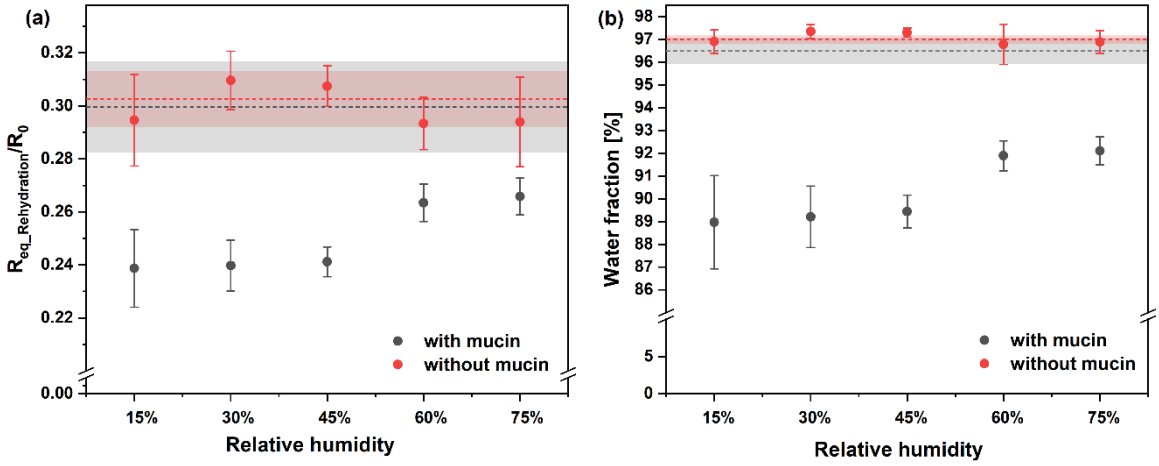

Figure 21. Relative change of the saliva droplet size and water uptake upon rehydration at RH = 97%. The RH on the x-axis gives the equilibrium RH prior to rehydration. (a) Ratio of the equilibrium size following rehydration ($R_{eq\_Rehydration}$) to the initial droplet size as a function of the RH at which saliva droplets initially underwent evaporation. The dashed lines indicate the average ratio of saliva droplets that evaporated at 97%, with the shaded area showing the standard deviation. (b) Water fraction of saliva droplets with and without mucin after achieving the equilibrium at rehydration. The dashed lines indicate the reference at 97% RH.

For AS droplets, the hygroscopic growth at 97% RH remains unaffected by the evaporation process under different RH conditions. All size ratios revert to the reference interval (0.303 ± 0.01), and the water content of the rehydrated saliva droplets reaches as high as 97 *w*%, consistent with the water content in the reference droplets. However, ASM droplets are less hygroscopic. The size recovery of ASM droplets during rehydration at 97% RH is incomplete. The size ratio decreases to (0.241 ± 0.009) and the water content falls to less than 90 *w*% when droplets initially evaporate under dry conditions (RH ≤ 45%). In comparison, the reference size ratio is (0.299 ± 0.017), with a reference water fraction of 96.5 *w*%. However, the hygroscopicity of evaporated ASM droplets under 60% and 75% RH conditions is slightly higher. The size ratio increases to (0.260 ± 0.006), and the water content within the droplets correspondingly rises to 92 *w*%.

The difference in the hygroscopicity between ASM droplets and AS droplets implies that the presence of mucin retards the water uptake process, even at humidity where the droplets preserve their apparent liquid or semi-liquid state. As discussed in Section 3.1.2 (Figure 19), SEM images of saliva droplets collected from EDB provide a more detailed insight into the

underlying factors contributing to the disparities in hygroscopic properties. When RH ≤ 45%, the mucin forms a layer on the surface of saliva droplets, covering salt crystals. This layer hinders the water uptake by saliva droplets with mucin. Even at high RH, the ASM droplets do not recover their sizes compared to AS saliva droplets. This observation suggests that the presence and the state of mucin are influential factors contributing to the limitation observed in the hygroscopic growth of saliva droplets. Our results align closely with a previous study by Choi and Chan (2002), who reported that organic components exert a strong influence on the hygroscopic behavior of inorganic components and the growth factor of droplets containing inorganic and organic mixtures are lower than those of the pure inorganic species.

3.1.4 Light scattering patterns of levitated saliva droplets

To further elucidate how the presence of mucin influences the evaporation and hygroscopic growth of saliva droplets, the morphology of levitated saliva droplets based on their light scattering patterns is discussed here. In Figure 22, I compare the light scattering patterns of an AS droplet (Figure 22(a)) and an ASM droplet (Figure 22(b)) under changing RH conditions. At the beginning, a saliva droplet was trapped at 97% RH and levitated for 10 minutes. Then, RH was decreased step by step from 97% to 25%, all while the saliva droplet remained stably levitated. After reaching 25% RH, the RH was adjusted back to 97% in one step and the light scattering patterns were continuously recorded while the droplet remained stably levitated under these conditions.

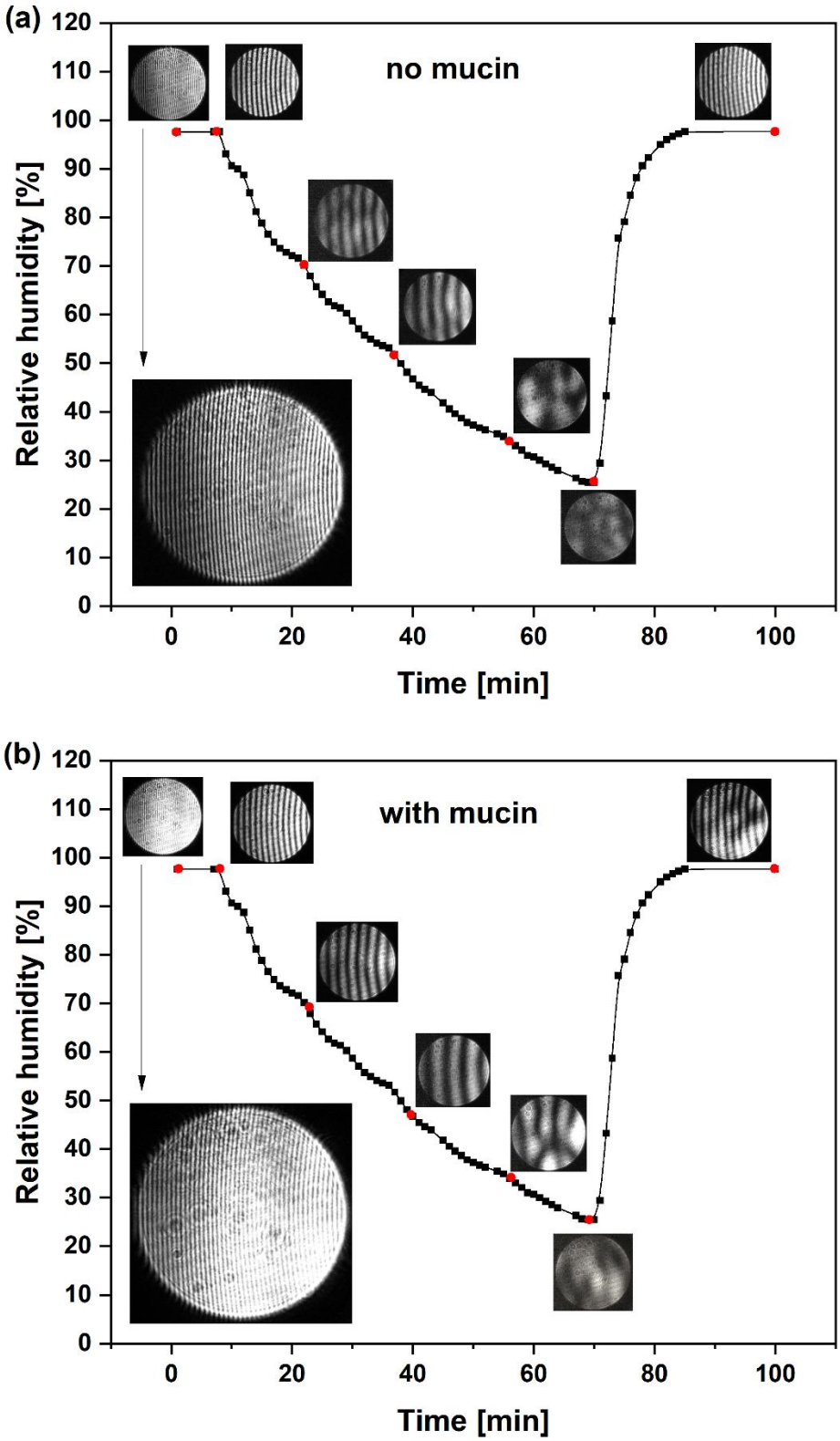

Figure 22. Series of light scattering patterns of saliva droplets with changing RH: (a) A representative saliva droplet without mucin. (b) A representative saliva droplet with mucin. The red dots indicate time and RH at which the light scattering patterns were recorded. An enlarged version of the initial light scattering patterns of both droplets is shown in the lower left corner of the graph for clarity.

In Figure 22(a), for the AS droplet, with decreasing RH, the diminishing number of vertical stripes in the light scattering patterns reflects a reduction in droplet size. A noticeable distortion of the scattering pattern is observed after the RH drops down to 70% (Figure S9), suggesting onset of crystallization within the levitated droplet and a loss of its original spherical shape. As evaporation proceeds, the number of stripes in the scattering patterns reduces and the stripes become increasingly irregular. A distinct increase in the number of stripes on the light scattering patterns could be observed following humidification.

The ASM droplet (Figure 22(b)) preserves its spherical shape for a longer time compared with the AS droplet, as indicated by the stripes remaining regular until the RH drops below 45%. At this point, the scattering patterns become irregular. This suggests that the droplet undergoes significant changes in morphology, possibly deviating from its spherical shape. This conclusion is consistent with the observation that saliva particles become non-spherical at RH below 50% (Walker et al., 2021).

Upon comparing the light scattering patterns of the two types of saliva droplets, it becomes evident that the onset of pattern distortion in mucin-containing droplets is noticeably delayed in comparison to mucin-free droplets. This observation suggests that the presence of mucin contributes to the prolonged preservation of a spherical shape of the saliva droplet. This effect is likely due to the specific properties of mucin, such as viscoelasticity and surface activity: (1) Viscoelastic properties of mucin (Mccullagh et al., 1995) may allow droplets to retain their spherical shape during evaporation through its ability to resist deformation for a more extended period. (2) Mucin can affect the surface tension of the saliva droplets (Mikos and Peppas, 1989). By altering the surface tension, mucin may influence the tendency for droplet to deform during evaporation. This could also contribute to the spherical shape being preserved for a longer time.

3.1.5 Conclusions

I investigated the role of mucin in artificial saliva droplets from two aspects: (1) evaporation process and hygroscopic growth of levitated artificial saliva droplets in an EDB; (2) the evolution of microphysical structure and morphology of artificial saliva droplets using light scattering patterns and SEM, in order to extend the understanding of the RH-dependent infectivity of viruses loaded in saliva droplets. The presence of mucin influences both evaporation kinetics and equilibrium thermodynamics of artificial saliva droplets, which cannot be explained by the presence as an additional soluble component alone. I hypothesize, that it facilitates the formation of a semi-permeable viscous layer on the surface of saliva droplets during evaporation under low-to-moderate humidity conditions ($5 < RH \leq 45\%$). This mucin-

rich surface layer reduces the water evaporation rate and retains a small extra fraction of water within the saliva droplets, thereby maintaining a favorable environment for viruses and other pathogens. Additionally, mucin hinders water uptake during rehydration, leading to reduced hygroscopic growth and, consequently, smaller droplet sizes. Respiratory particles that form a semi-solid organic surface layer before contacting a solid surface would be more readily resuspended by everyday human activity or through advection by air currents. Reduced hygroscopic growth of saliva droplets upon repeated inhalation would facilitate deeper penetration of virus-laden particles into the human respiratory tract thus increasing potential infections to the lungs.

The complex phase behavior of respiratory droplets within the environmentally relevant humidity range may contribute to the observed variability in pathogen infectivity in the aerosol phase (Guo et al., 2020; Niazi et al., 2021b). The observations from this study suggest that the formation of a mucin-enriched layer on the outer surface of saliva droplets may help explain the RH-dependent infectivity of viruses. The concentration of mucin in saliva can vary significantly depending on physiological factors such as hydration status, age, and underlying health conditions. Varying mucin concentrations may result in virus-laden respiratory droplets forming organic shells of differing solidity, thereby influencing viral transmissibility by either protecting or exposing the pathogens to environmental factors such as temperature, humidity, and UV radiation. The impact of mucin concentration on the physicochemical properties of respiratory droplets will be further discussed in Section 3.2.

3.2 Measurements of simplified model respiratory droplets: NaCl-mucin droplets

The findings from the Section 3.1 highlight the significant role of mucin in influencing the behavior of saliva droplets. The evaporation, rehydration, and phase changes of complex organic-inorganic systems which contain more than ten components are significantly more complex and diverse than those observed in simple inorganic systems. To better isolate and understand the role of mucin in influencing droplet behavior, and assess the effects of varying mucin concentrations on the physicochemical properties of saliva droplets under different RH conditions, the complex composition of artificial saliva is simplified using model systems composed of the representative salt and protein.

This section focuses on two key salivary components: NaCl, a representative inorganic salt, and mucin, a high-molecular-weight glycoprotein which is abundant in saliva (Pöhlker et al., 2023;

Santarpia et al., 2024) and serves here as a representative protein component. Mucin levels can vary significantly depending on oral health status and individual physiology. It has been reported that mucin concentrations can be elevated by a factor of 4 in infected individuals, potentially leading to substantial differences in phase separation and other physicochemical behaviors of respiratory droplets (Spicer and Martinez, 1984).

To investigate the influence of mucin on respiratory droplet behavior, NaCl-mucin droplets were studied with mucin mass fractions (X_{mucin}) ranging from 0.1 to 0.85. For comparison, the mucin concentration in the artificial saliva examined in Section 3.1 was 0.6 g/L, corresponding to X_{mucin} = 0.532. This extended mass fraction range (0.1-0.85) was selected to capture physiologically relevant conditions and to systematically explore the effect of lower and higher mucin contents on droplet properties.

The focus of this section is to provide a comprehensive understanding of how mucin affects evaporation and rehydration behavior, the efflorescence and deliquescence phenomena, and the resulting morphological transformations in saliva-like droplets. By isolating these effects in a simplified system, the study aims to elucidate the physicochemical role of mucin in modulating the respiratory droplet behavior under varying ambient conditions.

The following parts present experimental investigations of:

1. Evaporation of NaCl-mucin droplets containing different mucin concentrations under controlled RH conditions, and the residual water fraction at equilibrium.
2. Morphology NaCl-mucin droplets at equilibrium under varying RH conditions.
3. Efflorescence and deliquescence transitions during droplet dehydration and rehydration.

3.2.1 Evaporation behavior of levitated NaCl-mucin droplets

The evaporation behavior of pure aqueous NaCl droplets, 0.3 g/L mucin-NaCl droplets, and 0.6 g/L mucin-NaCl droplets at a well-controlled temperature of (17.8 ± 0.3) °C under 30% RH and 80% RH conditions is shown in Figure 23. The initial NaCl concentration in all droplets was identical to the total molar concentration of inorganic components in the artificial saliva droplets (after 20% *v/v* dilution), as discussed in Section 3.1. The 0.6 g/L mucin concentration also corresponded to that used in the artificial saliva experiments described earlier in Section 3.1.

Single droplets with an initial radius of (48 ± 2) μm were injected into the trap after stabilizing the temperature and RH for 30 minutes. As evaporation proceeds, droplets shrink in size due to

water loss and reach equilibrium when the vapor pressure of water in the droplet equals the surrounding vapor pressure. As shown in Figure 23(a), no significant difference is observed in the evaporation kinetics among the three types of droplets under 30% RH conditions, suggesting that mucin does not significantly influence droplet evaporation under dry conditions. Tian et al. (2024) investigated the effect of mucin on the evaporation of AS and Dulbecco's modified Eagle's medium (DMEM) droplets at 40% RH using an EDB. They reported that the addition of mucin to both AS and DMEM droplets only marginally limited the evaporation rate in the latter stages of drying when compared with non-mucin droplets. Furthermore, they examined the effect of different mucin concentrations (0.1% *w/v*, 0.3% *w/v*, and 0.5% *w/v*) in DMEM droplets and found that the evaporation rates were comparable at 40% RH. This indicates that the impact of mucin is not strongly dependent on concentration at low RH.

At 80% RH (Figure 23(b)), the evaporation profiles of three types of droplets initially follow a similar trend. However, at later stages, the droplets with higher mucin concentrations show slightly slower evaporation kinetics before reaching equilibrium. This trend is consistent with observations from artificial saliva droplets at 75% RH, where droplets containing mucin also exhibited slower evaporation. Additionally, the 0.6 g/L mucin-NaCl droplet shows a larger equilibrium size under 80% RH compared to the other two droplets, as shown in Table 3, suggesting that mucin slows water loss and retains moisture at elevated humidity levels.

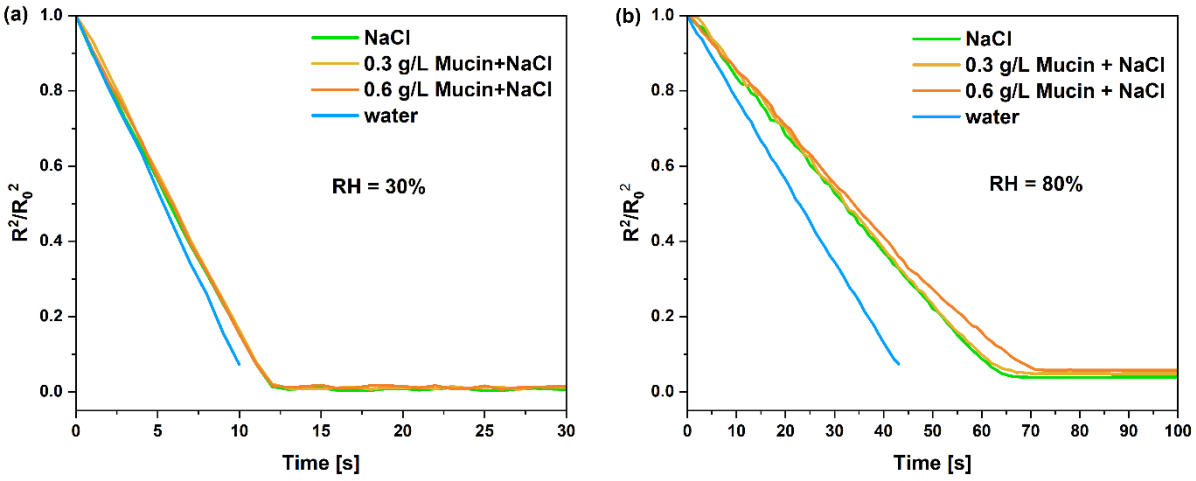

Figure 23. Evaporation of aqueous NaCl droplets, 0.3 g/L Mucin-NaCl droplets and 0.6 g/L Mucin-NaCl droplets at (a) RH = 30% and (b) RH = 80%.

Table 3. Relative size change of droplets with different mucin concentrations at 30% RH and 80% RH, shown as R_{eq}/R_{ce}. Here, R_{eq} is the droplet equilibrium radius, and R_{ce} is the concentration-equivalent radius (R_{ce} = 28 ± 1 μm), as defined in Section 3.1.1.

Droplet types	**30% RH**	**80% RH**
NaCl	0.132 ± 0.001	0.255 ± 0.001
0.3 g/L Mucin + NaCl	0.145 ± 0.001	0.278 ± 0.003
0.6 g/L Mucin + NaCl	0.165 ± 0.003	0.300 ± 0.002

Meng et al. (2025) demonstrated that the presence of mucin in ASM droplets promotes water retention by forming a mucin-enriched layer on the droplet surface during evaporation at intermediate RH (30%-45%). However, that study investigated only one single mucin concentration (3 g/L). Reported mucin concentrations in human saliva typically range from 1 to 5 g/L, depending on individual oral health conditions (Kesimer et al., 2017; Pan et al., 2025). Here, I extended the previous work to investigate whether similar water retention effects occur at lower/higher mucin concentrations, thereby evaluating the concentration dependence of this mechanism.

Figure 24 shows the residual weight fraction of water within droplets containing different mucin concentrations after reaching equilibrium. The residual weight fraction of water was determined by subtracting the theoretical dry particle mass from the final particle mass. The theoretical dry mass was calculated based on the initial concentrations of NaCl and mucin in the droplets, while the final particle mass was obtained from recorded light scattering patterns. Each data point represents the average of ten droplets, with error bars indicating the observed range.

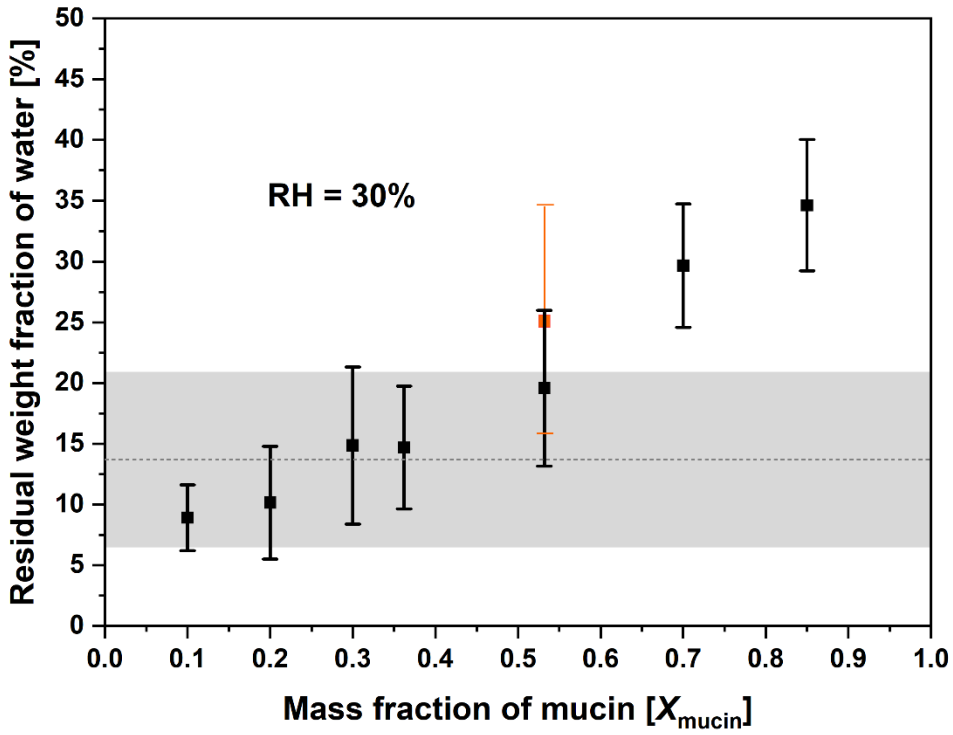

Figure 24. The residual weight fraction of water in NaCl-mucin droplets containing varying mucin mass fractions (ranging from 0.1 to 0.85) at equilibrium under 30% RH conditions is shown in black. For comparison, the residual weight fractions of water in artificial saliva droplets with the same mucin content (0.6 g/L, X_{mucin} = 0.532) and in artificial saliva droplets without mucin, both at equilibrium under 30% RH conditions, are shown in red and grey, respectively.

The density of NaCl-mucin droplets at equilibrium (30% RH) was estimated using the Aerosol Inorganic-Organic Mixtures Functional groups Activity Coefficients (AIOMFAC) model, as summarized in Appendix Table S4. AIOMFAC is a thermodynamic model that calculates activity coefficients in complex mixtures of inorganic salts and organic compounds present in droplets and aerosols (Zuend et al., 2011). Instead of treating entire molecules, the model uses functional groups as the basis for parameterization. Given that mucin is a highly glycosylated protein with long sugar side chains, the dominant functional groups relevant in this context are hydroxyl (-OH) from glycans and carboxyl (-COOH) from acidic amino acids and sialic acids (Bar Dayan et al., 2004; Curnutt et al., 2020). The number of functional groups per mucin macromolecule was estimated from its known glycan content and amino acid composition: approximately 65,000 -OH groups and 3,500 -COOH groups. These values were input into AIOMFAC along with the concentrations of inorganic ions (Na^+, Cl^-) to define the mixed

droplet composition. The model then calculated the equilibrium water activity at 30% RH and the corresponding equilibrium water content of the droplets. From this, the density of NaCl-mucin at equilibrium was derived by dividing the total mass of solute plus water by the droplet volume. The temperature input for all calculations was 290.95 K.

As shown in Figure 24, the water content of droplets increases progressively with rising mucin mass fraction, ranging from less than 10 *w*% in droplets at X_{mucin} = 0.1 to more than 30 *w*% at X_{mucin} = 0.85. This result supports the conclusion that mucin promotes water retention during evaporation, with the amount of water retained in droplets positively correlated with mucin mass fraction. This effect is attributable to the hygroscopic nature of mucin, which enables strong interactions with water molecules (Ushida and Murata, 2013). Mucin contains numerous hydrophilic functional groups, such as hydroxyl (-OH), and carboxyl (-COOH), which can form hydrogen bonds and electrostatic interactions with water molecules (Bar Dayan et al., 2004; Curnutt et al., 2020). As a result, increasing mucin concentration increases the number of available binding sites for water molecules.

Compared to the residual water retained by ASM droplets (Section 3.1, Figure 18), NaCl-mucin droplets retain a comparable amount of water at 30% RH. Although the mean value for NaCl-mucin droplets is slightly lower than that of ASM droplets, the overlap of error bars indicates that this difference is not statistically significant. Nevertheless, several factors may contribute to the observed trend: (1) Efflorescence and hygroscopicity of different salts. The tendency of a salt to retain water is reflected by its ERH value. NaCl has an ERH of 45-48% (Ahn et al., 2010; Li et al., 2014), below which it crystallizes and loses its ability to retain water. In contrast, artificial saliva contains a complex mixture of salts with varying ERH values. Hydrated salts such as $CaCl_2 \cdot H_2O$ and $MgCl_2 \cdot 7H_2O$ retain water as part of their crystalline structure and have much lower ERH (e.g., ~10% RH for $MgCl_2 \cdot 7H_2O$) (Peng et al., 2022). Additionally, potassium thiocyanate (KSCN) is highly hygroscopic. Albayrak et al. (2014) reported that KSCN-surfactant systems are stable at a salt/surfactant molar ratio of 2 with no observable salt crystallization at room temperature and 25-30% RH. In this thesis, KSCN concentration in ASM droplets (0.19 g/L) is likely too low to dry completely or crystallize at 30% RH. (2) Ion valency and water-binding strength. Multivalent ions (e.g., Ca^{2+}, PO_4^{3-}) in ASM salts tend to bind more water molecules than monovalent ions (e.g., Na^+) due to their higher charge density and stronger electrostatic interactions with water (Hribar et al., 2002). These factors may enhance water retention in ASM droplets, although their relatively low abundance means the overall effect is modest.

Compared to the AS droplets, the mean values suggest that NaCl-mucin droplets retain somewhat more water than AS droplets, although this difference also lies within the experimental uncertainty. This trend, while subtle, supports the view that mucin contributes to water retention. Overall, the results highlight that both mucin and inorganic salts play roles in regulating the water retention capacity of evaporating droplets.

3.2.2 Morphology of NaCl-mucin droplets extracted from the EDB

NaCl-mucin droplets were collected approximately two minutes after reaching equilibrium at 30% RH in the trap. The collected droplet samples were immediately transferred, stored, and analyzed under extremely dry conditions to prevent water uptake from surrounding environment, as described in Section 2.5. As shown in Figure 25, a series of SEM images captures the phase state of droplets at the moment they attached to the Si-wafer. The droplets, composed of NaCl and mucin, were prepared in a gradual increase in mucin mass fraction (X_{mucin}) from 0 (pure NaCl) to 1 (pure mucin). The pure NaCl droplet served as a baseline for understanding how mucin alters droplet morphology. The NaCl residue exhibits well-defined, faceted surfaces, characteristic of its cubic crystalline structure (Aquilano et al., 2009; Bunio et al., 2022; Hardy et al., 2023).

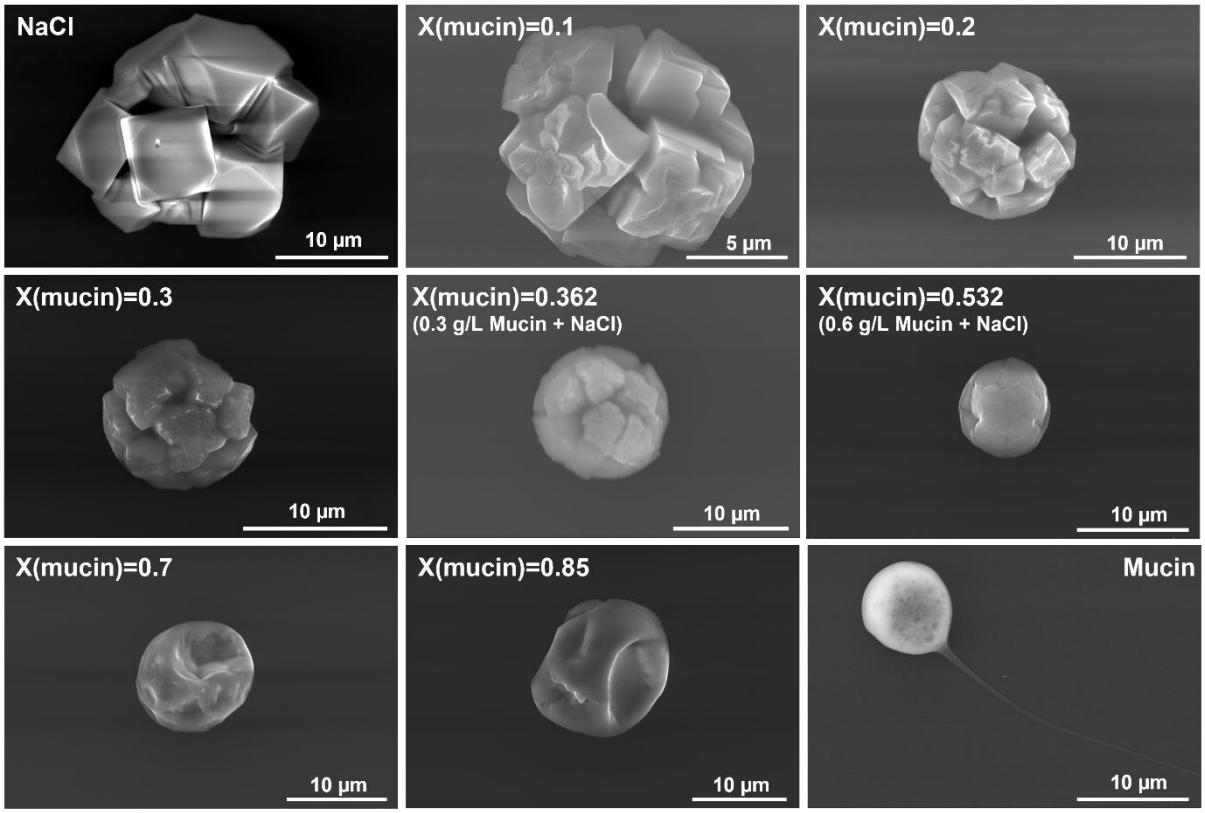

Figure 25. SEM images of representative dried NaCl-mucin particles collected from EDB after they reached the equilibrium state under 30% RH conditions. The mass fraction of mucin (X_{mucin}) is increased from 0 (pure NaCl) to 1 (pure mucin).

When mucin is introduced in small amounts (X_{mucin} = 0.1-0.2), the smooth surfaces and sharp edges of the NaCl crystals are interfered by the presence of mucin. Although crystal morphology of NaCl still dominates the appearance, its crystals appear embedded in or coated by mucin. For droplets with intermediate mucin concentrations (X_{mucin} = 0.3-0.532), the morphology become increasingly irregular, with a noticeable reduction in crystal faceting. This suggests that mucin begins to dominate the physical behavior of the system by forming a viscous, gel-like network on the droplet surface. At high mucin concentrations (X_{mucin} = 0.7-0.85), the particles display smooth, largely amorphous surfaces with visible surface depressions and an absence of any crystalline characteristics. This morphology indicates that high concentrations of mucin can potentially influence the crystallization of NaCl and lead to a predominantly viscous dried state. More SEM images can be found in Appendix Figure S10. Seyfert et al. (2022) investigated the evaporation of droplets containing NaCl and mucin on superhydrophobic substrates and found that mucin strongly influences the final shape of dried droplet residuals, resulting in salt crystals coated by mucin. They reported that the compactness of these dried droplets is relatively low, with a high void fraction that could potentially provide

pocket-like hydrous microenvironment where viruses may remain protected in dried droplet residues.

As discussed in Section 3.2.1, increasing the mucin mass fraction leads to enhanced water retention at equilibrium under 30% RH, as evidenced by a steady rise in residual water content. Correspondingly, SEM images reveal a morphological transition from crystalline NaCl structure to increasingly irregular, no-crystal-visible particles, reflecting the dominance of mucin's gel-forming properties. This suggests that, in addition to mucin's hygroscopic nature, another possible reason for the increased residual water content in droplets with higher mucin concentrations is the formation of mucin networks that physically trap water. Additionally, this morphological transformation may influence the crystallization behavior of NaCl, which will be further discussed in Section 3.2.3.

Interestingly, pure mucin droplet presents a smooth and slightly deformed spherical structure, with a long string-like, inner-hollowed "tail" extending from the main body, measuring approximately 200 nm in thickness. This feature is likely attributable to the viscoelastic properties of mucin, resulting in the stretching during the evaporation process within the trap (McCullagh et al., 1995). As water evaporates, mucin becomes increasingly concentrated and forms a polymeric network, resulting in enhanced elastic and adhesive behavior (Chace et al., 1989). Consequently, the mucin polymeric network is deformed and elongated under stresses such as capillary forces and electrostatic forces during evaporation, resulting in the observed "tail" structure. Although Coulombic instability, commonly referred to as the Rayleigh limit, can also cause droplet deformation and breakup under high charge conditions, it is unlikely to be the cause here. At the Rayleigh limit, the electric charge on the droplet surface exceeds the cohesive force of surface tension, leading to droplet fission and the emission of small droplets or jets (Duft et al., 2003). However, the smooth and continuous filament observed here differs from the characteristic breakup patterns of Coulombic instability. Instead, it suggests viscoelastic stretching of mucin during or following droplet collection as the more plausible explanation. A total amount of 15 pure mucin droplets were tested, and the consistency in shape and structure, along with the absence of droplet fission, further supports this conclusion. A detailed description of the "tail" can be found in Appendix Figure S11.

The evaporation process of some 0.3 g/L mucin-NaCl droplets under 30% RH conditions shows interesting phenomena. Light scattering patterns of droplets during evaporation were recorded continuously from the beginning until equilibrium was reached, as shown in Figure 26(a). The first light scattering pattern on the left corresponds to the droplet at the first second of

evaporation. As the droplet evaporates, its size decreases and the number of the vertical parallel stripes in the light scattering patterns decreases accordingly, as shown in the second and the third images in Figure 26(a). Upon reaching equilibrium, a noticeable distortion in the scattering patterns can be observed, characterized by the loss of regular vertical stripes, indicating that droplet undergoes morphology changes and the loss of original spherical shape. However, in some cases, a bright horizontal stripe at the end of evaporation can be observed, as shown in the last light scattering image in Figure 26(a). Such a bright stripe is characteristic of scattering from elongated objects, such as rods or cylinders.

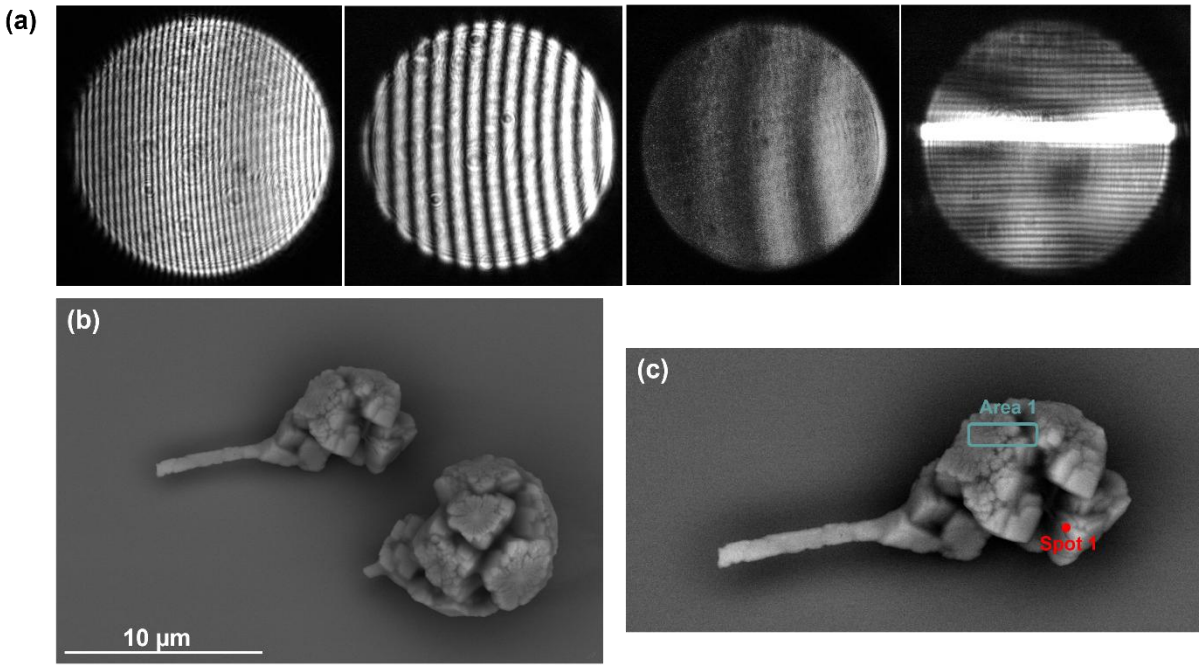

Figure 26. Light scattering patterns and SEM analysis a 0.3 g/L mucin-NaCl droplet collected from the EDB after reaching equilibrium at 30% RH. (a) Time-series of light scattering patterns captured during evaporation in the EDB at 30% RH. (b) SEM image of the final collected particle, which appears to have broken in half during deposition onto the Si-wafer. (c) Zoomed-in SEM image of one half of the droplet, showing a marked area in blue (Area 1) and a spot in red (Spot 1) selected for elemental identification and quantification.

To investigate this phenomenon further, a droplet exhibiting the bright horizontal stripe at equilibrium was collected and analyzed using SEM, as shown in Figure 26(b). The rapid evaporation at 30% RH leads to supersaturation of NaCl, resulting in multiple nucleation sites, with NaCl crystals embedded or covered by mucin, as evidenced by the rough surface features previously discussed. The SEM image shows that the droplet broke into two halves on the Si-wafer during collection, and a rod-like structure is observed extending from the main residual

body. This unusual morphology is particularly intriguing, as it differs from both the crystalline structure of pure NaCl and the "tail" structure observed in pure mucin droplets under the same conditions. The observation also indicates that the rod-like structure does not arise from contact with the Si-wafer but is already formed in the levitated state during evaporation. Possible mechanisms may explain this phenomenon: (1) Viscoelastic stretching of mucin at the point right before reaching equilibrium. As discussed previously, pure mucin droplets form a string-like "tail" due to their viscoelastic properties. During evaporation, the increasing concentration of mucin enhances polymer entanglement and elasticity. Under the combined influence of capillary stresses from shrinking surface area and electrostatic forces in the trap, this viscoelastic mucin network may undergo stretching, thereby altering NaCl crystal growth and contributing to the observed rod-like morphology. (2) Coulombic fission of the droplet (Duft et al., 2003). The droplet may undergo coulombic instability during evaporation, potentially exceeding the Rayleigh limit due to charge accumulation during levitation. In aqueous droplets, this typically results in the emission of small droplets or fission fragments. However, in viscous systems such as mucin-containing droplets, fission may proceed differently, rather than ejecting smaller droplets, deformation may be accommodated by elongation of the droplet body. For comparison, an example of a droplet undergoing Coulombic instability during evaporation is shown in Appendix Figure S12.

To understand the distribution of mucin and NaCl in droplet residues at equilibrium, elemental analysis was performed using EDX spectrometer (described in Section 2.5.2) on two distinct regions of the droplet collected from the EDB after equilibration at 30% RH, as shown in Figure 26(c). The element identification and quantification results are shown in Table 3. Area 1, representing a broader surface region, exhibits a relatively high carbon content (52.34 *wt*%, 69.90 *at*%), indicating a mucin-rich surface layer. In contrast, Spot 1, a localized region within the interior of the dried droplet associated with a crystalline domain, shows a lower carbon content and higher sodium and chloride contents. The difference in elemental composition between the surface and the interior of the droplet indicates the phase separation and inhomogeneous internal structure of the dried droplet, with most of NaCl crystallized within a mucin matrix. This is consistent with the findings of Huynh et al. (2021), who studied the evaporation and phase state of droplets containing NaCl with a protein mixture of mucin and albumin at 40% RH using fluorescence microscopy. They reported the formation of a protein-enriched shell at the droplet interface following evaporation, enclosing an NaCl-dominated inner core.

Table 3. Element identification and quantification of Area 1 and Spot 1 on one half of the 0.3 g/L mucin-NaCl droplet residue collected from 30% RH.

Elements	Area 1	Spot 1	Area 1	Spot 1
	Weight %		Atomic %	
C	52.3	9.7	69.9	21.4
O	6.6	-	6.7	-
N	1.2	-	1.4	-
Na	17.0	27.2	11.8	31.4
Cl	22.78	63.2	10.3	47.3

The final dried morphology and phase state of droplets equilibrated at three different RH levels: 30%, 45%, and 80% were analyzed, as shown in Figure 27. The top row (a-c) displays pure NaCl droplets, the middle row (d-f) presents NaCl-mucin droplets containing 0.3 g/L mucin, and the bottom row (g-i) shows NaCl-mucin droplets with 0.6 g/L mucin.

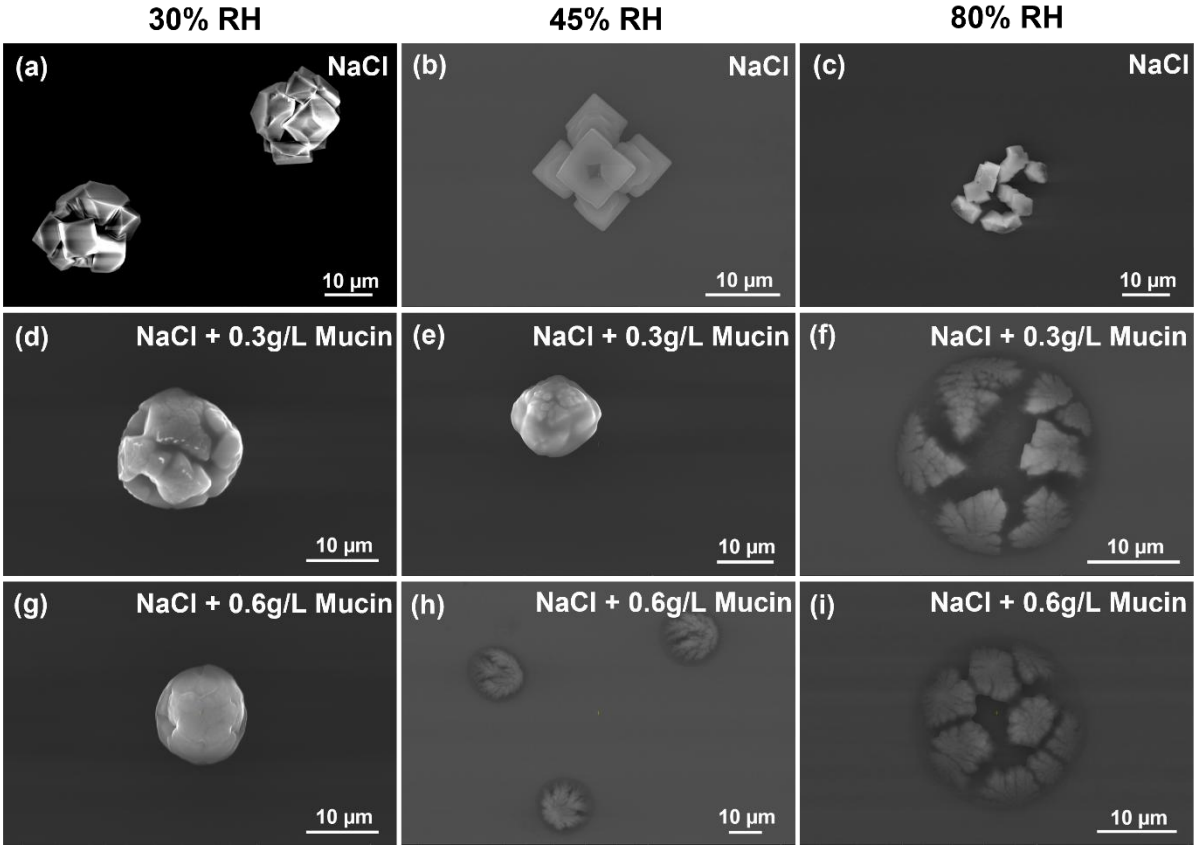

Figure 27. SEM images of NaCl particles, 0.3 g/L mucin-NaCl particles, and 0.6 g/L mucin-NaCl particles formed through evaporation and collected from EDB after they reached the equilibrium state under 30% RH, 45% RH, and 80% RH conditions.

Crystallization occurs when the RH drops below the ERH of NaCl, which ranges from 45% - 48% (Ahn et al., 2010; Li et al., 2014). However, the morphology of NaCl crystalline residues varies with RH. At 30% RH (Figure 27(a)), multiple nucleation sites are present, where smaller cubic crystals aggregate into a larger, compact cluster. At 45% RH (Figure 27(b)), fewer but larger NaCl crystals are formed, indicating that the rate of evaporation significantly influences the crystallization behavior of NaCl. Under dry conditions (30% RH), where the evaporation rate is high, water rapidly evaporates, leading to a sharp increase in NaCl concentration. As a result, supersaturation is reached abruptly, prompting rapid nucleation at multiple sites and the formation of numerous small crystals. In contrast, at intermediate RH (e.g., 45%), the slower evaporation rate allows supersaturation to be reached more gradually. This provides sufficient time for ions to redistribute within the droplet, resulting in fewer nucleation events and the growth of larger, well-defined crystals. This aligns with the findings of Hardy et al. (2023), who investigated the relationship between the drying rate of NaCl droplets and their final morphology. They reported that dried NaCl particles consisted of a collection of reproducible crystal shapes, with faster evaporation rates producing a greater number of smaller crystals.

At 80% RH (Figure 27(c)), the NaCl crystals appear smaller and more loosely distributed, because the droplet remained in a liquid state when equilibrium was reached in the trap, but upon collection, it was immediately exposed to very dry conditions (< 2% RH), which induced rapid crystallization on the Si-wafer surface. Consequently, small crystals (≤ 5 μm in diameter) formed during this post-collection drying process.

The addition of 0.3 g/L and 0.6 g/L mucin results in irregular structure under dry conditions (30% RH), with a notably thicker viscous mucin layer observed on the surface of 0.6 g/L mucin-NaCl droplet. At 45% RH, the droplet containing 0.3 g/L mucin (Figure 27(e)) still exhibits a solid state with crystalline features, indicating that the NaCl crystallized in the levitated droplet. The edges, however, appear more rounded compared to those collected at 30% RH. In contrast, droplets with 0.6 g/L mucin at 45% RH (Figure 27(h)) show a semi-liquid state, evidenced by their flattened “pancake” morphology and the presence of a dark surrounding area, which corresponds to the footprint of a liquid droplet upon deposition on the Si-wafer. This observation suggests that mucin at a concentration of 0.6 g/L influences the crystallization of NaCl, and also support the previous statement that mucin in higher concentrations can enhance water retention within droplets. However, this effect is not evident at the lower concentration of 0.3 g/L, and this will be further discussed in Section 3.2.3. At 80% RH, both 0.3 g/L and 0.6 g/L mucin-containing droplets (Figure 27(f) and (i)) remain in the liquid state at equilibrium.

3.2.3 Efflorescence and deliquescence behavior of levitated NaCl-mucin droplets

As discussed in Section 3.2.2, different mass fractions of mucin result in different droplet phase state and morphology, even under identical RH conditions. This indicates that mucin may play a significant role in influencing phase transitions and salt crystallization. To gain a deeper understanding of how mucin influences phase transitions in droplets, the rehydration and dehydration behaviors of levitated NaCl-mucin droplets containing different mucin concentrations were investigated across a wide range of RH conditions. The experimental details are described in Section 2.4.2.

The rehydration and dehydration curves of representative droplets containing different mass fraction of mucin (X_{mucin} = 0, 0.1, 0.2, 0.3, 0.362, 0.532, 0.7, 0.85 and 1) are shown in Figure 28. Each plot shows the droplet growth factor (GF) as a function of RH, with black data points representing rehydration and red data points representing dehydration. The red dashed line marks the RH at which efflorescence occurs, and the black dashed line marks the RH at which deliquescence occurs. The onset of the efflorescence and deliquescence was determined from changes in the light scattering patterns, as described in Section 2.4.2, where example images of light scattering patterns are provided.

Here, the growth factor (GF) was defined as $GF = R/R_{dme}$, where R is the droplet radius at a given RH and R_{dme} is the dry mass-equivalent radius, calculated from the theoretical dry mass of the droplet. This definition was chosen because droplets undergo severe deformation during evaporation, especially albumin-containing droplets (discussed in Section 3.3), making it difficult to determine their size reliably under dry conditions. By using the mass-equivalent radius as the reference, the GF of both mucin-containing and albumin-containing droplets can be compared consistently.

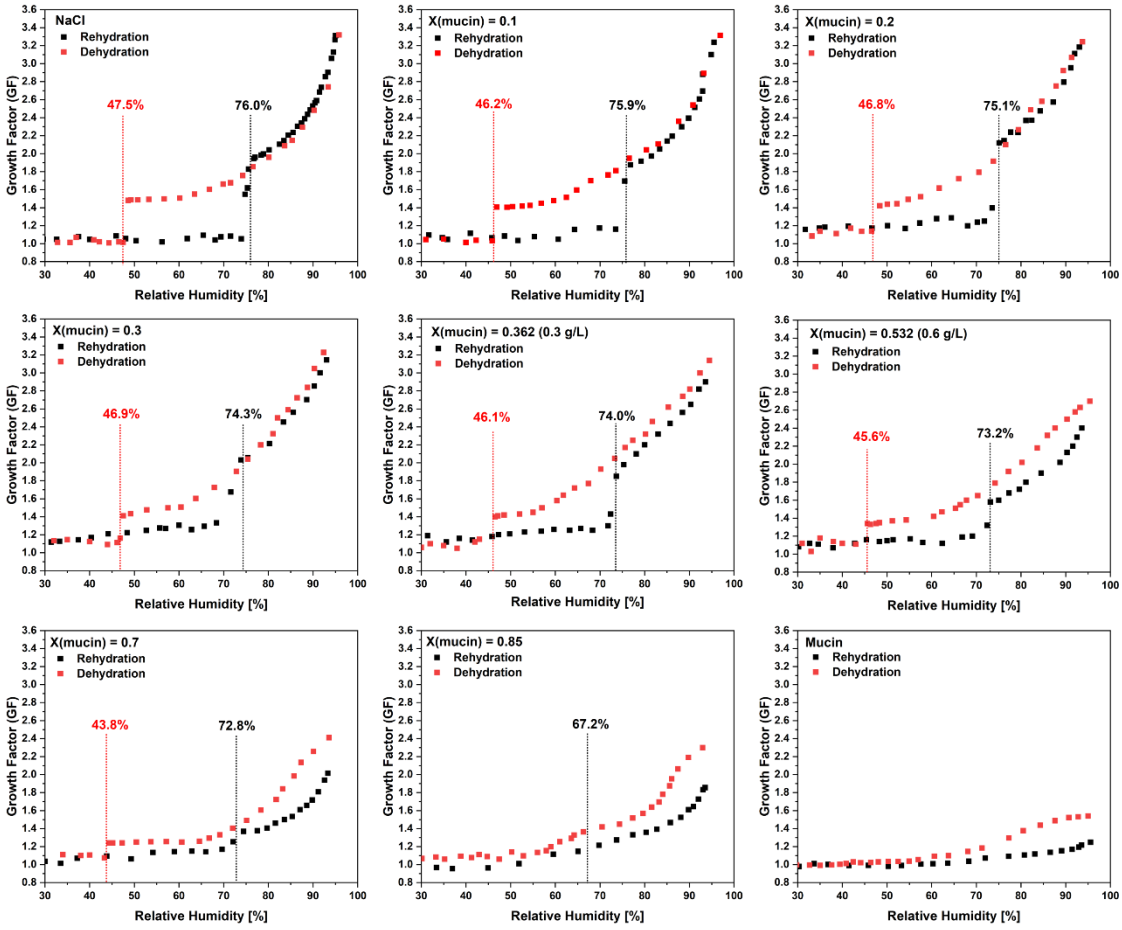

Figure 28. Rehydration and dehydration curves of representative droplets containing varying mass fraction of mucin, ranging from X_{mucin} = 0 (pure NaCl) to X_{mucin} = 1 (pure mucin). The black curves represent the rehydration process, while the red curves represent the dehydration process. Each data point corresponds to the growth factor (GF) of the droplet under the respective RH conditions. The black vertical dashed line indicates the deliquescence RH (DRH) of the droplet, and the red vertical dashed line marks the efflorescence RH (ERH).

For droplets composed entirely of NaCl, a sharp deliquescence jump in the GF is observed at 76% RH, and efflorescence occurs at 47.5% RH, indicating a clear phase transition between solid and liquid states. As the mucin mass fraction increases, these phase transitions become less pronounced. The deliquescence and efflorescence RH values shift slightly, and the discontinuities in the curves become more gradual, suggesting increasing suppression of crystallization. At higher mucin content, X_{mucin} = 0.7 and 0.85, the phase transitions become less distinct. In particular, for X_{mucin} = 0.85, no obvious efflorescence point reflected by the sudden change in droplet size can be identified. This indicates that droplet behavior is strongly influenced by high mucin concentrations. In the case of pure mucin, no sharp phase transitions are observed, and the growth factor changes smoothly with RH, reflecting a continuous

hygroscopic behavior. These findings highlight the critical role of mucin in modulating the water uptake and phase behavior of respiratory droplets.

Under the identical humid conditions (95% RH), droplet hygroscopicity varies across different mucin mass fractions. For pure NaCl droplets, the rehydration and dehydration GFs converge closely at 95% RH, indicating a reversible process between water uptake and water loss. At low mucin content (X_{mucin} = 0.1-0.2), the presence of mucin does not significantly affect the overall water uptake behavior, as the GFs remain comparable during both hydration cycles. However, at moderate mucin content (X_{mucin} = 0.3-0.362), the rehydration GFs are slightly lower than the dehydration GFs after the droplet has passed deliquescence RH, suggesting mucin-induced suppression of water uptake by the droplet. This disparity becomes more pronounced at higher mucin contents (X_{mucin} = 0.532-0.85), where the rehydration GFs are consistently lower than the dehydration GFs throughout the entire deliquescence process. Such behavior indicates a suppression effect caused by the mucin at high concentrations, potentially due to hindered water diffusion during rehydration or enhanced water retention during dehydration via mucin-water binding interactions. In addition, as shown in the SEM images in Figure 25, a high mass fraction of mucin leads to the formation of a dense mucin network on the droplet surface under dry conditions. During rehydration, this surface structure may act as a physical barrier, limiting water uptake. Organic compounds have received significant attention due to their ability to alter the physicochemical properties of inorganic aerosols (Huynh et al., 2022; Mikhailov et al., 2004; Richards et al., 2020). It is often assumed that organic-inorganic mixture particles undergo phase separation into a “core-shell” morphology, with an organic shell encasing an inorganic crystalline core (Harmon et al., 2010). The presence of this organic shell may reduce the degree of water uptake and modify the deliquescence RH of the inorganic component. For example, Choi and Chan (2002) investigated the effects of five different organic species on the water uptake behavior of NaCl using an EDB and found that the growth factors of organic-inorganic mixtures were lower than those of pure inorganic particles.

Figure 29 provides an overview of how mucin influences the crystallization and hygroscopic phase transitions of NaCl in NaCl-mucin droplets. Figure 29(a) shows the ERH as a function of mucin mass fraction. In this study, the ERH was obtained at the RH at which the light scattering patterns of levitated droplets suddenly became irregular, indicating a phase transition. The ERH of pure NaCl droplets served as a baseline for evaluating the influence of mucin on droplet phase behavior. Based on measurements from 20 individual NaCl droplets, the ERH is determined to be 47.5% with a statistical standard deviation (SD) of ± 0.2%. However, when

the accuracy of the RH control system (± 1.5%) is taken into account, error propagation gives an overall uncertainty of ± 1.5%. This value is consistent with previously reported ERH values for NaCl of 45-48% (Ahn et al., 2010; Li et al., 2014). For droplets with low mucin content (X_{mucin} = 0.1-0.2), the ERH does not differ significantly from that of pure NaCl, suggesting that NaCl continues to dominate the phase behavior in these systems. This observation is consistent with findings by Huynh et al. (2022), who investigated model respiratory droplets containing NaCl and mucin at a 10:1 mass ratio and reported that the phase behavior of respiratory droplets with a low-protein content is similar to the characteristic efflorescence behavior of NaCl. As the mucin content increases, the efflorescence is delayed, reflected by a reduction in the ERH. A pronounced decrease in ERH is observed when the mucin mass fraction (X_{mucin}) increases beyond 0.5, with ERH = 45.6 (± 0.2 SD) % at X_{mucin} = 0.532 (0.6 g/L mucin), and ERH = 43.5 (± 0.3 SD) % at X_{mucin} = 0.7, the quoted uncertainties represent statistical standard deviations. Similar findings were reported by Gao et al. (2008), who studied the effects of organics on the ERH of NaCl particles and found that the water-soluble organics could significantly suppress salt crystallization, with ERH reductions of over 30% RH when the organic mole fraction exceeded 0.5. In this study, the suppression of ERH caused by mucin can be attributed to the several mechanisms:

(1) Kinetic inhibition of crystallization: As water evaporates, mucin increases droplet viscosity. This reduced molecular mobility slows down ion diffusion, making it more difficult for Na^+ and Cl^- ions to aggregate into a crystal. Balabushevich et al. (2018) reported that a large number of physical entanglements stabilized by covalent and noncovalent interactions, such as electrostatic, hydrogen bonding, or other specific binding interactions, are present in the mucus layer. These interactions enhance the viscoelasticity of the mucin and form a mesh network filter that reduces the rates at which molecules and particles diffuse and penetrate. As a result, crystallization is delayed until a lower RH is reached, reducing the observed ERH.

(2) Hydrophilic nature of mucin: Mucin can retain water due to its hydrophilicity (Ushida and Murata 2013), as discussed in Section 3.2.1. This water-retaining property allows mucin to bind more water and helps maintain a locally higher humidity within the droplet. Consequently, even if the surrounding RH falls to the ERH of pure NaCl (47.5 ± 0.2 %), the water activity within droplets may still be too high to trigger crystallization, thereby delaying efflorescence to lower environmental RH.

(3) Entrapment of NaCl in confined mucin pockets: Mucin may encapsulate regions of aqueous NaCl solution, restricting the spatial freedom required for crystal nucleation and prolonging the

supersaturated state of the droplet. Seyfert et al. (2022) studied the morphology and structure of dried droplets containing NaCl and mucin on an omniphobic substrate, i.e., a surface engineered to repel both water and oil-based liquids. They reported that the addition of mucin produced structures with a large void fraction that offered potential pockets, potentially acting as confinement zones for dissolved salts.

Additionally, droplets with X_{mucin} = 0.85 were tested. However, no efflorescence can be observed because the light scattering patterns became gradually irregular without exhibiting any sudden change. This suggests a transition from salt-dominant to mucin-dominant droplet behavior at high mucin concentrations.

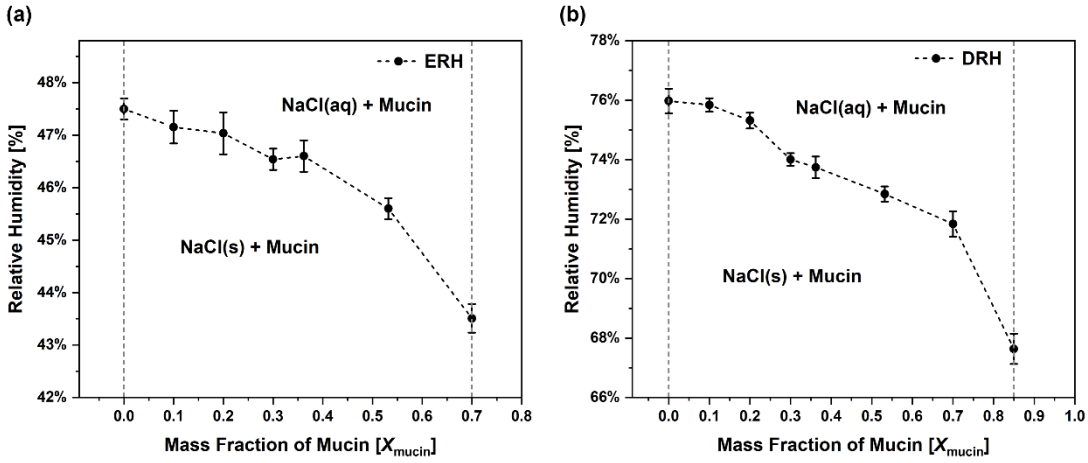

Figure 29. (a) Efflorescence relative humidity (ERH) and (b) deliquescence relative humidity (DRH) of droplets containing NaCl with varying mass fraction of mucin (X_{mucin}). Each data point represents the average ERH and DRH values, with error bars indicating the standard deviations (SD) obtained from 20 individual measurements.

Figure 29(b) shows the DRH as a function of mucin mass fraction. The DRH was determined as the RH at which the light scattering patterns of levitated droplets suddenly became regular again, characterized by the appearance of vertical straight stripes that indicate the droplets have become spherical and homogeneous. On the basis of 20 individual NaCl droplets data, the obtained DRH of NaCl in this study is 76.0 (± 0.4 SD) %, which aligns well with reported values (75-76%) from previous studies (Ahn et al., 2010; Alshawa et al., 2009).

As the mucin mass fraction (X_{mucin}) increases, the DRH gradually decreases, from 76.0 (± 0.4 SD) % for pure NaCl to 67.6 (± 0.5 SD) % at X_{mucin} = 0.85. This trend indicates that mucin promotes the deliquescence of NaCl, with a particularly notable drop in DRH when X_{mucin}

exceeds 0.7. This suggests a threshold concentration beyond which mucin begins to significantly influence and dominate the droplet deliquescent behavior.

One possible explanation for the observed decrease in DRH with increasing mucin content is the interactions between mucin and NaCl. Mucin is known to behave as a polyelectrolyte due to its polymeric network of charged sugar groups (oligosaccharides), primarily carboxyl and sulfate groups, which can dissociate in aqueous environments (Du et al., 2021; Nystrom et al., 2010). This dissociation imparts a net negative charge to mucin, characteristic of polyelectrolyte behavior. The reduction in DRH in the presence of mucin is consistent with the theoretical prediction by Wexler and Seinfeld (1991), who proposed that the DRH of an electrolyte can be lowered by the addition of a second electrolyte. Mechanistically, this effect arises because the second electrolyte lower the total water activity in the system, which shift the equilibrium between the solid and dissolved phases toward dissolution at lower RH. Even though mucin is a macromolecular polyelectrolyte rather than a small inorganic salt, its dissociated functional groups contribute to the ionic strength of the droplet solution, thereby lowering the equilibrium water activity and effectively lowering the DRH of NaCl.

To further elucidate mucin's water-uptake behavior, water-cycle experiments were performed on pure mucin droplets (0.6 g/L), as shown in Figure 30. A total of 50 pure mucin droplets were tested and a representative case is presented here. The levitated droplet was first dried at 20% RH and held at equilibrium for 3 minutes. The RH was then increased from 20% to approximately 95% by setting the final RH and allowing the system to equilibrate. The RH increase was not an instantaneous jump but a gradual adjustment, during which light scattering patterns were recorded at one-second intervals.

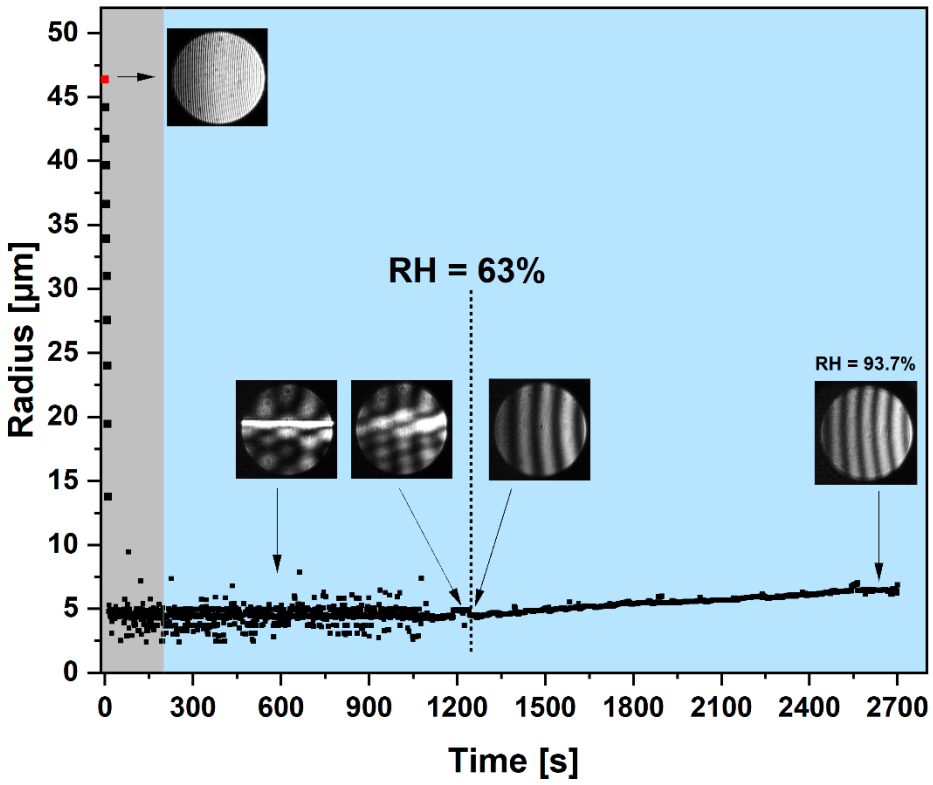

Figure 30. Evaporation and subsequent rehydration behavior of a representative pure mucin droplet. The grey-shaded region represents the evaporation process at 20% RH. The blue-shaded region represents the rehydration process, where the RH is gradually increased. Light scattering patterns captured at selected time points illustrate the shape and phase changes throughout the drying and water uptake processes. The vertical black dashed line marks a notable transition near RH = 63.0%. The red dot in the figure at the beginning represents the first second of droplet evaporation, and the corresponding light scattering pattern is shown next to it.

During the evaporation phase, the droplet radius decreases from approximately 47 µm to 5 µm, indicating significant water loss. At equilibrium, a bright horizontal stripe in the light scattering patterns is observed again, indicating a "tail-like" structure of dried mucin droplet as previously discussed in Figure 25 (Section 3.2.2). During the rehydration phase, this horizontal stripe gradually widens and becomes increasingly diffuse, with its sharp edges fading, suggesting the progressive breakdown of the "tail" structure as the droplet absorbs water.

A notable transition occurred at RH = 63.0%, where the bright horizontal stripe disappears and regular vertical stripes reappear in the light scattering patterns. This shift indicates that the mucin droplet has absorbed sufficient water to undergo a morphological transition from an

irregular, heterogeneous structure to a more homogeneous and spherical state. As RH continues to increase beyond this point, the droplet radius grows slowly and continuously, reflecting the steady and limited water uptake behavior of mucin. Unlike inorganic salts such as NaCl, which exhibit a sharp deliquescence jump at a specific RH, mucin demonstrates a gradual and continuous rehydration process, consistent with its hygroscopic nature.

Mucin modifies the phase behavior of NaCl-mucin droplets by promoting water retention and enhancing NaCl solubilization under humid conditions. In NaCl-mucin droplets, particularly those with high mucin content, mucin enables greater water retention even at relatively low RH, resulting in a lower ERH. During rehydration, mucin begins to absorb water at an early stage, and this absorbed water may effectively serve as a solvent reservoir, facilitating the early NaCl dissolution. This mechanism provides an additional explanation for the observed decrease in DRH of NaCl with increasing mucin content.

3.2.4 Conclusions

In this Section, the role of mucin in modulating the physicochemical behavior of NaCl-mucin model respiratory droplets was investigated under varying RH conditions. Mucin, the major glycoprotein in respiratory fluids, not only influences the evaporation kinetics of droplets under humid conditions but also strongly affects the thermodynamic endpoint and final morphology of dried particles. Under dry conditions, mucin tends to migrate toward the droplet surface during evaporation, forming a viscous, semi-permeable, elastic, gel-like layer. This surface layer facilitates greater water retention at equilibrium, with higher mucin content corresponding to increased water retention within the droplet.

Mucin itself behaves as a hygroscopic substance, gradually absorbing water as RH increases but without exhibiting a sharp deliquescence transition like crystalline salts. As RH increases, dried mucin particles gradually absorb water, soften and grow in size continuously, even at relatively low RH, yet they do not fully transition to a liquid state even near 95% RH. As a result, the presence of mucin reduces the overall hygroscopicity NaCl-mucin droplets, with higher mucin content leading to lower growth factors. Moreover, as mucin concentration increases, both the ERH and DRH of NaCl in NaCl-mucin droplets decrease, indicating a transition from NaCl-dominated to mucin-governed hygroscopic behavior.

Given the variability in mucin content among individuals and the dynamic environmental conditions encountered during airborne transmission, these findings provide fundamental insights into the role of mucin in determining droplet behavior. They also underscore the need

to account for compositional complexity, particularly the presence of mucin and other proteins, when modeling the physicochemical dynamics of respiratory droplets in real-world settings.

3.3 Measurements of simplified model respiratory droplets: NaCl-albumin droplets

Unlike mucin, albumin is a smaller, globular protein found in lower quantities in saliva but is abundant in the deep lung fluid (Larsson et al., 2012). It is often used as a model protein due to its well-defined physicochemical properties and ease of handling in experiments. In this thesis, NaCl-albumin droplets were employed as a second simplified yet biologically relevant model respiratory system, representing and capturing key physicochemical characteristics of exhaled droplets originating from the lower respiratory tract. To enable direct comparison with NaCl-mucin droplets, all experimental conditions and tested albumin concentrations were kept consistent with those used in the NaCl-mucin experiments described in Section 3.2.

This section aims to investigate the influence of albumin on the physicochemical properties of model respiratory droplets. The effects of albumin are examined from the aspects of evaporation kinetics, particle morphology, phase transitions, rehydration process, and efflorescence and deliquescence behavior of NaCl in NaCl-albumin droplets. A deeper exploration of how albumin alters the physicochemical properties of droplets during evaporation and rehydration can provide valuable insight into its potential role in modulating pathogen survival in exhaled respiratory droplets. Furthermore, comparison between the effects of mucin and albumin elucidates how different proteins in respiratory fluids govern droplet behavior under varying environmental conditions. This is critical for improving predictive models of respiratory droplet dynamics and for assessing the risks associated with airborne transmission of infectious diseases.

The following sections present investigations of:

1. Evaporation behavior of NaCl-albumin droplets containing different albumin concentrations under varying RH conditions, including a comparison between NaCl-albumin and NaCl-mucin droplets.
2. Morphology and shape evolution of NaCl-albumin droplets during evaporation.
3. Hygroscopic growth behavior of NaCl-albumin droplets and their comparison with NaCl-mucin droplets.

4. Efflorescence and deliquescence behavior of NaCl in NaCl-albumin droplets during dehydration and rehydration.

3.3.1 Evaporation behavior of levitated NaCl-albumin droplets

The evaporation behavior of levitated NaCl-albumin droplets containing different concentrations of albumin (0 g/L (pure NaCl), 0.3 g/L and 0.6 g/L) was investigated at a constant temperature of (17.8 ± 0.3) °C under low (30%) and high (80%) RH conditions, as shown in Figure 31. A total of 20 droplets were examined for each composition, with representative examples presented in the figure. The evaporation kinetics of the pure NaCl droplets, modeled using the SADKAT, are indicated by the black dotted line. The close agreement between the experimental data for the pure NaCl droplet and the SADKAT model under both RH conditions confirms the accuracy and reliability of the experimental measurements.

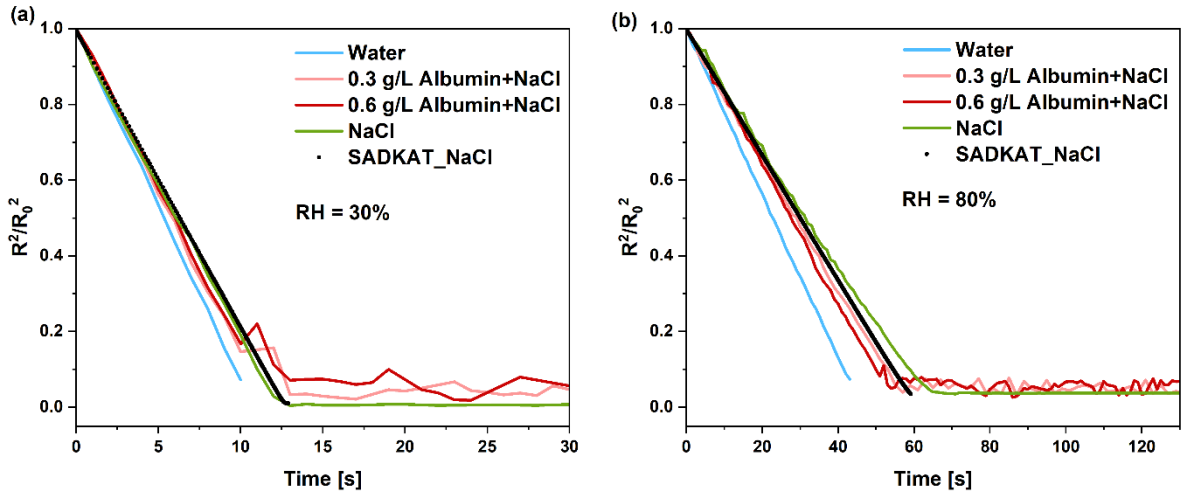

Figure 31. Normalized squared radius as a function of time for water, NaCl, and NaCl-albumin droplets at two different RH conditions: (a) 30% RH and (b) 80% RH. Evaporation of an aqueous NaCl droplet modeled by SADKAT is shown in black dotted line.

At 30% RH, during the early stage of the evaporation process, the evaporation behavior of droplets is similar to that of pure water droplets, showing a linear decrease trend. As evaporation progresses into the middle stage, difference in the droplet evaporation behavior can be observed. Compared to the pure water droplet, the evaporation rates of both aqueous NaCl and NaCl-albumin droplets slow down. However, it is noteworthy that the NaCl-albumin droplets exhibit a slightly faster evaporation rate than the aqueous NaCl droplet. Similar findings were reported

by Lin et al. (2020), who investigated the evaporation rate of 1-µL droplets with different chemical compositions (NaCl, sodium dodecyl sulfate (SDS) and BSA) at 20%, 50% and 80% RH. They observed that BSA droplets (1 g/L) generally evaporated faster than NaCl and SDS droplets under 20% and 50% RH conditions.

In the late stage of the evaporation at 30% RH, droplets containing albumin exhibit a distinct "jump and fall" behavior in apparent size. The term "apparent size" is used here because this "jump and fall" behavior does not reflect the real physical size changes but instead arise from distortions in the light scattering patterns as the droplet loses its spherical structure and undergoes morphological deformation.

Although the scattering patterns become irregular, size determination remains possible because the analysis is based on the average peak distance, which can still be extracted even from disturbed patterns (see Section 2.3.5). Moreover, as the deformed droplet rotates in the trap, the scattering patterns intermittently capture orientations that preserve recognizable features, allowing reliable tracking of size evolution. This explains the significant fluctuations observed in the normalized squared radius shown in Figure 31. This phenomenon is further explored in Section 3.3.2.

At 80% RH, droplet evaporation proceeds more slowly compared to the dry conditions. NaCl-albumin droplets still show a slightly higher evaporation rate than the pure NaCl droplet. However, the sudden size distortion observed in the later stage is less prominent under this higher humidity. When comparing NaCl-albumin droplets containing 0.6 g/L and 0.3 g/L albumin, the higher-concentration sample (0.6 g/L) exhibits morphological disturbances earlier than the lower-concentration sample (0.3 g/L). This suggests that the effect of albumin on droplet morphology during evaporation is concentration-dependent.

Figure 32 further supports this conclusion by showing the light scattering patterns recorded over ten consecutive seconds after equilibrium was reached at 80% RH. In the case of pure NaCl droplet (top row), the light scattering patterns remain sharp and regularly spaced, indicating a stable spherical shape and homogenous internal structure. The NaCl + 0.3 g/L albumin droplet (middle row) shows visible disturbances and wiggles in the scattering patterns, implying minor changes in the droplet's structure and internal heterogeneities introduced by albumin. This indicates that albumin begins to influence droplet behavior but is not yet dominant. In contrast, the NaCl + 0.6 g/L albumin droplet (bottom row) displays significant disruption in the light scattering patterns. The stripes become irregular, distorted, or even disappear over time, indicating a loss of spherical shape and/or increasing internal complexity.

The morphology of droplets collected from EDB at their equilibrium state is further discussed in Section 3.3.2. These results highlight the strong influence of albumin at higher concentrations on both evaporation kinetics and morphology of droplets.

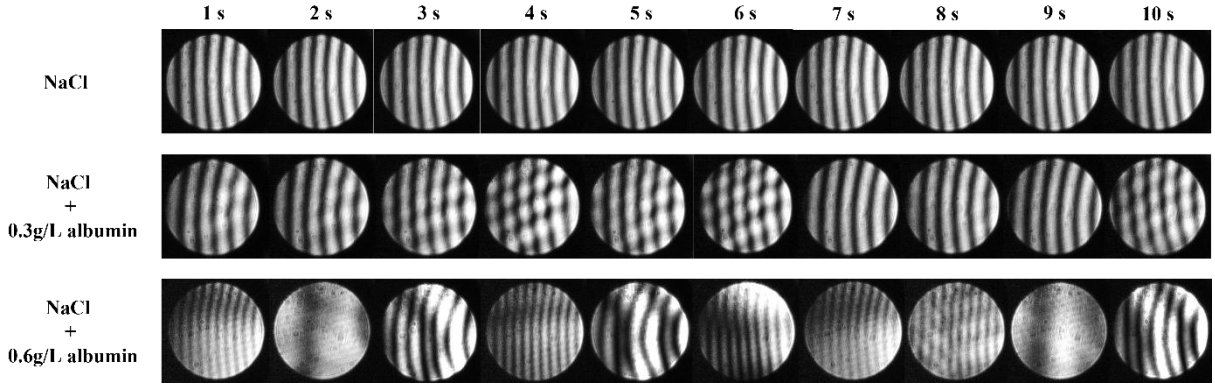

Figure 32. Time-resolved light scattering patterns of levitated droplets: pure NaCl (top row), NaCl + 0.3 g/L albumin (middle row), and NaCl + 0.6 g/L albumin (bottom row) at their equilibrium state under 80% RH conditions. Each image shows the droplet at 1-second intervals from 1 to 10 seconds at their equilibrium.

A possible explanation for the accelerated evaporation observed in NaCl-albumin droplets compared to aqueous NaCl droplets is the role of albumin in lowering surface tension at the air-liquid interface. The addition of NaCl to water increases surface tension (Zhang and Carloni, 2012). For example, adding 1 M NaCl into water can increase the surface tension of water to approximately 74.05 mN/m at 23 °C, compared to around 72.5 mN/m for pure water (Ozdemir et al., 2009). This is because the ions (Na^+ and Cl^-) in NaCl interact more strongly with water molecules than water molecules interact with each other, thereby enhancing cohesive forces at the droplet surface. As a result, NaCl droplets exhibit a lower evaporation rate than pure water droplets under the same conditions. Conversely, albumin acts as a surface-active agent. When dissolved in water, it tends to adsorb at the air-water interface, disrupting hydrogen bonding between water molecules and thus lowering the surface tension (Campbell et al., 2015). Absolom et al. (1981) reported that serum albumin, when dissolved in water at concentrations ranging from 0.01% to 5.5% (*w/v*), reduces the surface tension of water from 72.5 mN/m to approximately 50 mN/m. Therefore, in NaCl-albumin droplets, water molecules are held less tightly at the interface, making it easier for them to escape into the vapor phase. This reduced surface tension likely contributes to the slightly faster evaporation rate observed in the presence of albumin compared to pure NaCl droplets.

To clearly distinguish the effects of varying albumin mass fractions on droplet evaporation, the evaporation behavior of NaCl-albumin droplets with low ($X_{albumin}$ = 0.1) and high ($X_{albumin}$ = 0.85) albumin content under 30% RH conditions was investigated. As shown in Figure 33, five independently tested droplets are presented for both low-albumin (blue) and high-albumin (red) conditions, and their evaporation profiles are compared with those of pure water and pure NaCl droplets under identical conditions. As expected, the pure water droplet exhibits the fastest evaporation due to the absence of solutes. In contrast, the pure NaCl droplet evaporates more slowly as the dissolved salt lowers water activity, thereby suppressing the evaporation rate. When a low concentration of albumin ($X_{albumin}$ = 0.1) is added, the evaporation behavior remains nearly identical to that of pure NaCl droplets, indicating that at this mass fraction, albumin has a minimal impact on evaporation kinetics. NaCl continues to dominate the droplet's physicochemical behavior by influencing both water activity and surface tension. However, at a higher albumin concentration ($X_{albumin}$ = 0.85), the evaporation rate increases relative to both pure NaCl and low-albumin droplets. Additionally, the evaporation curves become more irregular and exhibit greater fluctuations in the later stages of drying. These findings are consistent with observations of Lin et al. (2020), who investigated the evaporation behavior of droplets containing 1g/L NaCl, 0.1 g/L BSA, and 1 g/L BSA under 20%, 50%, and 80% RH conditions. Their results showed that droplets containing BSA evaporated more quickly than pure NaCl droplets, and that droplets with higher BSA concentrations exhibited faster evaporation rates than those with lower BSA content. This similarly supports the conclusion that increased albumin concentration enhances the evaporation rate, likely due to its surface-active properties that modify the interfacial dynamics of the droplet when present in sufficient concentration.

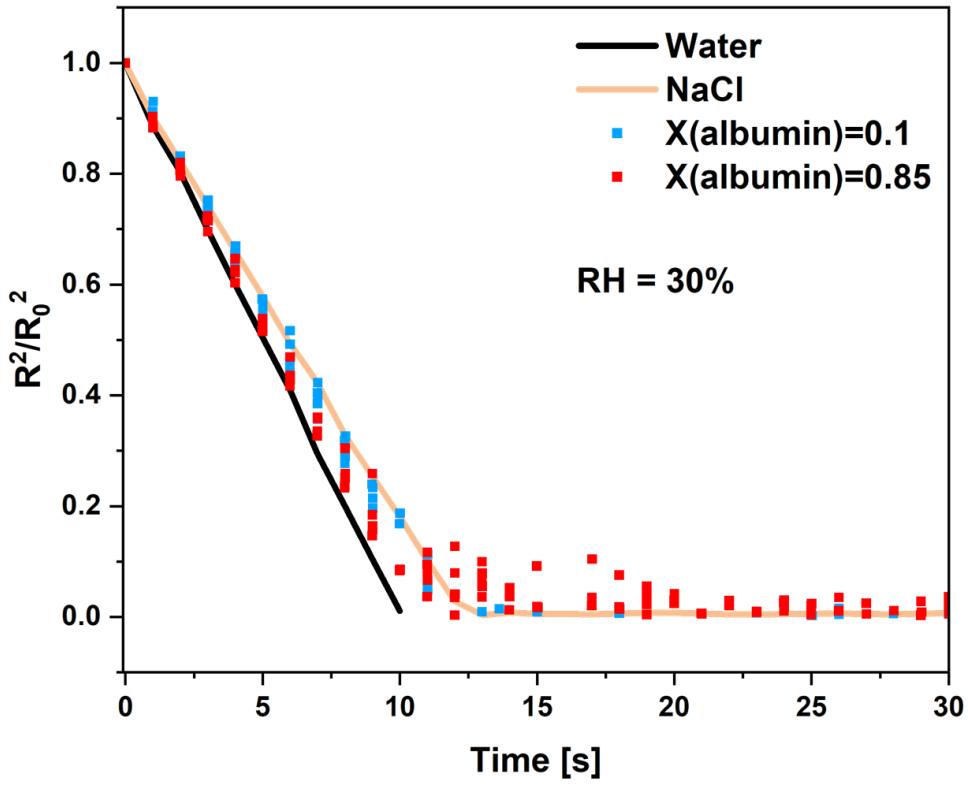

Figure 33. Normalized squared droplet radius (R^2/R_0^2) as a function of time for pure water, NaCl, and NaCl-albumin droplets containing low ($X_{albumin}$ = 0.1) and high ($X_{albumin}$ = 0.85) albumin mass fraction at 30% RH. For both types of NaCl-albumin droplets, five independent measurements are presented for each composition to illustrate experimental variability.

In order to compare the influence of two major respiratory proteins, mucin and albumin, on droplet evaporation behavior. NaCl droplets containing equal concentrations of each protein (0.6 g/L) were tested under a range of RH conditions: very dry (5% RH), dry (30% RH), moderate (45% RH), and humid (80%). This allows us to assess how environmental conditions and protein type affect droplet evaporation behavior, as illustrated in Figure 34. For each protein type and RH condition, 20 droplets were tested, and representative droplets are shown in the figure to capture the typical behavior observed.

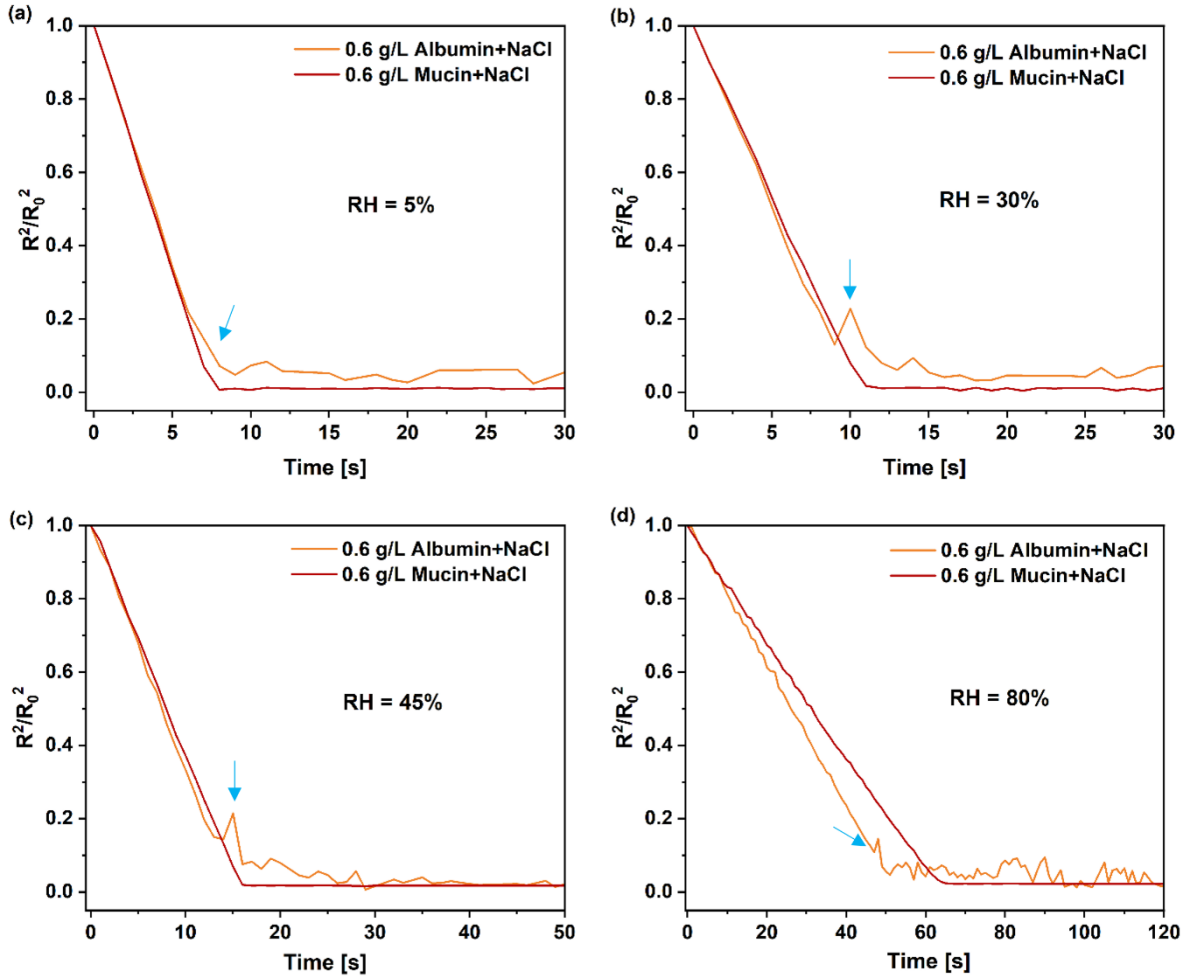

Figure 34. Normalized squared droplet radius (R^2/R_0^2) as a function of time for NaCl-albumin and NaCl-mucin droplets with equal protein concentrations (0.6 g/L) under varying RH conditions: (a) 5% RH, (b) 30% RH, (c) 45% RH, and (d) 80% RH. The earlier deviation in the NaCl-albumin droplet size evolution is indicated by blue arrows in the figure.

At very low humidity (5% RH, Figure 34(a)), both NaCl-mucin and NaCl-albumin droplets exhibit rapid evaporation with nearly identical profiles, indicating that under extremely dry conditions, the influence of either protein on evaporation kinetics is minimal and the evaporation process is primarily driven by the low ambient humidity. As the RH increases to 30% RH (Figure 34(b)), the evaporation curves for both droplets still nearly overlap during the initial stage, but subtle differences begin to emerge later. The NaCl-mucin droplet exhibits a slightly slower evaporation rate in the later stage. As previously discussed in Section 3.2.1 (Figure 23), the evaporation behavior of the 0.6 g/L mucin + NaCl droplet closely resembles that of a pure NaCl droplet, suggesting that the formation of the viscous, semi-permeable, gel-like mucin layer does not significantly influence droplet evaporation at this RH. The slightly faster evaporation of the NaCl-albumin droplet may be attributed to the presence of albumin,

which, as discussed earlier, can lower surface tension and thereby enhance evaporation. A similar trend is seen at 45% RH (Figure 34(c)), with the NaCl-albumin droplet continuing to evaporate slightly faster during the later stages. This effect becomes more pronounced at 80% RH (Figure 34(d)), where the NaCl-mucin droplet shows a noticeably slower evaporation rate than the NaCl-albumin droplet. As discussed in Figure 23 (Section 3.2.1), the evaporation of NaCl-mucin droplet is slower than that of the pure NaCl droplet at 80% RH, indicating that mucin begins to exert a more pronounced effect on droplet evaporation under high humidity conditions, even when the droplets remain in the liquid state at equilibrium without the formation of a semi-permeable, solid/semi-solid mucin layer. The observed difference in evaporation rates between NaCl-mucin and NaCl-albumin droplets can be attributed to two factors: (1) albumin accelerates evaporation by reducing droplet surface tension, and (2) mucin slows down evaporation via stronger mucin-water binding interactions, especially under humid conditions. These findings suggest that both mucin and albumin modulate droplet evaporation in a humidity-dependent manner, with their effects becoming more significant at moderate to high RH levels.

Interestingly, NaCl-albumin droplets consistently exhibit an earlier deviation in droplet apparent size evolution, as reflected by the "jump" in the normalized squared radius (R^2/R_0^2) in Figure 34 (highlighted by blue arrows), regardless of the RH conditions. This is observed using the light scattering patterns, which provide insight into the structural and morphological changes of droplets during evaporation. These scattering patterns provide visual evidence of the droplet's phase state and internal homogeneity at equilibrium, both of which are influenced by protein type and RH in this case. For NaCl-albumin droplets, as water evaporates, albumin may rapidly accumulate at the air-liquid interface, increasing surface roughness and initiating early disruption in droplet uniformity. Previous studies have shown that both mucin and albumin tend to aggregate under stress conditions, such as drying or increased ionic strength in solution (Bansil and Turner, 2006; Brahma et al., 2005; Weston et al., 2023). Our findings suggest that albumin aggregates more readily than mucin under these conditions, contributing to earlier morphological instability.

Figure 35 shows representative light scattering patterns of both droplet types at equilibrium under various RH conditions. While the scattering patterns change dynamically even at equilibrium, only a representative one-second scattering pattern from the temporal sequence is shown for clarity. Notably, droplets containing two different respiratory proteins exhibit markedly different light scattering patterns at their equilibrium. For NaCl-mucin droplets, the

light scattering patterns under dry conditions (5% and 30% RH) are heavily distorted and lack distinct stripes, indicating substantial deformation and loss of sphericity in shape due to severe water loss and potential onset of crystallization. At 45% RH, however, the scattering patterns still maintain regular and well-spaced stripes, suggesting a homogeneous liquid phase and preserved spherical shape in droplets. Under more humid conditions (80% RH), the scattering patterns remain regular and even exhibit an increased number of stripes, suggesting not only a liquid, spherical state but also a larger equilibrium droplet size due to reduced water loss.

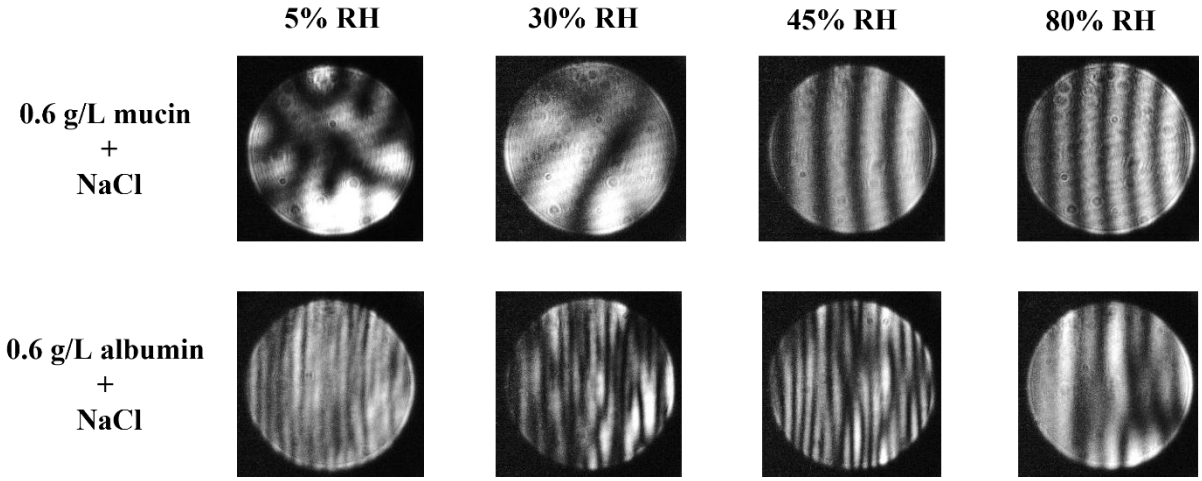

Figure 35. Representative light scattering patterns of 0.6 g/L mucin + NaCl (top row) and 0.6 g/L mucin + NaCl (bottom row) droplets at their equilibrium state under different RH conditions: 5%, 30%, 45%, and 80%.

In contrast, for NaCl-albumin droplets, they consistently exhibit clear distortions and irregular scattering patterns under all RH conditions examined. These disrupted patterns indicates that albumin plays a dominant role in destabilizing droplet morphology at equilibrium, leading to structural collapse and loss of sphericity irrespective of humidity level. These observations highlight the strong impact of protein composition on droplet stability and morphology during evaporation.

The persistent deformation of NaCl-albumin droplets across all RH conditions may be attributed to albumin's inability to form a stabilizing viscoelastic layer like mucin can. Albumin, being a smaller, globular and surface-active protein, may initially migrate to the air-water interface during evaporation but lacks the structural robustness to preserve droplet sphericity as water evaporates. A detailed discussion of droplet morphology at equilibrium is presented in Section 3.3.2.

These findings suggest that while both mucin and albumin impact droplet evaporation and morphology, mucin is more effective in preserving spherical shape of droplets under drying stress, especially at moderate to high RH. In contrast, albumin slightly accelerates evaporation compared with aqueous NaCl droplets, and induces substantial structural deformation. These differences may have implications for droplet rehydration capacity and pathogen encapsulation, which will be further explored in the following sections.

3.3.2 Morphology of NaCl-albumin droplets extracted from the EDB

As discussed in the previous section, evaporation measurements provide insight into the evaporation kinetics and structural deformation of NaCl-albumin droplets. Notably, droplets containing albumin exhibit earlier distortions in light scattering patterns during evaporation compared to those containing mucin. This behavior appears to be independent of RH conditions but strongly dependent on albumin concentration. However, the exact morphology and phase state of albumin-contained droplets at equilibrium, as well as their relationship to albumin concentration, remain unclear.

In order to complement the analysis of evaporation behavior, I further investigated the final morphologies of NaCl-albumin droplets with varying albumin mass fractions (X_{albumin}), ranging from 0 (pure NaCl) to 1 (pure albumin), after reaching equilibrium under 30% RH conditions, as shown in Figure 36. All experimental conditions were consistent with those used for mucin, as described in Section 3.2. The droplet collection procedure has been described in detail in Section 2.5. Briefly, NaCl-albumin droplets were collected 2 minutes after the initial disturbance of the light scattering pattern at 30% RH and immediately transferred for SEM analysis under dry conditions to minimize environmental interference.

Figure 36 presents representative SEM images that capture the phase state of the droplets upon contact with the Si-wafer. For each condition, 10 droplets were collected, and representative images are shown here. Additional SEM images are provided in the Appendix Figure S13.

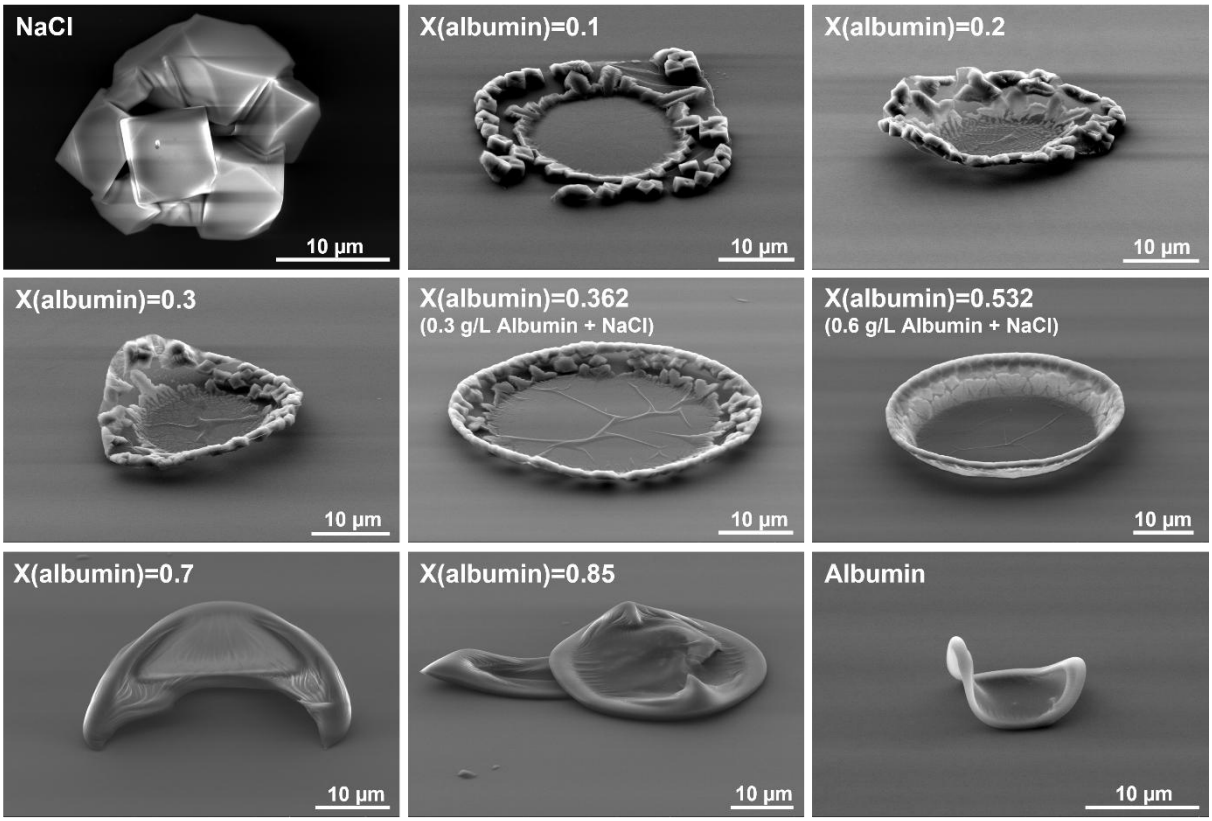

Figure 36. SEM images of representative dried NaCl-albumin droplet residues collected from the EDB after reaching equilibrium under 30% RH conditions. The droplets contain varying mass fractions of albumin ($X_{albumin}$), ranging from 0 (pure NaCl, top left) to 1 (pure albumin, bottom right).

The pure NaCl residue displays characteristic cubic crystals, resulting from the crystallization of NaCl. The addition of albumin significantly alters the morphology of the dried particles. For droplets with low albumin content ($X_{albumin}$ = 0.1), the dried droplet residues collected from the EDB exhibit a distinct bowl-like shape, featuring a smooth, concave center that adheres strongly to the substrate. A thickened edge, 6-8 µm in width, is raised and partially detached from the substrate. NaCl crystals are clearly visible along this edge, indicating solute accumulation at the droplet periphery, which is likely driven by solute migration during evaporation. The bumpy outer rim results from NaCl crystallization at the droplet edge, where the small crystals are dispersed and wrapped in a transparent albumin film. In contrast, the central region lacks visible NaCl crystals and is instead covered by a thin film of albumin.

As the albumin mass fraction increases from $X_{albumin}$ = 0.1 to $X_{albumin}$ = 0.362, the shadow along the droplet periphery highlights the topographical curvature and confirms the bowl-like shape. NaCl crystals remain visible at the elevated edge. Notably, the central region now displays fine,

wrinkle-like patterns, which may result from the increased albumin concentration providing more material for thin film formation during evaporation.

When the albumin content reaches $X_{albumin}$ = 0.532, the droplet still retains a bowl-like shape, however, its morphology begins to transition. The edge become smoother and more continuous, while crystallization features become less distinct, suggesting that albumin plays a progressively dominant role in determining the final morphology.

At higher albumin content, $X_{albumin}$ = 0.7-0.85, the bowl-like shape disappears. The structures become increasingly collapsed and wrinkled, though an albumin film remains in the center. NaCl crystals are no longer visible at the edges, as they are enveloped by a thick, ring-shaped layer of albumin.

At $X_{albumin}$ = 1 (pure albumin), the albumin droplet residue shows a highly deformed morphology characterized by a pronounced rim, curled edges, and smooth surfaces. These features are distinct from typical crystalline residues and indicative of the unique drying behavior of albumin. This morphology suggests the formation of a viscoelastic, hydrogel-like film during evaporation, likely resulting from the gelation of albumin.

Gelation is the process by which a liquid or sol transforms into a gel, a solid-like material characterized by an interconnected molecular network. In the case of globular proteins, such as albumin, this transformation typically involves partial unfolding and subsequent aggregation, which promotes the development of a continuous network as water content decreases (Gosal and Ross-Murphy, 2000). The gelation behavior of globular proteins has been extensively studied (Easa et al., 1996; Ziegler and Foegeding, 1990), and albumin is widely recognized as a key gelling agent in biological and food systems (Boye et al., 1996).

In this study, the evaporation process concentrates albumin within the droplet, promoting intermolecular interactions and network formation. As water continues to evaporate, this network undergoes solidification, resulting in a gel-like structure, as observed in the SEM image. Mikhailov et al. (2004), in their investigation of the hydration and dehydration of NaCl-BSA aerosol particles, similarly reported the formation of a gel-like microstructure containing embedded NaCl crystallites at intermediate RH.

Overall, the transition from well-defined crystalline residues (pure NaCl) to distorted and irregular structure becomes increasingly evident with rising albumin content. Even at lower concentrations, albumin appears to influence final morphology, suggesting its significant role in modulating the physical state of the levitated drying droplet.

Wang et al. (2023) investigated the drying process of sessile droplets containing NaCl and HSA, and reported that the presence of NaCl significantly promote the accumulation of HSA at the peripheral region, as shown in Figure 37. Since this evolution process took place on a substrate, the final morphology closely resembles the structures observed in our SEM images. These findings prompt further questions about the timing of droplet collection: Is it appropriate to collect droplets just two minutes after they reach equilibrium? Could they still be in a liquid or semi-liquid state at that point, and if so, might evaporation continue after collection, thereby leaving a bowl-like shape? Might residual water still be present within the droplet?

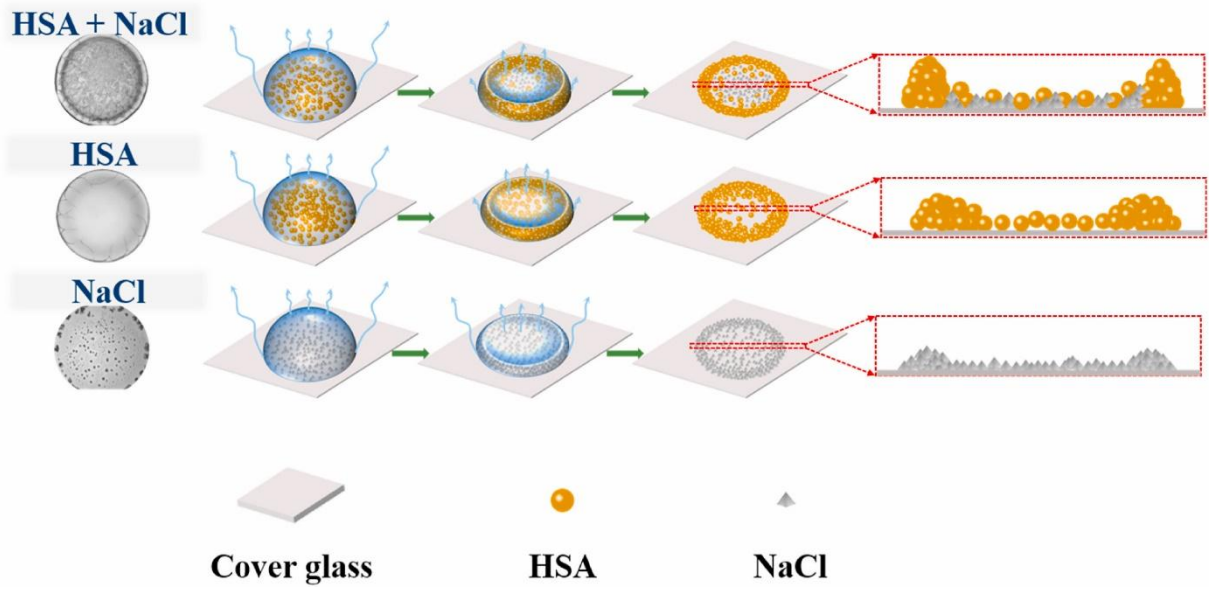

Figure 37. Schematics of drying process of sessile droplets of NaCl-HSA, pure HSA, and NaCl droplets. Figure reproduced from Wang et al., 2023.

To explore these questions, additional experiments were conducted to assess whether droplet morphology changes with extended levitation time. Specifically, I tested 0.6 g/L albumin + NaCl droplets under 30 % RH conditions and increased the levitation time to 30 minutes. Figure 38 shows the comparison between droplets collected at approximately 2 minutes (Figure 38(a-c)) and 30 minutes (Figure 38(d-f)) after reaching equilibrium. They all display a characteristic bowl-like morphology with a thickened peripheral ring and a collapsed central region composed of a thin albumin film. This consistent structure suggests that albumin accumulates at the droplet interface during evaporation and that the morphology stabilizes relatively early in the equilibrium phase.

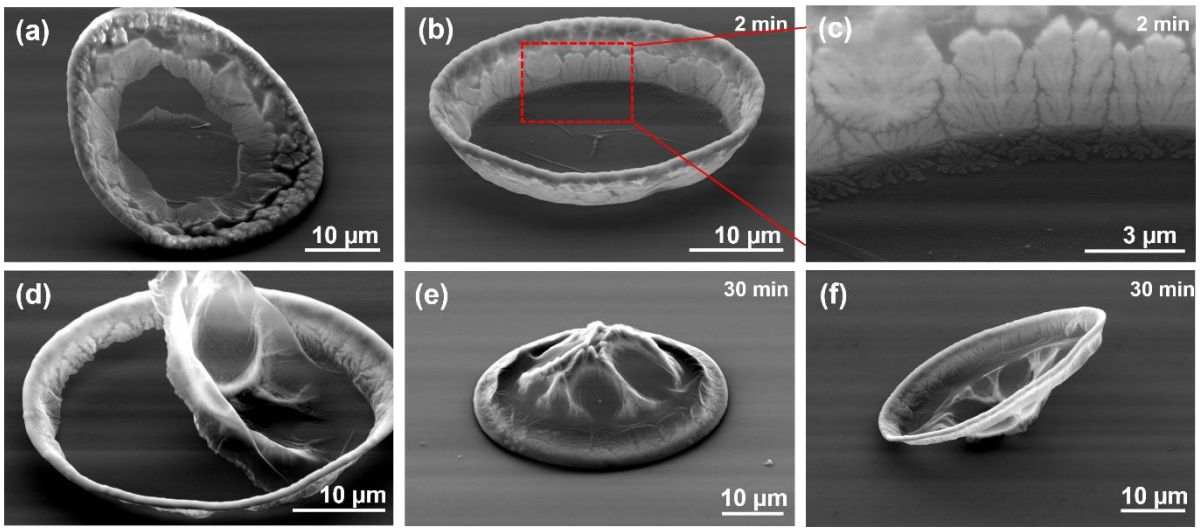

Figure 38. SEM images of dried NaCl-albumin (0.6 g/L) droplet residues collected from the EDB after reaching equilibrium at 30% RH. (a-c): Droplets collected approximately 2 minutes after reaching equilibrium; (c) is a magnified view of the boxed region in (b), showing the NaCl crystals growing inside of the albumin film. (d-f): Droplet collected approximately 30 minutes after reaching equilibrium.

However, the two sets of droplets exhibit different characteristics in the central collapsed region. Droplets collected 2 minutes after reaching equilibrium show a smooth albumin film that is well attached to the Si-wafer. In contrast, droplets collected 30 minutes later shows a more robust central film that is not attached to the Si-wafer. This observation leads me to hypothesize that, at the 2-minute mark, the albumin matrix remains partially hydrated, and after 30 minutes, sufficient water has been lost from the system.

As shown in Figure 38(a) and (d), the central films of both droplets exhibit partial tearing and rupture, likely resulting from the mechanical disruption during deposition onto the Si-wafer. However, the nature of these ruptures differs. In Figure 38(a), the smooth albumin film appears well-adhered to the Si-wafer, and likely retains some water, making it more flexible and cohesive, allowing it to conform to the Si-wafer surface without detaching. In contrast, the albumin film in Figure 38(d) is partially peeled from the Si-wafer surface, indicating a greater degree of water loss. The resulting brittleness and shrinkage likely reduce adhesion of the albumin film.

Overall, the duration of droplet levitation under steady airflow does not significantly influence the resulting equilibrium morphology. Droplets collected at both 2 minutes and 30 minutes after reaching equilibrium consistently exhibited a bowl-like structure. The primary difference is that extended levitation (30 minutes) appears to result in greater water loss from the droplet.

To further verify that the distinctive bowl-like shape results from evaporation of the NaCl-albumin droplets while levitated in the trap, it is essential to visually examine the real-time evaporation process of these droplets. Figure 39(a) presents HSV camera images of a 0.6 g/L albumin + NaCl droplet evaporating under 30% RH conditions, capturing the progressive volume reduction and morphological deformation prior to reaching equilibrium. A comparison with a droplet containing the same concentration of mucin (Figure 39(b)) clearly demonstrates both the validity of the observed deformation and the pronounced differences in morphological evolution between the two droplet types.

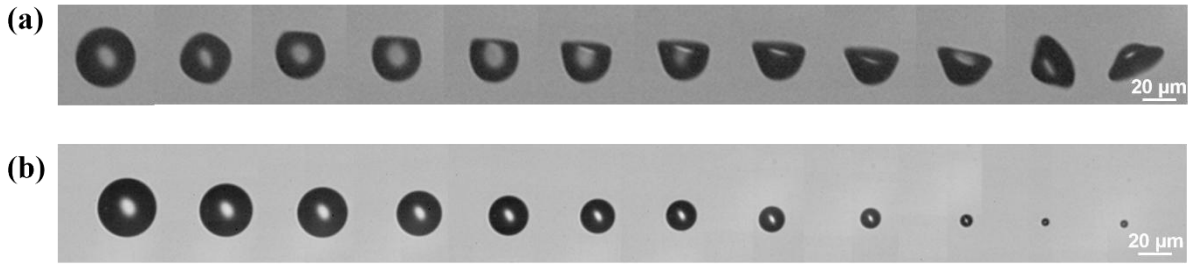

Figure 39. High-speed video (HSV) camera images of levitated droplets evaporating under 30% RH conditions, illustrating the morphological transformation prior to reaching equilibrium. (a) A representative 0.6 g/L albumin + NaCl droplet, (b) a representative 0.6 g/L mucin + NaCl droplet. Videos were recorded at a frame rate of 30,000 frame per second (fps). The sequence shown corresponded to a duration of 3 seconds, highlighting representative morphological changes during this period. Scale bar: 20 µm.

As shown in Figure 39(a), the droplet initially maintains a spherical shape, indicative of uniform surface tension and a homogeneous internal composition. However, as evaporation progresses, the levitated droplet gradually loses its spherical shape. Notably, the upper region of the droplet begins to flatten while the lower half remains relatively rounded. This morphological transition suggests non-uniform evaporation across the droplet surface. With continued water loss, the flattening at the top deepens into a concave surface, while the bottom hemisphere retains its rounded structure, ultimately producing the characteristic UFO-like morphology observed in the trap.

In contrast, Figure 39(b) shows that the NaCl-mucin droplet undergoes a more uniform decrease in size while largely maintaining its near-spherical morphology, although the final shape is difficult to resolve due to its small size at the end of evaporation. This structural stability is also supported by the SEM images presented in Section 3.2.2. Comparing with NaCl-albumin droplets, the absence of significant deformation in NaCl-mucin system suggests that mucin

forms a relatively rigid and compact outer layer, which helps preserve droplet integrity and stabilizes its morphology even under substantial water loss.

The observed progressive shape changes observed in NaCl-albumin droplets likely reflect a disruption in interfacial uniformity caused by the accumulation of albumin at the air-water interface. Albumin, being surface-active, tends to move to the droplet surface early in the evaporation process and forms a thin interfacial film. As more water evaporates, this film becomes increasingly rigid, unable to accommodate volume shrinkage uniformly. This leads to structural collapse rather than uniformly shrinking into a sphere. Such deformation highlights the inability of albumin to form a mechanically robust stabilizing layer that can preserve droplet integrity throughout evaporation. In contrast, NaCl-mucin droplets maintain a more compact shape under same conditions, highlighting how different proteins modulate droplet morphology during evaporation. These findings emphasize the role of protein-specific interfacial behavior and mechanical properties in determining the final structure of evaporated respiratory droplets.

Comparison of the SEM images and HSV camera images reveals consistent morphology features: SEM images show a bowl-like morphology of the NaCl-albumin droplet residue deposited on the Si-wafer, while HSV images capture a UFO-like structure of the NaCl-albumin droplet residue in its levitated state. This resemblance further supports the conclusion that the pronounced deformation into a bowl-like morphology, as observed by SEM, originates during the evaporation process within the trap.

A striking observation from Figure 39 is the difference in final size after evaporation, despite the droplets having comparable initial masses. A more detailed and direct comparison is present in Figure 40. The NaCl-albumin droplet collapses into a much larger, irregular bowl-like residue, whereas the NaCl-mucin droplet shrinks to a smaller, compact spherical particle. This contrast highlights the fundamentally different roles played by the two proteins in shaping droplet phase behavior: albumin promotes deformation and low-density, highly irregular structures that occupy a larger volume, while mucin facilitates the formation of denser, more compact residuals. Consequently, even droplets of equal mass can yield markedly different end sizes depending on their protein composition, emphasizing the importance of protein-specific physicochemical properties in determining the morphology and density of respiratory droplet residues.

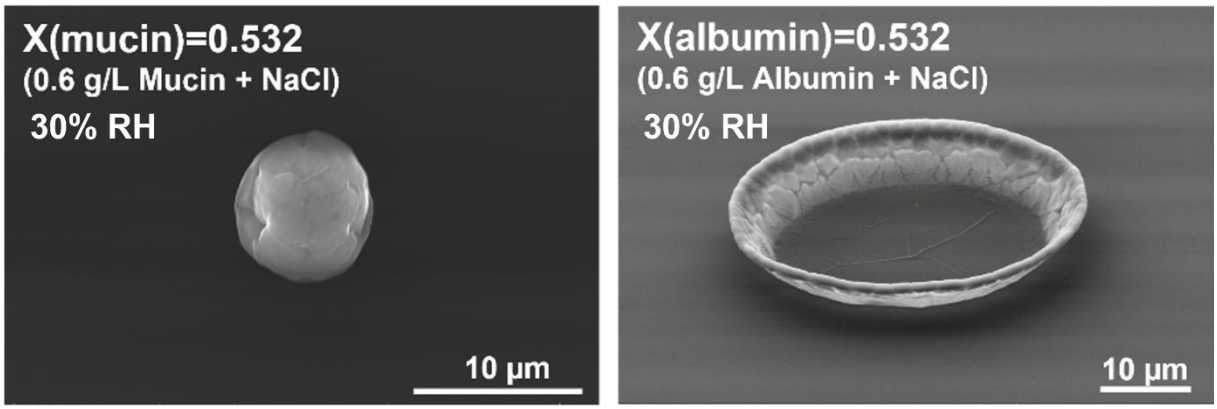

Figure 40. Comparison of NaCl-mucin and NaCl-albumin droplets (X_{mucin} = $X_{albumin}$ = 0.532) equilibrated at 30% RH. Both droplets were levitated, evaporated, and collected under identical conditions.

After characterizing the evaporation behavior and investigating the influence of albumin concentration on droplet morphology, the effects of different RH levels on the final morphology and phase state of NaCl-albumin droplets at equilibrium were examined. This analysis aims to further elucidate the combined impact of RH and albumin content on the final structural outcomes. The final morphology of the dried residues provides critical insight into how RH modulates NaCl-albumin interactions and governs distinct morphological transitions during evaporation. NaCl-containing droplets with two different albumin concentrations (0.3 g/L and 0.6 g/L) were studied under four RH conditions: 5%, 30%, 45%, and 80%. The resulting morphologies and phase state, captured after collection on Si-wafers, are presented in Figure 41.

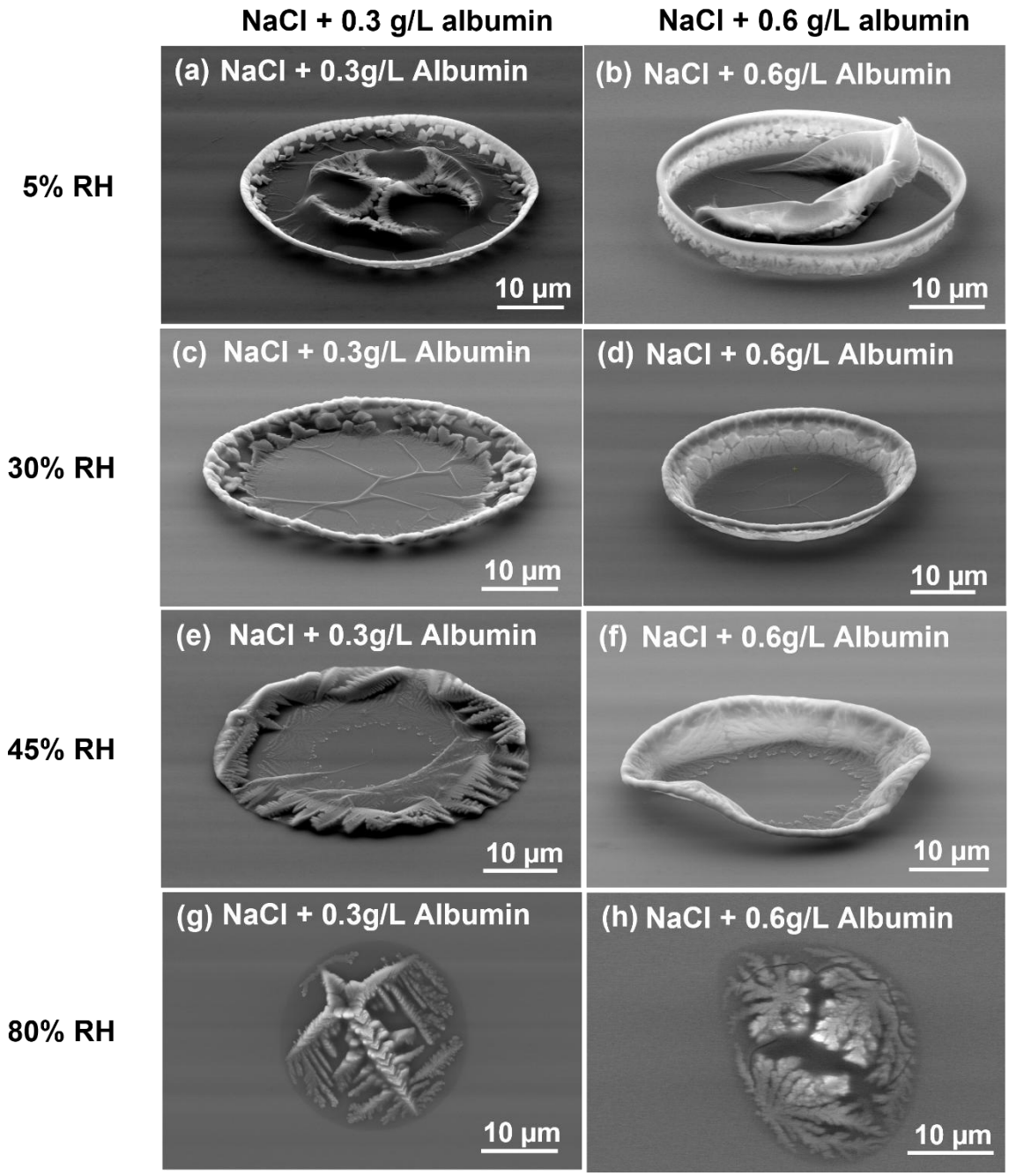

Figure 41. SEM images of NaCl-albumin droplets collected from EDB under various RH conditions. Droplets containing NaCl + 0.3 g/L albumin (left column) and NaCl + 0.6 g/L albumin (right column) were examined at equilibrium after evaporation at 5%, 30%, 45%, and 80% RH conditions.

These SEM images provide a clear comparison of NaCl-albumin droplet morphologies as a function of both RH conditions and albumin concentration. The interplay between drying conditions and albumin content give rise to distinct structural features, offering insights into the underlying physicochemical mechanisms governing droplet evaporation and solidification.

At 5% RH, droplets exhibit a bowl-like shape with raised edges. The droplet in Figure 41(b), which contains a higher albumin concentration (0.6 g/L), displays a more pronounced bowl-shaped edge compared to the 0.3 g/L sample in Figure 41(a). Under such extremely dry conditions, water evaporates rapidly, significantly weakening albumin's capacity to act as a temporary water reservoir. In the 0.6 g/L case (Figure 41(b)), the central albumin film appears brittle and fractured, consistent with the morphology shown in Figure 38(d), where rapid water loss leads to fragile and structurally compromised residues.

At 30% RH, droplets at both albumin concentrations maintain a well-defined bowl-like structure. NaCl accumulates prominently at the edges, while the central region remains relatively smooth, displaying visible wrinkles in the albumin film. Similar to the phenomenon observed under 5% RH, the droplet with higher albumin content (0.6 g/L) exhibits a more distinct bowl-shaped characteristic.

At 45% RH, the bowl-like morphology becomes less apparent in the droplet with 0.3 g/L albumin (Figure 41(e)). The droplet edge appears slightly elevated and thickened, concentrating most of the NaCl crystals. This crystallization pattern differs markedly from those observed at lower RH (Figures 41(a) and (c)) and suggests a shift in the crystallization mechanism. Under moderate humidity, slower evaporation allows more time for NaCl to nucleate and grow into larger crystals, as opposed to being rapidly confined in smaller domains due to fast water loss (Hardy et al., 2023). For the droplet containing 0.6 g/L albumin (Figure 41(f)), the increased albumin content further reshapes the final bowl-like morphology.

Under higher humidity (80% RH) conditions, droplets no longer retain a bowl-like shape upon collection onto the Si-wafer. For the droplet containing 0.3 g/L albumin (Figure 41(g)), the dark footprint suggests that the droplet remained in a liquid state at the time of collection. However, the droplet containing 0.6 g/L albumin (Figure 41(h)) appears to be in a semi-liquid or gel-like state at the time of collection. Its irregular dark footprint, deviating from a circular outline, suggests that the droplet may have undergone phase transformation driven by the higher albumin content. Moreover, visible cracks on the surface indicate that albumin had accumulated at the air-water interface to form a thin interfacial film prior to collection, highlighted cracks can be found in Appendix Figure S14. Upon sudden exposure to dry conditions after being collected onto the Si-wafer, this film likely contracted and fractured due to mechanical stress.

Collectively, these findings demonstrate that albumin significantly influences droplet morphology during evaporation under all RH conditions. It promotes early-stage morphological disruption and results in structurally diverse final residues, transitioning from spherical to

irregular UFO-like shapes under dry conditions. This behavior contrasts with the stabilizing effect of mucin, which better preserves droplet integrity and leads to more compact and cohesive dried morphologies.

The shape and morphology of respiratory droplets significantly influence their suspension time in air. Albumin-containing droplets form highly deformed bowl-like structures, experiencing higher aerodynamic drag. As a result, these irregular particles experience lower settling velocities and may remain airborne longer than compact, spherical particles of the same mass. By contrast, mucin-containing droplets tend to retain a more compact and relatively regular morphology, which promotes faster settling. This suggests that albumin-rich droplets may contribute more to long-range airborne transmission, whereas mucin-rich droplets are relatively more likely to deposit at shorter distances or contribute to surface-based (fomite) infection.

The albumin film formed on the droplet surface can partially retain water and slow down desiccation, especially under moderate to high RH conditions. This implies that, on the one hand, respiratory droplets containing albumin are capable of retaining a substantial amount of water, even under relatively dry conditions such as 30% RH, which may help protect embedded pathogens from dehydration. On the other hand, this temporary water-retention capacity may also enhance the droplet's hygroscopic potential. This is further explored in Section 3.3.3.

3.3.3 Rehydration study of levitated NaCl-albumin droplets and comparison with NaCl-mucin droplets

In the previous sections, I investigated the evaporation behavior and resulting morphologies of NaCl-albumin droplets under varying RH conditions. However, the transmission of respiratory pathogens is influenced not only by the drying process but also potential for rehydration. Once expelled into the air, respiratory droplets may undergo rehydration when they enter more humid environments, such as within the respiratory tract of a new host or under ambient conditions that fluctuate in humidity. Understanding how dried or semi-dried respiratory droplets reabsorb water is critical for assessing their ability to influence both droplet behavior and pathogen survival.

This section focuses on the rehydration behavior of NaCl-albumin droplets as a model for respiratory droplets originating from the deep lung. Particular emphasis is placed on the role of albumin in governing droplet hygroscopicity and structural reversibility upon water uptake. To elucidate specific effects of albumin, comparisons are made with mucin-containing droplets, aiming to offer new insights into how different proteins modulate droplet rehydration behavior.

First, I assessed the rehydration behavior of pure albumin droplets. A total of 20 pure albumin droplets were tested, with Figure 42 showing the representative evaporation and rehydration behavior of one such droplet. The tested concentration was 0.6 g/L, selected to match the conditions used in the pure mucin study for direct comparison. Initially, the droplet was exposed to a low-humidity environment (20% RH), as indicated by the gray-shaded region, during which it underwent drying and volume reduction. After reaching equilibrium for 3 minutes, the RH was gradually increased to approximately 95% RH, and the light scattering patterns of the droplet were recorded at one-second intervals to monitor the rehydration process.

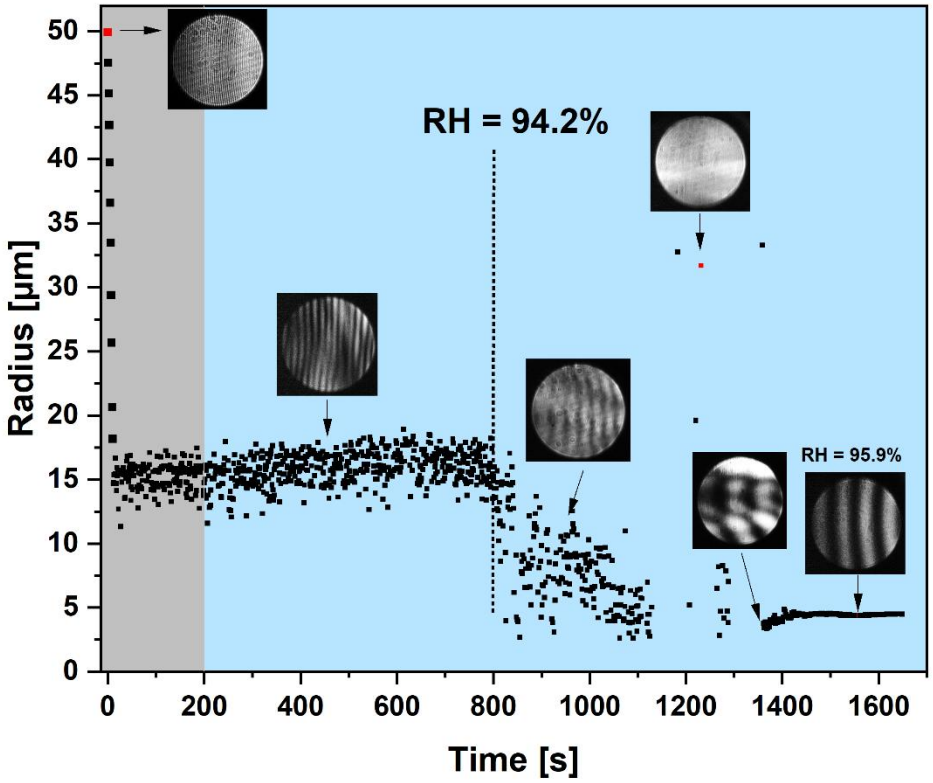

Figure 42. Evaporation and rehydration behavior of a representative pure albumin droplet. The grey-shaded region indicates the evaporation phase at 20% RH, and the blue-shaded region represents the rehydration phase during which the RH is gradually increased. Light scattering patterns captured at selected time points illustrate the shape and phase changes throughout both drying and water uptake processes. The vertical black dashed line marks a notable transition near RH = 94.2%. The red dot in the figure at the beginning of evaporation represents the first second of droplet exposure, with its corresponding scattering pattern shown next to it. The red dot during rehydration highlights the observed "jump" behavior, with its corresponding scattering pattern displayed above.

The light scattering pattern at the first second (marked by a red dot) indicates a homogeneous, spherical droplet with an initial radius of approximately 50 μm. As evaporation proceeds, the radius decreases, eventually fluctuating at around 15 μm, indicating that the droplet has lost its spherical shape and deformed into an irregular-shaped residue.

Upon entering the rehydration phase (blue-shaded region), the surrounding RH is progressively increased, and the droplet begins to respond. During the period between the onset of rehydration and the point marked by the dashed vertical line at 94.2% RH, the droplet radius shows a slightly increasing trend, although significant fluctuations persist. Throughout this phase, the light scattering patterns display closely packed, irregular, curved stripes, indicating a heterogeneous and non-spherical structure.

A sudden drop in radius is observed near 800 s, coinciding with the RH approaching 94.2%, as marked by the black vertical dashed line. This transition is reflected by notable changes in the scattering patterns, with less, but more curved and more widely spaced stripes appearing, indicating a shift in droplet morphology.

A particularly interesting feature is the "jump and fall" behavior observed during rehydration, highlighted by a red dot in the blue-shaded region. During the "jump and fall" behavior, the stripes in the light scattering patterns disappeared entirely, and the droplet exhibited unstable, oscillatory movement while levitating in the trap. This unexpected behavior during water uptake may be attribute to partial collapse or structural instability of the albumin film, potentially triggered by water penetration and rearrangement of the albumin matrix.

As RH gradually stabilizes near 95%, the droplet radius also stabilized, but at a value even lower than 5 μm. During this stage, regular and straight stripes reappear in the scattering patterns, indicating that the droplet has absorbed sufficient water to regain a more homogeneous and spherical form. Notably, even though RH remains constant between 800-1600 s, the droplet morphology continues to evolve significantly. This observation suggests that albumin does possess water absorption capacity, but effective rehydration occurs only under near-saturated humidity conditions. This behavior contrasts with that of mucin, which exhibits clear water uptake and swelling already at around 63% RH, as discussed previously in Section 3.2.3 and shown in Figure 30.

Albumin concentration plays a significant role in influencing the evaporation behavior and final morphology of NaCl-albumin droplets. Here I investigated the rehydration behavior of NaCl-

albumin droplets containing varying albumin mass fraction, $X_{albumin}$ = 0.1, 0.2, 0.3, 0.7, and 0.85, as shown in Figure 43. A total of ten droplets were tested for each condition, and each droplet was initially subjected to 20% RH until equilibrium was reached, the evaporation phase is highlighted in gray in the figure. After approximately 150 seconds, the RH was gradually increased to ~ 95% to initiate rehydration, with the rehydration phase indicated by the light-yellow shading. This figure illustrates how rehydration behavior of NaCl-albumin droplets is influenced by albumin content, revealing distinct variations in water uptake behavior and structural response across different concentrations.

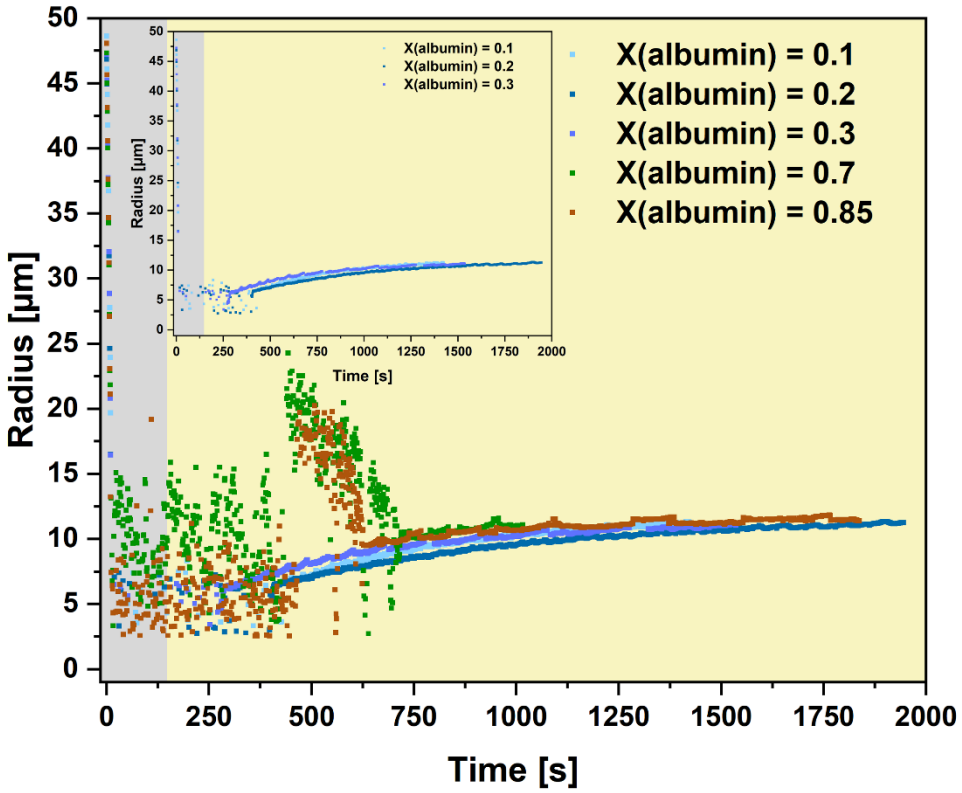

Figure 43. Rehydration behavior of NaCl-albumin droplets with varying albumin mass fraction ($X_{albumin}$ = 0.1, 0.2, 0.3, 0.7, and 0.85). The upper part of the main figure includes an inset highlighting the clear rehydration response of droplets with lower albumin content ($X_{albumin}$ = 0.1-0.3). The gray-shaded area indicates the evaporation phase, while the light yellow-shaded area indicates the rehydration phase.

The droplet radius was derived from light scattering patterns over time as the droplets were exposed to increasing humidity. Following initial evaporation, the droplets reach an equilibrium

state characterized by irregular, UFO-like structures. Upon rehydration, droplets begin to absorb water. As shown the upper inset in Figure 43, droplets with lower albumin content ($X_{albumin}$ = 0.1-0.3) exhibit a smooth and consistent increase in radius after a fluctuation period, indicating that these droplets enter a gradual and continuous water uptake phase after overcoming an initial instability. In contrast, droplets with higher albumin content ($X_{albumin}$ = 0.7 and 0.85) show more pronounced size fluctuations during the early stages of rehydration. Notably, these droplets exhibit a distinct "jump and fall" in apparent size before stabilizing, which mirrors that observed in the rehydration of pure albumin droplets. This suggests that at higher concentrations, albumin dominates the droplet behavior, and this is an effect that is less apparent at lower concentrations. The delayed onset of steady growth in high-albumin droplets likely results from the formation of a denser albumin film, which impedes water diffusion and thereby delays complete rehydration.

Furthermore, under controlled conditions where all droplets contain the same amount of NaCl, increasing the albumin mass fraction does not significantly influence the hygroscopic growth of the droplets. As illustrated in Figure 43, the final equilibrium radius following rehydration is nearly identical across all albumin concentrations. This observation implies that although albumin concentration strongly affects drying behavior and morphological transformations during rehydration, such as droplet deformation and internal structural rearrangement, it does not significantly alter the overall water absorption capacity. The hygroscopicity of the droplets remains primarily governed by the NaCl content. A more detailed analysis of droplet hygroscopicity will be presented in the following section.

To facilitate a direct comparison between the influence of albumin and mucin on droplet rehydration behavior, the evolution of droplet radius over time for each type is presented in Figure 44. Both droplets underwent the same drying and rehydration protocol: initial evaporation at 30% RH for approximately 2 minutes, followed by a gradual increase in RH to ~ 95% to induce rehydration. One representative droplet out of ten tested for each condition is shown.

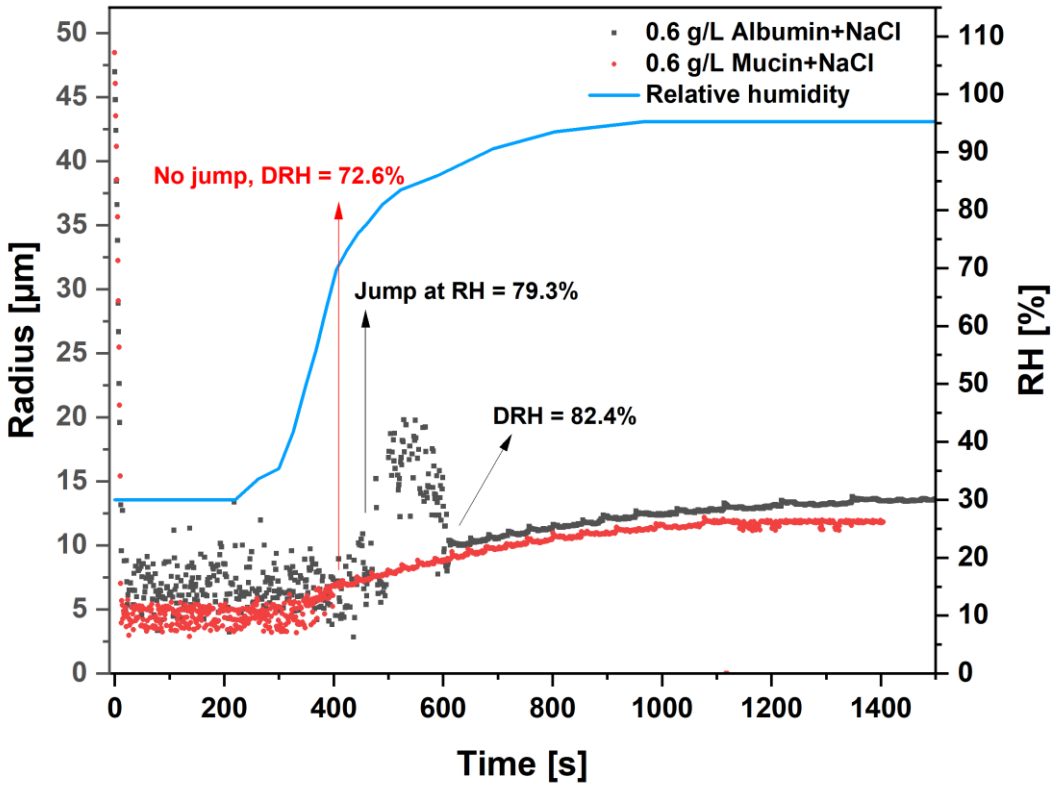

Figure 44. Comparison of the rehydration behavior of 0.6 g/L albumin + NaCl droplet (black) and 0.6 g/L mucin + NaCl droplet (red) under gradually increasing RH (blue) conditions.

Despite having the same protein concentration, the albumin-containing and mucin-containing droplets exhibit distinctly different rehydration behaviors. The NaCl-albumin droplet (black curve) displays a pronounced "jump and fall" at approximately 79.3% RH, following a DRH of 82.4%. The DRH in this thesis was identified as the RH at which the light scattering patterns transition from irregular to regular, straight stripes, signifying a homogeneous, liquid-like state where the solutes may have fully dissolved. In contrast, the NaCl-mucin droplet (red curve) demonstrates a smoother, more gradual increase in radius without a sharp deliquescence jump during rehydration, and shows a lower DRH of 72.6%.

This comparison highlights key differences in the hygroscopic behavior of droplets containing different proteins. Albumin appears to preserve the deliquescence behavior of NaCl, as evidenced by the "jump" behavior happened close to the DRH of pure NaCl. This suggests that NaCl remains at least partially accessible within the albumin matrix, allowing a distinct phase transition to occur once the RH surpasses the DRH threshold, leading to structural reorganization of the droplet as water uptake and salt dissolution progress. Mucin, however,

appears to facilitate a more continuous and gradual water uptake process. The absence of a sharp “jump” and lower DRH suggest that mucin forms a more hydrophilic matrix that gradually absorbs water and retains it, thereby creating a favorable microenvironment for NaCl to deliquesce in a more stable and controlled manner.

Following rehydration at 95% RH, the droplets were collected from the trap and compared with droplets that were evaporated and collected directly at equilibrium under 95% RH conditions, as shown in Figure 45. This comparison between NaCl-protein droplets that were equilibrated directly at high RH and those that underwent drying followed by rehydration provides key insights into the reversibility of their phase states and morphological transitions.

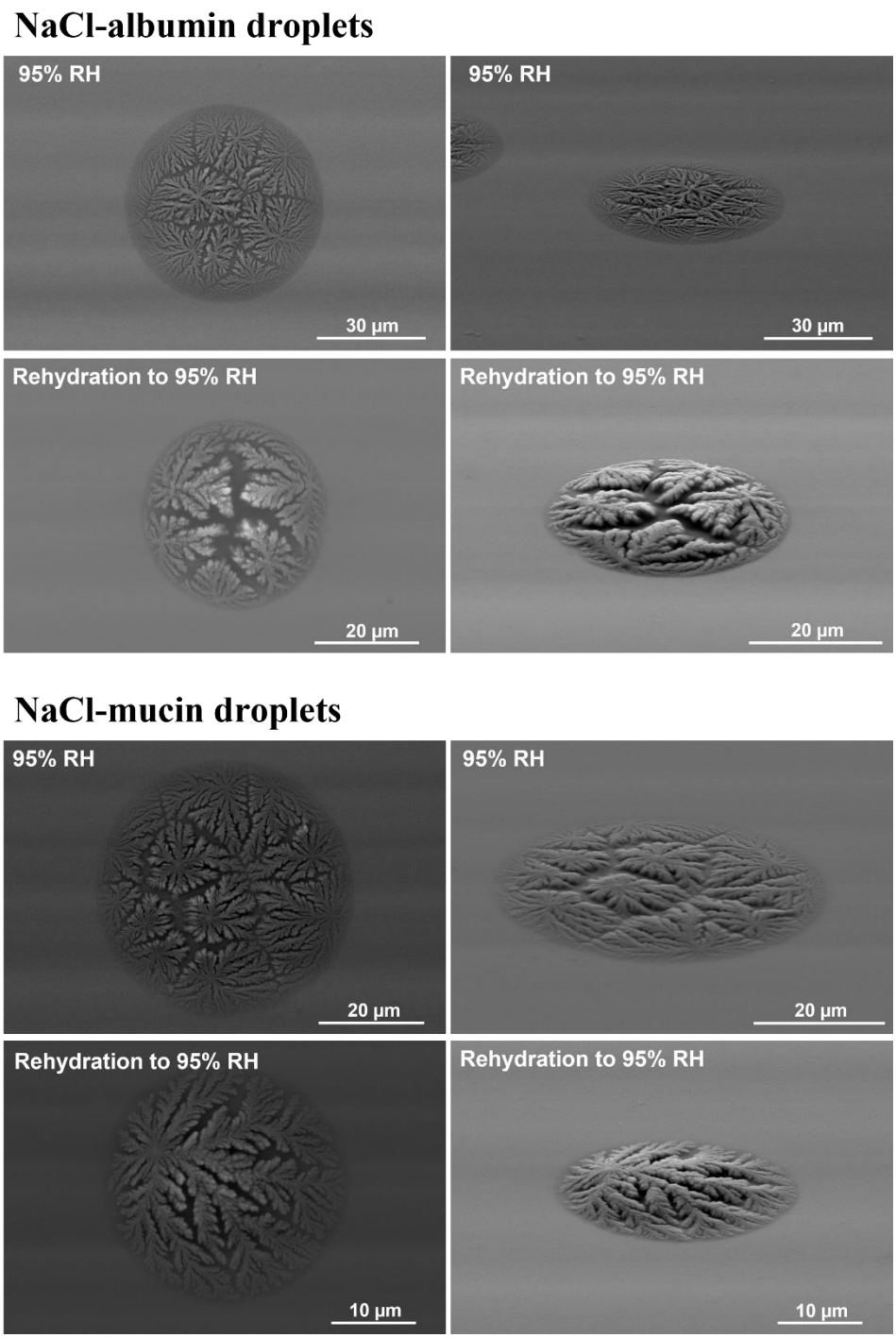

Figure 45. Morphological comparison of NaCl-protein droplets (0.6 g/L albumin or mucin) at 95% RH and after rehydration to 95% RH. The upper panels show the NaCl-albumin droplets, while the lower panels show the NaCl-mucin droplets. For each droplet, both a top view and a tilted view (60°) are presented.

For NaCl-albumin droplets, although both the droplets equilibrated at 95% RH and those rehydrated to 95% RH exhibit a liquid-like state, their final morphologies are different. At 95% RH, the NaCl-albumin droplet exhibits a relatively flat and smooth surface morphology with

evenly distributed NaCl crystal patterns, indicating a homogeneous distribution of solutes within the droplet. The rehydrated droplet, however, exhibits visible surface crack patterns (see highlighted examples in Appendix Figure S15), attributed to an albumin film formed during drying. These cracks suggest that albumin migrates to the droplet interface during drying and remained localized there during rehydration, rather than evenly redistributing into the droplet interior upon absorbing water. This highlights the irreversible structural changes induced by the initial drying phase, indicating that although water uptake occurs, the internal organization, particularly the NaCl-albumin matrix and interfacial albumin layer, does not fully revert to its original state.

In the case of NaCl-mucin droplets, those equilibrated at 95% RH show a flat surface morphology with multiple crystalline clusters. However, droplets rehydrated to 95% RH display a markedly different structure: a single nucleation site from which densely branched NaCl crystals grow, forming organized dendritic patterns across the droplet. This difference underscores that, despite reaching a liquid state again after rehydration, the structural and compositional organization of the droplet does not revert to that observed under direct humid conditions.

This section primarily focuses on the rehydration behavior of albumin and its influence when coexisting with NaCl in droplets. Overall, the findings indicate that albumin possesses hygroscopic capability and significantly influences rehydration behavior of NaCl-albumin droplets at high concentrations, often inducing droplet instability before reaching full deliquescence. Although rehydrated droplets return to a liquid phase, a portion of the albumin may remain concentrated at the droplet interface, impeding complete structural reorganization. In contrast, mucin facilitates earlier and more uniform rehydration, resulting in smoother morphological transitions. These contrasting behaviors highlight the distinct roles that respiratory proteins play in governing the phase transitions and structural evolution of exhaled respiratory droplets during rehydration. Further analysis of how albumin modulates the deliquescence and efflorescence behavior of NaCl-albumin droplets is presented in the following section.

3.3.4 Efflorescence and deliquescence behavior of levitated NaCl-albumin droplets

Understanding the efflorescence and deliquescence behavior of NaCl-albumin droplets is essential for elucidating the phase transitions and hygroscopic responses of respiratory droplets originating from the deep lung under varying ambient conditions. The phase state of respiratory

droplets, whether liquid, semi-solid, or solid, directly influences their ability to transport and preserve airborne pathogens (Huynh et al., 2022; Lin and Marr, 2020).

I previously observed a unique rehydration behavior of albumin, which significantly influences the water uptake process of NaCl-albumin droplets by inducing pronounced morphology changes that appear as a distinct “jump and fall” in droplet apparent size derived from light scattering patterns. However, this phenomenon is only evident at high albumin concentrations, suggesting that albumin must reach a critical content before it can significantly dominate the droplet rehydration process. This “jump and fall” behavior appears to postpone the DRH of NaCl-albumin droplets compared to the DRH of pure NaCl. To further investigate this hypothesis, rehydration and dehydration experiments were conducted on NaCl-albumin droplets containing varying albumin mass fraction, ranging from X_{albumin} = 0 (pure NaCl), 0.1, 0.2, 0.3, 0.362, 0.532, 0.7, 0.85, and 1 (pure albumin). These tested albumin mass fraction and all experimental conditions were identical to those in the mucin-containing droplet test, allowing for a direct comparison between the effects of these two respiratory proteins. Since reliable droplet size measurements cannot be obtained from light scattering patterns after efflorescence, the dry particle radius (r_{dry}) used to calculate the growth factor was instead derived from the theoretical dry mass, assuming complete water evaporation and that only NaCl and albumin remain.

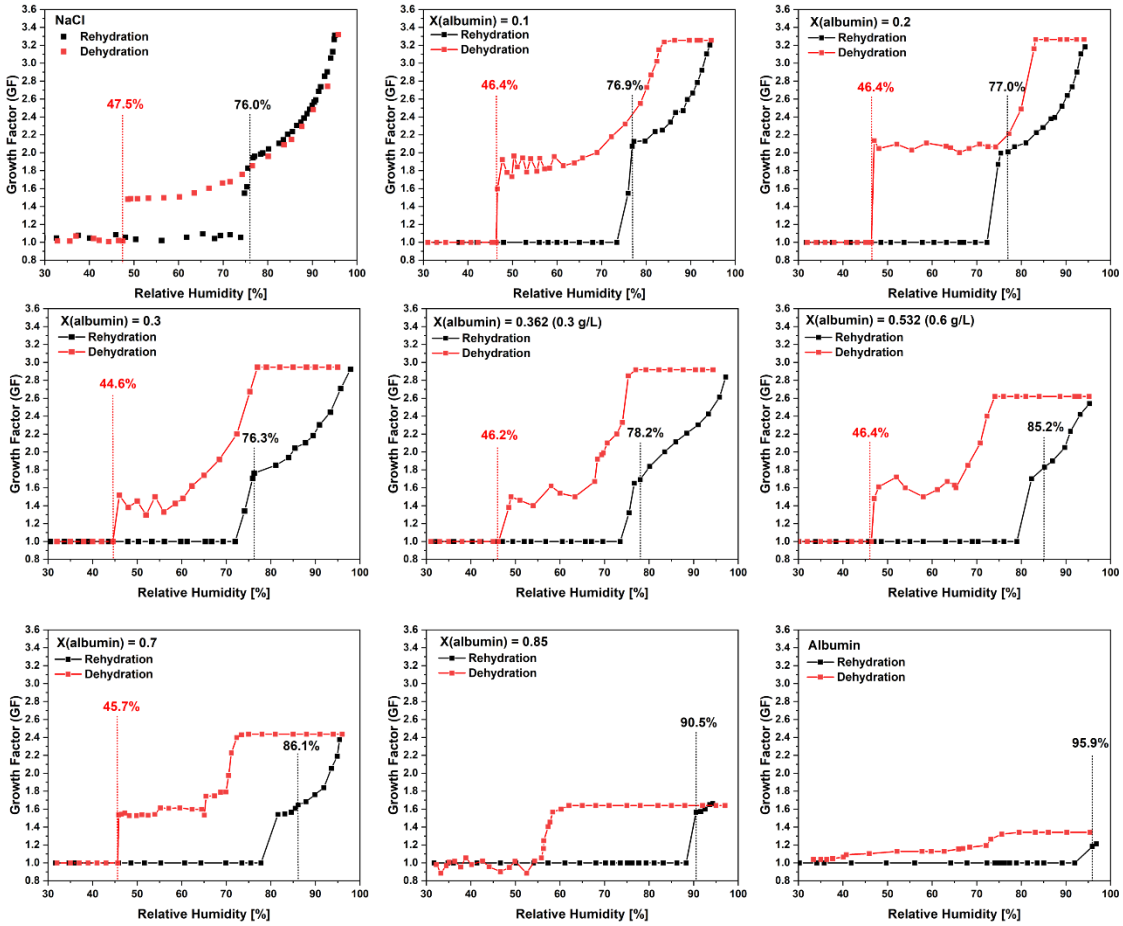

Figure 46. Rehydration and dehydration curves of representative NaCl-albumin droplets containing varying mass fraction of albumin, ranging from $X_{albumin}$ = 0 (pure NaCl) to $X_{albumin}$ = 1 (pure albumin). The black curves represent the rehydration process, while the red curves represent the dehydration process. Each data point corresponds to the growth factor (GF) of the droplet under the respective RH conditions. the black vertical dashed line marks the DRH of the droplet, and the red vertical dashed line marks the ERH.

Figure 46 systematically illustrates how the addition of albumin influences the dehydration and rehydration behavior of droplets. The pure NaCl droplet shows a classic rehydration and dehydration behavior with a sharp deliquescence transition at 76.0% RH and efflorescence at 47.5 % RH, consistent with literature values for NaCl (Ahn et al., 2010; Alshawa et al., 2009; Li et al., 2014).

At low albumin content ($X_{albumin}$ = 0.1-0.362), the droplets continue to exhibit clear deliquescence behavior during rehydration, with the DRH remaining close to that of pure NaCl. This indicates that NaCl still dominates the deliquescence process. However, an interesting phenomenon is observed during dehydration. The droplets remain stably levitated without noticeable changes in size as the RH decreases from 95% to approximately 80%. Below this

point, the droplets begin to shrink, as evidenced by a reduction in the number of stripes observed in the light scattering patterns. As dehydration progresses, the shrinkage slows, and fluctuations in apparent size are observed as the light scattering patterns start exhibiting some curved stripes, suggesting deformation of the droplet structure. As the scattering patterns become irregular, the size evaluation routine becomes unstable, leading to apparent variability in the droplet size. Notably, this fluctuation occurs at RH levels significantly higher than the ERH of pure NaCl, implying that NaCl has not yet undergone fully efflorescence. Instead, the observed instability may result from the migration of albumin toward the droplet interface, which disrupts the homogeneous internal structure of the droplet. As RH continues to decrease and approaches the ERH of pure NaCl, the stripes in the light scattering patterns disappear completely, indicating the onset of NaCl efflorescence.

At higher albumin content (X_{albumin} = 0.532-0.85), droplets still exhibit clear deliquescence behavior, however, the DRH increases significantly, reaching 85.2% for X_{albumin} = 0.532, 86.1% for X_{albumin} = 0.7, and 90.5% for X_{albumin} = 0.85. Given that the pure albumin droplet exhibits a very high DRH of 95.9%, this trend indicates that at higher concentrations, albumin begins to dominate the rehydration behavior of the droplet and suppresses the deliquescence of NaCl. As previously discussed, NaCl-albumin droplets with high albumin content exhibit distinct “jump and fall” in apparent size before reaching their DRH. This abrupt change occurs at the RH close to the DRH of pure NaCl, suggesting a more complex deliquescence mechanism is involved, potentially influenced by structural deformation and heterogeneity within the droplet.

Supporting this interpretation, Mikhailov et al. (2004) investigated the hygroscopic growth of aerosol particles composed of NaCl and BSA. They observed a pronounced reduction in particle diameter upon hydration, which they attributed to substantial microstructural rearrangements. Notably, this transition occurred at the RH similar to that for pure NaCl, implying that NaCl-albumin can exhibit unique structure and phase behavior during rehydration.

Taken together, these findings suggest the following interpretation: at higher albumin concentrations, the drying process leads to significant droplet deformation, resulting in a highly irregular morphology. As RH increases, the albumin film becomes increasingly permeable to water, gradually allowing substantial water penetration and interaction with the encapsulated NaCl. Once the RH reaches and exceeds the DRH of pure NaCl, sufficient water is absorbed for NaCl to initiate deliquescence. However, the dissolved NaCl remains confined within the rigid albumin film, as it has not been fully solubilized or softened. Consequently, the droplet begins to restructure and reorganize to regain a stable shape. As water uptake continues, the

thick albumin film eventually dissolves, allowing the droplet to restore a stable spherical shape, marking the completion of the deliquescence process.

During dehydration, a more pronounced “no-change” phase is observed at the onset of the process. For the droplet with $X_{\text{albumin}} = 0.7$, the RH must drop to approximately 70% to initiate dehydration; for $X_{\text{albumin}} = 0.85$, this threshold falls even lower, to around 60% RH. This delayed shrinkage likely results from several interrelated mechanisms:

First, albumin possesses hygroscopic properties and binds water strongly through hydrogen bonding (Borisover et al., 1995; Dong et al., 2019; Wei et al., 2019). These water molecules are retained within the albumin matrix and are less responsive to ambient RH changes, further stabilizing the droplet. With higher albumin content, the albumin network becomes denser, further restricting water mobility.

Second, albumin may preferentially migrate toward the droplet interface during evaporation, even under very humid conditions. Evidence for this behavior is provided in Figure 47, which shows a droplet containing NaCl and 0.6 g/L albumin evaporating at 95% RH until equilibrium is reached. Prior to equilibrium, a fluctuation in droplet apparent size is observed, highlighted by the red arrow, and the corresponding light scattering pattern displays wavy and curved stripes, indicating temporary inhomogeneities in the droplet. Upon reaching equilibrium, the droplet regains a homogeneous, spherical shape, and the light scattering pattern returns to a regular form, as indicated by the black arrow. This phenomenon suggests that even at 95% RH, a subtle outward flow can occur, concentrating albumin at the interface and inducing temporary structural heterogeneity. The system, however, is capable of self-stabilizing and regaining homogeneity. The interfacial accumulation of albumin may contribute to the formation of a viscoelastic film, which acts as a barrier to water diffusion.

Collectively, these effects may delay the onset of visible size reduction, highlighting that albumin plays a significant role in modulating the response of model respiratory droplets during dehydration.

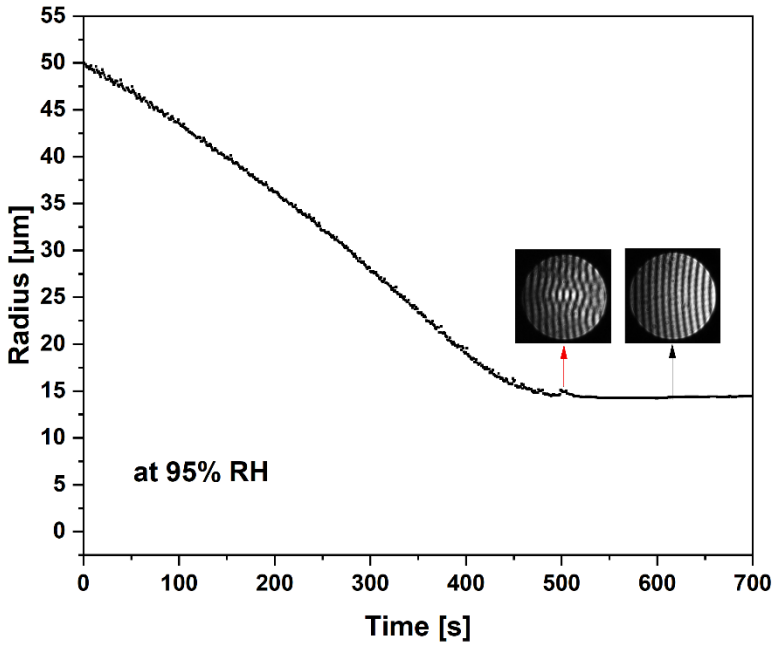

Figure 47. Evaporation profile of the NaCl-albumin droplet (albumin concentration: 0.6 g/L) at 95% RH. The red arrow marks the fluctuation in droplet apparent size prior to reaching equilibrium, with the corresponding light scattering pattern shown above. The black arrow shows the representative regular light scattering pattern of the droplet at equilibrium.

When comparing the growth factor of NaCl-albumin droplets during rehydration and dehydration under each concentration condition (Figure 46), it is noteworthy that the growth factor after rehydration is comparable to that at the onset of dehydration (~95% RH). This indicates that the presence of albumin does not inhibit complete water uptake at 95% RH, suggesting that the phase state of the droplets is reversible at this point. However, pure albumin droplets exhibit different behavior: the growth factor during rehydration is approximately 1.2, which is lower than that observed during dehydration. Similar findings were reported by Pöhlker et al. (2023), who compared the hygroscopic growth curves of BSA, NaCl, and KCl. Their study also predicted a growth factor of 1.2 for BSA as the RH approaches 100%, which is significantly lower than that of pure NaCl and KCl particles. These results suggest that the final hygroscopicity of NaCl-albumin droplets is primarily governed by NaCl, despite albumin significantly influencing droplet behavior throughout the rehydration process. This overlap in growth factors indicates that, regardless of whether the droplets reach 95% RH through water uptake or water loss, they arrive at a thermodynamically consistent final state.

To provide a clear and direct overview of how increasing albumin content influences the phase transition behavior of NaCl-albumin droplets, Figure 48 presents the ERH and DRH of droplets with varying albumin mass fractions. As shown in Figure 48(a), the ERH fluctuates slightly with albumin mass fraction but remains within a narrow range (45-47%) across all tested values. This suggests that while albumin may hinder NaCl efflorescence, the effect is relatively limited, lowering the ERH by only 1-2%, and appears to be largely independent of albumin mass fraction.

Similar observations were reported by Mikhailov et al. (2004), who investigated the aerosol particles composed of BSA and NaCl during dehydration and hydration. In their study, the ERH of NaCl-BSA droplets decreased with increasing BSA mass fraction, from 41% at $X_{\text{albumin}} = 0$ to 37% at $X_{\text{albumin}} = 0.75$. Although the absolute ERH values differ from those reported in this thesis, such discrepancies are expected due to differences in experimental conditions, along with a reported measurement uncertainty of ± 2% in their study. Given that the ERH decreased by only 4% across a 75% increase in albumin mass fraction, their results support the conclusion that albumin can inhibit the nucleation of NaCl crystals within droplets. However, the magnitude of this inhibition appears limited, which is consistent with our observation that the presence of albumin only marginally affects the ERH of NaCl-albumin droplets.

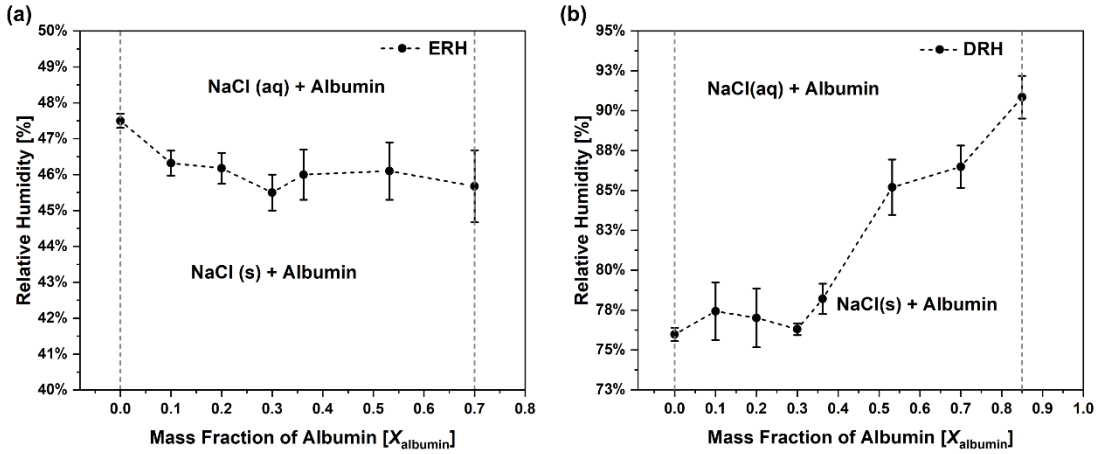

Figure 48. (a) Efflorescence relative humidity (ERH) and (b) deliquescence relative humidity (DRH) of droplets containing NaCl with varying mass fraction of albumin (X_{albumin}). Each data point represents the average ERH and DRH values, with error bars indicating the standard deviations obtained from 20 individual measurements.

In contrast, albumin plays a more important role in influencing the DRH of droplets during rehydration, as shown in Figure 48(b). At low albumin content, $X_{\text{albumin}} \leq 0.362$, the DRH

remains relatively constant (~76-79%), closely aligned with that of pure NaCl. This indicates that, at low concentrations, albumin does not noticeably influence the deliquescence behavior of NaCl. However, as the albumin mass fraction increases ($X_{albumin} > 0.362$), a significant rise in DRH is observed, reaching values above 90% at $X_{albumin} = 0.85$. This sharp increase indicates that, at higher concentrations, albumin begins to dominate the rehydration process and significantly delay the deliquescence of NaCl. The observed effect is likely attributed to the formation of a denser albumin film. Overall, at low albumin concentrations, water can easily penetrate the albumin matrix and interact with NaCl, triggering deliquescence at the RH close to the DRH of pure NaCl. As albumin concentration increases, water can still diffuse through the denser albumin matrix, however, due to significant droplet deformation during evaporation, NaCl deliquesces within an irregular shaped droplet. The droplet must then undergo structural reorganization to recover a stable, spherical morphology. This restructuring delays the observable deliquescence response, resulting in a higher DRH.

During efflorescence measurements, in which droplets gradually lose water, I observed that as the RH decreased below the ERH, the light scattering patterns abruptly became irregular, showing no discernible stripes. For example, the stripes were no longer observed when RH drops to 30%. This behavior contrasted with the scattering patterns recorded during standard evaporation experiments conducted directly at 30% RH, where the stripes were still present, although they appeared highly distorted. Since light scattering patterns provide insight not only into droplet homogeneity but also into shape and internal structure, the observed differences, despite occurring at the same final RH, may suggest a notable morphological distinction between droplets subjected to different drying pathways.

This observation led to the hypothesis that droplets undergoing slow evaporation may develop a different final morphology compared to those experiencing fast evaporation. To test this hypothesis, I compared droplets dried under both conditions and collected at 30% RH. In the slow evaporation conditions, the droplet was first equilibrated at 95% RH. The RH was then gradually decrease to 30%, which took approximately 20 minutes, after which the droplet was maintained at 30% RH until it was fully dried. In the fast evaporation condition, droplets were exposed directly to 30% RH from the beginning. The resulting droplet morphologies are shown in Figure 49, with the corresponding light scattering patterns displayed in the upper right corner of each image.

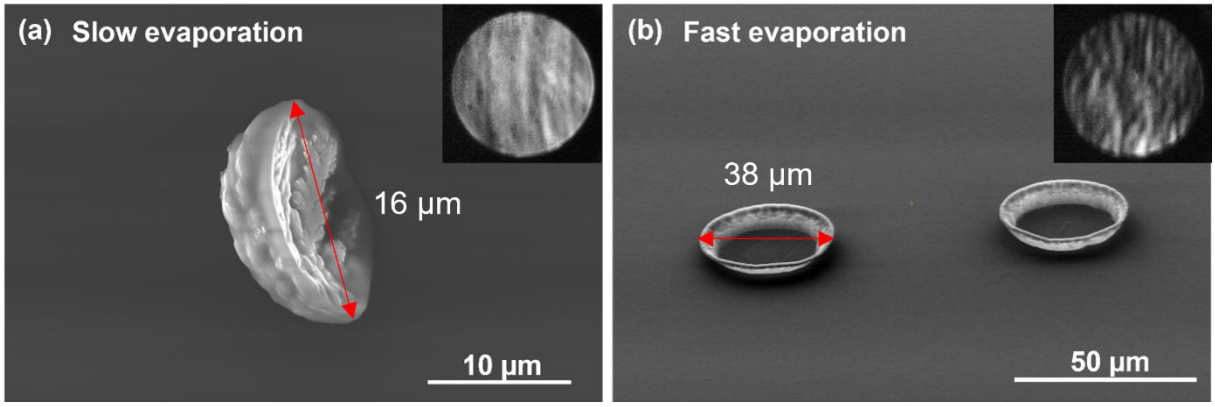

Figure 49. SEM images of NaCl-albumin (0.6 g/L) droplets dried under different evaporation conditions at 30% RH. (a) Slow evaporation: the droplet was first introduced into a 95% RH environment, followed by a gradual reduction to 30% RH, where it was held until fully dried. (b) Fast evaporation: the droplet was directly exposed to a 30% RH environment immediately after injection. The corresponding light scattering patterns at the end of drying are shown in the upper right corner of each image.

Distinct differences in droplet size, shape, and morphology are observed under slow and fast evaporation conditions. Under slow evaporation (Figure 49(a)) conditions, the droplet exhibits a compact and cohesive structure with a thicker shell and higher structural integrity. In contrast, droplets formed under fast evaporation (Figure 49(b)) conditions display a collapsed, bowl-like morphology with irregular deformation. These differences can be attributed to the extended drying time during slow evaporation, which allows for more extensive internal restructuring. Both NaCl and albumin have more time to diffuse and aggregate within the droplet. It seems like albumin can diffuse toward the surface at a rate comparable to the moving boundary, preventing the formation of the thin albumin "skin". Consequently, the droplet maintains a more compact structure and smaller final size compared to the fast-evaporated case.

The gradual water loss under slow evaporation likely facilitates the migration of albumin to the droplet interface, where it forms a surface film, while NaCl crystallizes internally, encapsulated by this albumin matrix. The droplet surface displays pronounced wrinkling and internal folding, suggesting that the albumin matrix undergoes non-uniform contraction during drying. In contrast, droplets subjected to fast evaporation (Figure 49(b)) exhibit a thinner, less compact, and more irregular morphology, as previously discussed in Section 3.3.2. The rapid loss of water likely traps albumin at the interface before NaCl crystallization can occur, resulting in less structural organization.

This comparison highlights the significant role of evaporation rate in determining the final morphology of NaCl-albumin droplets. These findings are particularly relevant to

understanding the behavior of respiratory droplets, where environmental conditions can dramatically influence the drying process and resulting residue structures.

3.3.5 Conclusions

This section investigated the evaporation behavior, hygroscopic properties, phase transitions, and morphological evolution of NaCl-albumin droplets across a range of albumin mass fractions under varying RH conditions, with a particular focus on how albumin influences evaporation, rehydration, efflorescence, and deliquescence droplets. The findings demonstrate that albumin plays a multifaceted role in modulating both the physical state and structural morphology of droplets.

During evaporation, the presence of albumin slightly accelerates evaporation compared to NaCl solution droplets and significantly alters the droplet structural morphology. Dried droplets exhibit pronounced deformation and collapse, often forming a UFO-shaped or bowl-like morphology, characterized by a thin central layer of albumin and NaCl crystallizing around the periphery, partially encapsulated by an albumin film. These features differ substantially from the well-defined crystalline structures of pure NaCl and also contrast with NaCl-mucin droplets, which display more compact and cohesive structures under dry conditions. This highlights albumin's unique ability to reshape droplet morphology during water loss. Additionally, slower evaporation results in denser and more cohesive residues, emphasizing the influence of drying rate on final droplet structure. Moreover, NaCl-albumin droplet residues exhibit a noticeably larger final size than NaCl-mucin residues under identical conditions, despite containing the same total solute mass. This observation suggests that albumin-containing residues possess a lower effective density, which reduces their settling velocity and consequently allows them to remain suspended in air for long periods.

During rehydration, the albumin film formed on the droplet surface remains permeable to water, allowing water molecules to penetrate and reach encapsulated NaCl, thereby triggering deliquescence. While albumin does not significantly alter the overall hygroscopicity of the NaCl-albumin system, as evidenced by the full recovery of the droplet growth factor after rehydration, it does influence the droplet behavior during the rehydration process. At high albumin mass fractions, a characteristic "jump and fall" in droplet apparent size is observed before steady growth resumes, suggesting a structural reconstruction phase prior to the formation of a stable spherical droplet.

With respect to phase transitions, the study finds that albumin exerts only a modest inhibitory effect on NaCl efflorescence. Although ERH values fluctuate slightly with increasing albumin concentration, the suppression is minimal and appears largely independent of concentration. In contrast, albumin has a more pronounced impact on deliquescence of NaCl. Higher albumin mass fractions lead to delayed (higher) DRH values, typically occurring after the observed "jump and fall" behavior. This delay is likely due to internal inhomogeneities and altered spatial distribution of NaCl, both induced by the presence of albumin.

Taken together, these findings reveal the critical role of albumin in governing the physicochemical behavior of mixed-component respiratory droplets. The formation of irregular, deformed residues with relatively larger final sizes and lower effective density suggests that NaCl-albumin droplets may remain suspended in air for longer periods due to reduced settling velocity. This prolonged airborne lifetime could enhance the potential for long-range aerosol transmission. Moreover, albumin's ability to retain water within its matrix at ambient RH levels (30-60%) may create creating protective microenvironments for pathogens to survive. Consequently, albumin-rich droplets may contribute to extended airborne persistence and sustained infectivity under indoor conditions.

4. Conclusions and outlook

The recognition of airborne transmission as a major route for respiratory pathogens has underscored the importance of controlling this pathway to effectively limit the spread of infection (Morawska and Cao, 2020; Wang et al., 2021). Numerous studies have demonstrated that environmental factors, such as humidity, temperature, CO_2, and light, significantly impact the survival of respiratory pathogens (Guo et al., 2021; Lin et al., 2020; Luo et al., 2023; Niazi et al., 2021b; Schuit et al., 2020; Smither et al., 2020). However, it is important to note that in real-world conditions, these environmental factors are not direct determinants of pathogen survival. Instead, they act indirectly by altering the physicochemical properties of exhaled respiratory droplets, thereby influencing the survival and infectivity of the pathogens loaded within. However, research on the physicochemical transformations that respiratory droplets undergo after exhalation, especially under varying environmental conditions, remains limited.

To address this gap, this thesis investigated the physicochemical behavior of respiratory droplets following exhalation, with a particular focus on evaporation and hygroscopic growth behavior, phase transitions, and final droplet morphology. Three systems were studied: artificial saliva droplets with and without mucin, NaCl-mucin droplets, and NaCl-albumin droplets. The

latter two served as simplified model respiratory systems to isolate and examine the effects of two important biologically relevant proteins. Mucin is highly abundant in saliva, while albumin is more prevalent in lung fluids (Pöhlker et al., 2023). This distinction enables a deeper understanding of whether respiratory droplets originating from different regions of the respiratory tract exhibit different evaporation behavior, hygroscopic behavior, and morphological structures, which can influence their potential for both airborne and surface-mediated transmission.

In the following two sections, I summarized the key findings based on experimental results across the three different systems, discussed their implications for the environmental behavior of respiratory droplets and the spread of pathogens, and identified open questions as well as the importance of this work for other fields of research.

4.1 Conclusions and implications for airborne transmission of respiratory pathogens

The evaporation and hygroscopic growth behavior of levitated droplets were studied using an EDB. The evolution of microphysical structure, morphology, and phase state of levitated droplets were investigated using SEM, HSV camera, and light scattering patterns. The results and key findings from three model respiratory systems as well as the implications for airborne transmission of respiratory pathogens are summarized in the following:

Measurements of artificial saliva system: The measurements on artificial saliva highlight the complex interplay between organic and inorganic components in determining droplet behavior under varying RH conditions, revealing the significant role of mucin in shaping the physicochemical properties of respiratory droplets. A direct comparison between artificial saliva droplets with and without mucin demonstrates that mucin not only influences evaporation kinetics but also alters the equilibrium thermodynamic state of droplets. Under dry conditions (lower than 45% RH), mucin tends to form a semi-permeable, viscous surface layer that enables the droplet to retain water, potentially creating a microenvironment conducive to pathogen survival. Additionally, mucin contributes to the prolonged maintenance of a spherical droplet shape during dehydration. Moreover, it impedes rehydration, leading to reduced hygroscopic growth and a smaller final droplet size after water uptake.

Measurements of NaCl-mucin system: This simplified NaCl-mucin system, serving as a surrogate model for saliva, enables a more detailed depiction of the role of mucin in respiratory

droplets. Given mucin's tendency to form a semi-permeable, viscous surface layer at the concentration of 0.6 g/L under dry conditions, the system was employed to test more mucin concentrations and explore the corresponding physicochemical mechanisms. The results indicate that mucin concentration has minimal effect on the evaporation kinetics under dry conditions (30% RH); however, under humid conditions (80% RH), droplets with higher mucin content exhibit noticeably slower evaporation rate. Mucin also influences the droplet equilibrium thermodynamics: increased mucin concentrations lead to larger equilibrium droplet sizes and greater residual water retention. SEM images reveal that the droplet morphology and phase state are closely linked to both RH and mucin content. It is confirmed that most mucin migrates to the droplet surface during evaporation under dry conditions, forming a viscous outer layer that envelops NaCl crystals. However, there is still a smaller fraction of mucin remains in the central part, coexisting with NaCl crystals. As mucin concentration increases, the outer mucin layer thickens progressively, eventually forming a complete coating over the NaCl crystals and rendering them visually undetectable. This layer significantly affects both efflorescence and deliquescence behaviors of droplets: with increasing mucin content, both the ERH and DRH decrease. These findings suggest that the mucin layer acts as a semi-permeable physical barrier, slowing water loss and inhibiting NaCl efflorescence during dehydration, while facilitating earlier water uptake and promoting NaCl deliquescence during rehydration. However, droplets with higher mucin content are unable to fully recover their original size during rehydration, with water uptake capacity becoming increasingly suppressed as mucin concentration increases.

Measurements of NaCl-albumin system: NaCl-albumin, serving as another simplified model of respiratory fluid, extends the scope of this research from saliva to lung fluid by enabling comparisons of the physicochemical properties of droplets originating from different regions of the respiratory tract. This simplified model emphasizes the role of protein composition in influencing the respiratory droplet behavior. Experimental results show that the presence of albumin accelerates droplet evaporation. Under identical conditions, droplets with higher albumin concentrations exhibit faster evaporation rates compared to NaCl solution droplets and undergo morphological transitions at earlier stages. In the late stages of evaporation, droplets experience a sudden and pronounced structural transformation, from an initially homogeneous spherical shape to a highly irregular, UFO-like/bowl-like morphology. SEM images reveal that this highly irregular structure consists of a gel-like albumin film in the center part with NaCl crystals forming around the periphery, which are fully covered by the semi-transparent albumin film. As the albumin content increases, the peripheral NaCl crystals become less visible, and

the overall morphology increasingly resembles that of pure albumin residues, indicating that albumin plays a dominant role in determining the final structure and morphology. This albumin film also appears capable of retaining some water; however, the exact amount cannot be quantified in this study. In addition, albumin exhibits a strong tendency to migrate toward the droplet interface, even under highly humid conditions. This interfacial migration can disrupt internal homogeneity and contribute to structural deformation during phase transitions. As a result, albumin influences both efflorescence and deliquescence behaviors of NaCl. While the presence of albumin slightly reduces the ERH, suggesting that albumin can inhibit NaCl crystallization to some extent, this effect does not show a strong dependence on albumin concentration. In contrast, albumin concentration has a pronounced influence on deliquescence behavior. At higher albumin concentrations, the DRH shifts to elevated values, and droplets exhibit a disturbance ("jump and fall") in apparent size during rehydration, indicating internal restructuring and morphological reconstruction prior to reaching equilibrium. Notably, despite inducing significant structural deformation and reshaping, albumin does not alter the final hygroscopicity of the droplets. This underscores albumin's unique role in modulating water uptake behavior and phase transitions, particularly in lung-derived respiratory droplets.

Implications for airborne transmission of respiratory pathogens: The findings from the artificial saliva, NaCl-mucin, and NaCl-albumin systems collectively demonstrate that respiratory droplet composition plays a critical role in determining their evaporation behavior, phase transitions, final morphology, and water uptake capacity, all of which directly influence droplet fate in the air and on surfaces, as well as the transmission potential of loaded pathogens. Mucin promotes the formation of compact, relatively spherical residues that stabilize the droplet structure during evaporation. As a result, mucin-rich droplets, such as those originating from the oral cavity, are likely to remain airborne for some time before settling onto surfaces. In contrast, albumin-rich droplets, which are more representative of deep lung fluids, tend to adopt highly irregular shapes with lower effective density upon drying, potentially leading to longer airborne lifetimes. However, their ability to retain water and delay salt crystallization may enhance pathogen viability, thereby increasing the risk of fomite-based transmission. Furthermore, respiratory droplets that form a solid organic surface layer prior to deposition are more likely to be resuspended into the air by human activity or air movement (Nikfar et al., 2021), facilitating their re-entry into the respiratory tract. Mucin-rich droplets, due to their lower hygroscopic growth and smaller rehydrated size, may penetrate deeper into the lungs, potentially increasing the risk infections. In contrast, albumin-rich droplets, with their larger size and irregular morphology upon rehydration, are more likely to be captured in the upper

respiratory tract (Guo et al., 2020). Importantly, changes in physicochemical properties directly linked to survivability of pathogens. Mucin has been shown to offer protective effects for viruses in aerosols, even under dry conditions (Lin and Marr, 2020; Zuo et al., 2014; Alexander et al., 2022). Our findings provide a possible explanation for this phenomenon: the compact mucin surface layer retains water and shields viruses from environmental stresses, thereby enhancing viral stability. In contrast, albumin-rich droplets lack a similarly rigid protective shell under dry conditions. Although albumin has been reported to preserve the infectivity of bacteriophages like MS2 and phi6 under intermediate and high humidity (Lin et al., 2020), this effect diminishes at low RH. Our results suggest that the thin albumin film formed under dry conditions is insufficient to protect viral particles, leading to inactivation through rapid water loss and elevated solute concentrations. In contrast, under humid conditions, albumin-rich droplets remain more liquid-like, supporting higher pathogen survival rates.

4.2 Outlook

This thesis systematically investigated the physicochemical transformations of model respiratory droplets under varying RH conditions, with a particular focus on how two key protein components, mucin and albumin, influence evaporation behavior, phase transitions, structure and morphology, and hygroscopic growth behavior. These insights significantly advance our understanding of the physicochemical behavior of respiratory droplets and offer important implications for the airborne transmission of infectious pathogens.

Despite these advances, several important questions remain unresolved. While the results provide strong evidence that mucin and albumin differentially affect droplet behavior, in physiological reality, these proteins coexist rather than act in isolation (Pöhlker et al., 2023). This raises a critical question: how do droplets behave when both mucin and albumin are present simultaneously? Given that mucin promotes the preservation of droplet morphology through the formation of a dense, semi-permeable outer layer, while albumin significantly disrupts droplet shape and structure even at relatively low concentrations, the interplay between these two proteins may introduce complex phase behaviors and structural transformations. It remains unclear how such coexistence would affect droplet hygroscopicity, phase transitions, and ultimately, the airborne lifetime and pathogen survival within these droplets.

Furthermore, future studies should extend simplified model respiratory systems to encompass more realistic, multi-component droplet compositions. These may include lipids, surfactants, enzymes, and even viable pathogens (Boat and Cheng, 1980; Larsson et al., 2012; Wang et al.,

2021). An important emerging area of research involves understanding the influence of pH dynamics on respiratory droplet behavior after exhalation (Luo et al., 2023; Haddrell et al., 2023; Haddrell et al., 2024). Since pH changes can modulate protein conformation and phase behavior, their impact on mucin-rich or albumin-rich droplets may significantly affect both droplet transformation and pathogen viability.

Finally, this study demonstrates that droplets originating from different regions of the respiratory tract exhibit distinct physicochemical behaviors after exhalation. These differences could influence not only primary transmission pathways, such as airborne and fomite-based transmission, but also the risk associated with secondary inhalation. Differentiating between upper and lower respiratory tract droplets based on biochemical characteristics is therefore crucial for accurate transmission modeling and risk assessment. Integrating this knowledge into infection control strategies such as indoor ventilation design, surface disinfection practices, and public health guidance, could significantly enhance our ability to mitigate the spread of respiratory pathogens, especially during future outbreaks or pandemics.

References

Absolom, D. R., Van Oss, C. J., Zingg, W., and Neumann, A. W.: Determination of surface tensions of proteins II. Surface tension of serum albumin, altered at the protein-air interface, *Biochimica et Biophysica Acta (BBA) - Protein Structure*, 670, 74-78, 10.1016/0005-2795(81)90050-7, 1981.

Ahlawat, A., Wiedensohler, A., and Mishra, S. K.: An Overview on the role of relative humidity in airborne transmission of SARS-CoV-2 in indoor environments, *Aerosol and Air Quality Research*, 20, 1856-1861, 10.4209/aaqr.2020.06.0302, 2020.

Ahn, K. H., Kim, S. M., Jung, H. J., Lee, M. J., Eom, H. J., Maskey, S., and Ro, C. U.: Combined use of optical and electron microscopic techniques for the measurement of hygroscopic property, chemical composition, and morphology of individual aerosol particles, *Analytical Chemistry*, 82, 7999-8009, 10.1021/ac101432y, 2010.

Albayrak, C., Barim, G., and Dag, O.: Effect of hygroscopicity of the metal salt on the formation and air stability of lyotropic liquid crystalline mesophases in hydrated salt-surfactant systems, *Journal of Colloid and Interface Science*, 433, 26-33, 10.1016/j.jcis.2014.07.008, 2014.

Alexander, R. W., Tian, J., Haddrell, A. E., Oswin, H. P., Neal, E., Hardy, D. A., Otero-Fernandez, M., Mann, J. F. S., Cogan, T. A., Finn, A., Davidson, A. D., Hill, D. J., and Reid, J. P.: Mucin transiently sustains coronavirus infectivity through heterogenous changes in phase morphology of evaporating aerosol, *Viruses*, 14, 10.3390/v14091856, 2022.

Ali, M., Lillehoj, E. P., Park, Y., Kyo, Y., and Kim, K. C.: Analysis of the proteome of human airway epithelial secretions, *Proteome Science*, 9, 4, 10.1186/1477-5956-9-4, 2011.

Alshawa, A., Dopfer, O., Harmon, C. W., Nizkorodov, S. A., and Underwood, J. S.: Hygroscopic growth and deliquescence of NaCl nanoparticles coated with surfactant AOT, *The Journal of Physical Chemistry A*, 113, 7678-7686, 10.1021/jp809869r, 2009.

Aquilano, D., Pastero, L., Bruno, M., and Rubbo, M.: {100} and {111} forms of the NaCl crystals coexisting in growth from pure aqueous solution, *Journal of Crystal Growth*, 311, 399-403, 10.1016/j.jcrysgro.2008.11.006, 2009.

Backstrom, M., Ambort, D., Thomsson, E., Johansson, M. E., and Hansson, G. C.: Increased understanding of the biochemistry and biosynthesis of MUC2 and other gel-forming mucins through the recombinant expression of their protein domains, *Molecular Biotechnology*, 54, 250-256, 10.1007/s12033-012-9562-3, 2013.

Balabushevich, N.G., Sholina, E.A., Mikhalchik, E.V., Filatova, L.Y., Vikulina, A.S., and Volodkin, D.: Self-assembled mucin-containing microcarriers via hard templating on $CaCO_3$ Crystals, *Micromachines*, 9, 307, 10.3390/mi9060307, 2018.

Baliga, S., Muglikar, S., and Kale, R.: Salivary pH: A diagnostic biomarker, *Journal of Indian Society of Periodontology*, 17, 461-465, 10.4103/0972-124X.118317, 2013.

Bansil, R. and Turner, B. S.: Mucin structure, aggregation, physiological functions and biomedical applications, *Current Opinion in Colloid & Interface Science*, 11, 164-170, 10.1016/j.cocis.2005.11.001, 2006.

Bar Dayan, Y., Vilkin, A., and Niv, Y.: Gallbladder mucin plays a role in gallstone formation, *European Journal of Internal Medicine*, 15, 411-414, 10.1016/j.ejim.2004.07.010, 2004.

Bardow, A., Moe, D., Nyvad, B., and Nauntofte, B.: The buffer capacity and buffer systems of human whole saliva measured without loss of CO_2, *Archives of Oral Biology*, 45, 1-12, 10.1016/S0003-9969(99)00119-3, 2000.

Bicer, E. M.: Compositional characterisation of human respiratory tract lining fluids for the design of disease specific simulants (Doctoral dissertation, King's College London), 2015.

Boat, T. F. and Cheng, P. W.: Biochemistry of airway mucus secretions, *Federation Proceedings*, 39, 3067–3074, 1980.

Bogdanovica, S., Zemitis, J., and Bogdanovics, R.: The Effect of CO_2 concentration on children's well-being during the process of learning, *Energies*, 13, 10.3390/en13226099, 2020.

Bohren, C. F. and Huffman, D. R.: Absorption and scattering by a sphere, in: absorption and scattering of light by small particles, edited by: Craig F. Bohren, and Huffman, D. R., 82-129, 10.1002/9783527618156.ch4, 1998.

Borisover, M. D., Sirotkin, V. A., and Solomonov, B. N.: Thermodynamics of water binding by human serum albumin suspended in acetonitrile, *Thermochimica Acta*, 254, 47-53, 10.1016/0040-6031(94)02108-Z, 1995.

Boye, J. I., Alli, I., and Ismail, A. A.: Interactions Involved in the gelation of bovine serum albumin, *Journal of Agricultural and Food Chemistry*, 44, 996-1004, 10.1021/jf950529t, 1996.

Brahma, A., Mandal, C., and Bhattacharyya, D.: Characterization of a dimeric unfolding intermediate of bovine serum albumin under mildly acidic condition, *Biochimica et Biophysica Acta (BBA) - Proteins and Proteomics*, 1751, 159-169, 10.1016/j.bbapap.2005.06.007, 2005.

Bunio, L. B., Wang, J., Kannaiyan, R., and Gates, I. D.: Evaporation and crystallization of NaCl-water droplets suspended in air by acoustic levitation, *Chemical Engineering Science*, 251, 10.1016/j.ces.2022.117441, 2022.

Campbell, R. A., Ang, J. C., Sebastiani, F., Tummino, A., and White, J. W.: Spread films of human serum albumin at the air-water interface: optimization, morphology, and durability, *Langmuir*, 31, 13535-13542, 10.1021/acs.langmuir.5b03349, 2015.

Campos Munoz, A., Jain, N. K., and Gupta, M.: Albumin Colloid. *BTI - StatPearls*, 2024.

Chace, K. V., Naziruddin, B., Desai, V. C., Flux, M., and Sachdev, G. P.: Physical properties of purified human respiratory mucus glycoproteins: effects of sodium chloride concentration on the aggregation properties and shape, *Experimental Lung Research*, 15, 721-737, 10.3109/01902148909062857, 1989.

Chen, X., Zhou, X., Xia, X., Xie, X., Lu, P., and Feng, Y.: Modeling of the transport, hygroscopic growth, and deposition of multi-component droplets in a simplified airway with realistic thermal boundary conditions, *Journal of Aerosol Science*, 151, 105626, 10.1016/j.jaerosci.2020.105626, 2021.

Choi, M. and Chan, C.: The effects of organic species on the hygroscopic behaviors of inorganic aerosols, *Environmental Science & Technology*, 36, 2422-2428, 10.1021/es0113293, 2002.

Corfield, A. P.: Mucins: a biologically relevant glycan barrier in mucosal protection, *Biochimica et Biophysica Acta (BBA) – General Subjects*, 1850, 236-252, 10.1016/j.bbagen.2014.05.003, 2015.

Curnutt, A., Smith, K., Darrow, E., and Walters, K. B.: Chemical and microstructural characterization of pH and [$Ca(^{2+})$] dependent sol-gel transitions in mucin biopolymer, *Scientific Reports*, 10, 8760, 10.1038/s41598-020-65392-4, 2020.

Dalla Barba, F., Wang, J., and Picano, F.: Revisiting D^2-law for the evaporation of dilute droplets, *Physics of Fluids*, 33, 051701, 10.1063/5.0051078, 2021.

Davies, J. F., Price, C. L., Choczynski, J., and Kohli, R. K.: Hygroscopic growth of simulated lung fluid aerosol particles under ambient environmental conditions, *Chemical Communications*, 57, 3243-3246, 10.1039/d1cc00066g, 2021.

Davis, E. J. and Schweiger, G.: The airborne microparticle: Its physics, chemistry, optic, and transport phenomena, *Springer Science & Business Media*, 10.1007/978-3-642-56152-8, 2002.

Delliere, S., Neveux, N., De Bandt, J. P., and Cynober, L.: Transthyretin for the routine assessment of malnutrition: A clinical dilemma highlighted by an international survey of experts in the field, *Clinical Nutrition*, 37, 2226-2229, 10.1016/j.clnu.2018.09.021, 2018.

Dong, Q., Yu, C., Li, L., Nie, L., Zhang, H., and Zang, H.: Analysis of hydration water around human serum albumin using near-infrared spectroscopy, *International Journal of Biological Macromolecules*, 138, 927-932, 10.1016/j.ijbiomac.2019.07.183, 2019.

Du, J., Lewis, O. L., Keener, J. P., and Fogelson, A. L.: Modeling and simulation of the ion-binding-mediated swelling dynamics of mucin-like polyelectrolyte gels, *Gels*, 7, 10.3390/gels7040244, 2021.

Duft, D.: Laborexperimente zur Mikrophysik der Wolken, Dissertation, 2011.

Duft, D., Achtzehn, T., Müller, R., Huber, B. A., Leisner, T.: Coulomb fission: Rayleigh jets from levitated microdroplets, *Nature*, 421, 128, 10.1038/421128a, 2003.

Easa, A. M., Hill, S. E., Mitchell, J. R., and Taylor, A. J.: Bovine serum albumin gelation as a result of the Maillard reaction, *Food Hydrocolloids*, 10, 199-202, 10.1016/S0268-005X(96)80035-X, 1996.

Ebert, M., Weinbruch, S., Rausch, A., Gorzawski, G., Helas, G., Hoffmann, P., and Wex, H.: Complex refractive index of aerosols during LACE 98#x2010; as derived from the analysis of individual particles, *Journal of Geophysical Research: Atmospheres*, 107, 10.1029/2000jd000195, 2002.

Effros, R. M., Peterson, B., Casaburi, R., Su, J., Dunning, M., Torday, J., Biller, J., and Shaker, R.: Epithelial lining fluid solute concentrations in chronic obstructive lung disease patients and normal subjects, *Journal of applied physiology (Bethesda, Md. : 1985)*, 99(4), 1286–1292, 10.1152/japplphysiol.00362.2005, 2005.

Egesten, A., Frick, I. M., Morgelin, M., Olin, A. I., and Bjorck, L.: Binding of albumin promotes bacterial survival at the epithelial surface, *Journal of Biological Chemistry*, 286, 2469-2476, 10.1074/jbc.M110.148171, 2011.

Elzoghby, A. O., Samy, W. M., and Elgindy, N. A.: Albumin-based nanoparticles as potential controlled release drug delivery systems, *Journal of controlled release : official journal of the Controlled Release Society*, 157, 168-182, 10.1016/j.jconrel.2011.07.031, 2012.

Gao, Y., Yu, L. E., and Chen, S. B.: Effects of organics on efflorescence relative humidity of ammonium sulfate or sodium chloride particles, *Atmospheric Environment*, 42, 4433-4445, 10.1016/j.atmosenv.2008.02.002, 2008.

Garcia-Fojeda B., González-Carnicero Z., de Lorenzo A., Minutti C. M., de Tapia L., Euba B., Iglesias-Ceacero A., Castillo-Lluva S., Garmendia J. and Casals C.: Lung Surfactant Lipids Provide Immune Protection Against Haemophilus influenzae Respiratory Infection. *Frontiers in immunology*, 10, 458, 10.3389/fimmu.2019.00458, 2019.

Gosal, W. and Ross-Murphy, S.: Globular protein gelation, *Current Opinion in Colloid & Interface Science*, 5, 188-194, 10.1016/S1359-0294(00)00057-1, 2000.

Groth, R., Cravigan, L. T., Niazi, S., Ristovski, Z., and Johnson, G. R.: In situ measurements of human cough aerosol hygroscopicity, *Journal of the Royal Society, Interface*, 18, 20210209, 10.1098/rsif.2021.0209, 2021.

Guo, L., Yang, Z., Zhang, L., Wang, S., Bai, T., Xiang, Y., and Long, E.: Systematic review of the effects of environmental factors on virus inactivation: implications for coronavirus disease 2019, *International Journal of Environmental Science and Technology*, 18, 2865-2878, 10.1007/s13762-021-03495-9, 2021.

Guo, Y., Wei, J., Ou, C., Liu, L., Sadrizadeh, S., Jin, T., Tang, L., Zhang, Y., and Li, Y.: Deposition of droplets from the trachea or bronchus in the respiratory tract during exhalation: A steady-state numerical investigation, *Aerosol Science and Technology*, 54, 869-879, 10.1080/02786826.2020.1772459, 2020.

Gustin, K. M., Belser, J. A., Veguilla, V., Zeng, H., Katz, J. M., Tumpey, T. M., and Maines, T. R.: Environmental conditions affect exhalation of H3N2 seasonal and variant influenza viruses and respiratory droplet transmission in ferrets, *PLoS One*, 10, e0125874, 10.1371/journal.pone.0125874, 2015.

Haddrell, A., Lewis, D., Church, T., and Reid, J.: Novel instrument to measure water uptake, dissolution and hygroscopic growth of an individual levitated aerosol particle in an environment identical to the lung (relative humidity > 99.5%), *Aerosol Science and Technology*, 58, 915-929, 10.1080/02786826.2024.2330482, 2024.

Haddrell, A., Otero-Fernandez, M., Oswin, H., Cogan, T., Bazire, J., Tian, J., Alexander, R., Mann, J. F. S., Hill, D., Finn, A., Davidson, A. D., and Reid, J. P.: Differences in airborne stability of SARS-CoV-2 variants of concern is impacted by alkalinity of surrogates of respiratory aerosol, *Journal of the Royal Society, Interface*, 20, 20230062, 10.1098/rsif.2023.0062, 2023.

Han, S. and Mallampalli, R. K.: The Role of Surfactant in Lung Disease and Host Defense against Pulmonary Infections, *Annals of the American Thoracic Society*, 12(5), 765–774, 10.1513/AnnalsATS.201411-507FR, 2015.

Hardy, D. A., Robinson, J. F., Hilditch, T. G., Neal, E., Lemaitre, P., Walker, J. S., and Reid, J. P.: Accurate measurements and simulations of the evaporation and trajectories of

individual solution droplets, *The journal of physical chemistry. B*, 127, 3416-3430, 10.1021/acs.jpcb.2c08909, 2023.

Harmon, C. W., Grimm, R. L., McIntire, T. M., Peterson, M. D., Njegic, B., Angel, V. M., Alshawa, A., Underwood, J. S., Tobias, D. J., Gerber, R. B., Gordon, M. S., Hemminger, J. C., & Nizkorodov, S. A.: Hygroscopic growth and deliquescence of NaCl nanoparticles mixed with surfactant SDS. *The journal of physical chemistry. B*, 114(7), 2435–2449, 10.1021/jp909661q, 2010.

Hinds, W.C.: Aerosol Technology, Properties, Behaviour, and Measurement of Airborne Particles. *John Wiley & Sons Inc*., New York, 1999

Hoffmann, N.: Experimental study on the contact freezing of supercooled micro-droplets in electrodynamic balance, Dissertation 2015.

Hribar, B., Southall, N. T., Vlachy, V., and Dill, K. A.: How ions affect the structure of water. *Journal of the American Chemical Society*, 124(41), 12302–12311, 10.1021/ja026014h, 2002.

Huang, B. X., Kim, H. Y., and Dass, C.: Probing three-dimensional structure of bovine serum albumin by chemical cross-linking and mass spectrometry, *J. Am. Soc. Mass Spectrom.*, 15, 1237-1247, 10.1016/j.jasms.2004.05.004, 2004.

Hutapea, T. P. H., Madurani, K. A., Syahputra, M. Y., Hudha, M. N., Asriana, A. N., Suprapto, and Kurniawan, F.: Albumin: Source, preparation, determination, applications, and prospects, *Journal of Science: Advanced Materials and Devices*, 8, 10.1016/j.jsamd.2023.100549, 2023.

Huynh, E., Olinger, A., Woolley, D., Kohli, R. K., Choczynski, J. M., Davies, J. F., Lin, K., Marr, L. C., and Davis, R. D.: Evidence for a semisolid phase state of aerosols and droplets relevant to the airborne and surface survival of pathogens, Proc. *Natl. Acad. Sci. U S A*, 119, 10.1073/pnas.2109750119, 2022.

Jing, B., Peng, C., Wang, Y., Liu, Q., Tong, S., Zhang, Y., and Ge, M. F.: Hygroscopic properties of potassium chloride and its internal mixtures with organic compounds relevant to biomass burning aerosol particles, *Scientific Reports*, 7, 43572, 10.1038/srep43572, 2017.

Johnson, G. R., Morawska, L., Ristovski, Z. D., Hargreaves, M., Mengersen, K., Chao, C. Y. H., Wan, M. P., Li, Y., Xie, X., Katoshevski, D., and Corbett, S.: Modality of human expired aerosol size distributions, *Journal of Aerosol Science*, 42, 839-851, 10.1016/j.jaerosci.2011.07.009, 2011.

Kesimer, M., Ford, A. A., Ceppe, A., Radicioni, G., Cao, R., Davis, C. W., Doerschuk, C. M., Alexis, N. E., Anderson, W. H., Henderson, A. G., Barr, R. G., Bleecker, E. R., Christenson, S. A., Cooper, C. B., Han, M. K., Hansel, N. N., Hastie, A. T., Hoffman, E. A., Kanner, R. E., Martinez, F., Paine, R., 3rd, Woodruff, P. G., O'Neal, W. K., and Boucher, R. C.: Airway mucin concentration as a marker of chronic bronchitis, *N. Engl. J. Med.*, 377, 911-922, 10.1056/NEJMoa1701632, 2017.

Khor, Y. H., Teoh, A. K., Lam, S. M., Mo, D. C., Weston, S., Reid, D. W., and Walters, E. H.: Increased vascular permeability precedes cellular inflammation as asthma control deteriorates, *Clin. Exp. Allergy*, 39, 1659-1667, 10.1111/j.1365-2222.2009.03349.x, 2009.

Kubala, E., Strzelecka, P., Grzegocka, M., Lietz-Kijak, D., Gronwald, H., Skomro, P., and Kijak, E.: A Review of selected studies that determine the physical and chemical properties of saliva in the field of dental treatment, *Biomed. Res. Int.*, 6572381, 10.1155/2018/6572381, 2018.

Kudo, E., Song, E., Yockey, L. J., Rakib, T., Wong, P. W., Homer, R. J., and Iwasaki, A.: Low ambient humidity impairs barrier function and innate resistance against influenza infection, *Proc. Natl. Acad. Sci. U S A*, 116, 10905-10910, 10.1073/pnas.1902840116, 2019.

Langmuir, I.: The evaporation of small spheres, *Physical Review*, 12, 368-370, 10.1103/PhysRev.12.368, 1918.

Larsson, P., Mirgorodskaya, E., Samuelsson, L., Bake, B., Almstrand, A. C., Bredberg, A., and Olin, A. C.: Surfactant protein A and albumin in particles in exhaled air, *Respir. Med.*, 106, 197-204, 10.1016/j.rmed.2011.10.008, 2012.

Lewis, D.: Why the WHO took two years to say COVID is airborne, *Nature*, 604, 26-31, 10.1038/d41586-022-00925-7, 2022.

Li, L., Li, Z., Bi, J., Li, H., Wang, S., Shao, C., and Song, Y.: The association between serum albumin/prealbumin level and disease severity in non-CF bronchiectasis, *Clin. Exp. Pharmacol. Physiol.*, 47, 1537-1544, 10.1111/1440-1681.13331, 2020.

Li, X., Gupta, D., Eom, H. J., Kim, H., and Ro, C. U.: Deliquescence and efflorescence behavior of individual NaCl and KCl mixture aerosol particles, *Atmospheric Environment*, 82, 36-43, 10.1016/j.atmosenv.2013.10.011, 2014.

Lieber, C., Melekidis, S., Koch, R., and Bauer, H. J.: Insights into the evaporation characteristics of saliva droplets and aerosols: Levitation experiments and numerical modeling, *J. Aerosol Sci.*, 154, 105760, 10.1016/j.jaerosci.2021.105760, 2021.

Lin, K. and Marr, L. C.: Humidity-dependent decay of viruses, but not bacteria, in aerosols and droplets follows disinfection kinetics, *Environ. Sci. Technol.*, 54, 1024-1032, 10.1021/acs.est.9b04959, 2020.

Lin, K., Schulte, C. R., and Marr, L. C.: Survival of MS2 and Phi6 viruses in droplets as a function of relative humidity, pH, and salt, protein, and surfactant concentrations, *PLoS One*, 15, e0243505, 10.1371/journal.pone.0243505, 2020.

Liu, J. and Duan, Y.: Saliva: a potential media for disease diagnostics and monitoring, *Oral Oncol.*, 48, 569-577, 10.1016/j.oraloncology.2012.01.021, 2012.

Liu, L., Wei, J., Li, Y., and Ooi, A.: Evaporation and dispersion of respiratory droplets from coughing, *Indoor Air*, 27, 179-190, 10.1111/ina.12297, 2017.

Liu, Q., Wu, B., Xie, R., Luo, Y., Zheng, D., Liu, G., and Zhang, H.: Association between serum albumin and pulmonary function in adolescents: analyses of NHANES 2007-2012, *BMC Pulm Med.*, 24, 554, 10.1186/s12890-024-03341-x, 2024.

Liu, Y., Li, T., Deng, Y., Liu, S., Zhang, D., Li, H., Wang, X., Jia, L., Han, J., Bei, Z., Li, L., and Li, J.: Stability of SARS-CoV-2 on environmental surfaces and in human excreta, *J. Hosp. Infect.*, 107, 105-107, 10.1016/j.jhin.2020.10.021, 2021.

Lowen, A. C., Mubareka, S., Steel, J., and Palese, P.: Influenza virus transmission is dependent on relative humidity and temperature. *PLoS pathogens*, 3(10), 1470–1476, 10.1371/journal.ppat.0030151, 2007.

Luo, B., Schaub, A., Glas, I., Klein, L. K., David, S. C., Bluvshtein, N., Violaki, K., Motos, G., Pohl, M. O., Hugentobler, W., Nenes, A., Krieger, U. K., Stertz, S., Peter, T., and Kohn, T.: Expiratory aerosol pH: the overlooked driver of airborne virus inactivation, *Environ. Sci. Technol.*, 57, 486-497, 10.1021/acs.est.2c05777, 2023.

Majorek, K. A., Porebski, P. J., Dayal, A., Zimmerman, M. D., Jablonska, K., Stewart, A. J., Chruszcz, M., and Minor, W.: Structural and immunologic characterization of bovine, horse, and rabbit serum albumins, *Mol. Immunol.*, 52, 174-182, 10.1016/j.molimm.2012.05.011, 2012.

Marr, L. C., Tang, J. W., Van Mullekom, J., and Lakdawala, S. S.: Mechanistic insights into the effect of humidity on airborne influenza virus survival, transmission and incidence, *J. R. Soc. Interface*, 16, 20180298, 10.1098/rsif.2018.0298, 2019.

McCullagh, C. M., Jamieson, A. M., Blackwell, J., and Gupta, R.: Viscoelastic properties of human tracheobronchial mucin in aqueous solution, *Biopolymers*, 35, 149-159, 10.1002/bip.360350203, 1995.

Meng, Y., Kiselev, A., Duft, D., Dresch, T., and Leisner, T.: Role of mucin in controlling evaporation and hygroscopic behavior of human respiratory droplets and potential implications for spreading of pathogens, *Aerosol Science and Technology*, 59, 1122-1136, 10.1080/02786826.2025.2505036, 2025.

Meurman, J. H., Rantonen, P., Pajukoski, H., and Sulkava, R.: Salivary albumin and other constituents and their relation to oral and general health in the elderly, *Oral Surg. Oral Med. Oral Pathol. Oral Radiol. Endod.*, 94, 432-438, 10.1067/moe.2002.122345, 2002.

Mikhailov, E., Vlasenko, S., Niessner, R., and Pöschl, U.: Interaction of aerosol particles composed of protein and saltswith water vapor: hygroscopic growth and microstructural rearrangement, *Atmos. Chem. Phys.*, 4, 323-350, 10.5194/acp-4-323-2004, 2004.

Mikos, A. G. and Peppas, N. A.: Measurement of the surface tension of mucin solutions, *International Journal of Pharmaceutics*, 53, 1-5, 10.1016/0378-5173(89)90354-2, 1989.

Mishra, V. and Heath, R. J.: Structural and biochemical features of human serum albumin essential for eukaryotic cell culture, *Int. J. Mol. Sci.*, 22, 10.3390/ijms22168411, 2021.

Morawska, L. and Cao, J.: Airborne transmission of SARS-CoV-2: The world should face the reality, *Environ. Int.*, 139, 105730, 10.1016/j.envint.2020.105730, 2020.

Morawska, L., Buonanno, G., Mikszewski, A., and Stabile, L.: The physics of respiratory particle generation, fate in the air, and inhalation, *Nat. Rev. Phys.*, 4, 723-734, 10.1038/s42254-022-00506-7, 2022.

Morawska, L., Johnson, G. R., Ristovski, Z. D., Hargreaves, M., Mengersen, K., Corbett, S., Chao, C. Y. H., Li, Y., and Katoshevski, D.: Size distribution and sites of origin of droplets expelled from the human respiratory tract during expiratory activities, *Journal of Aerosol Science*, 40, 256-269, 10.1016/j.jaerosci.2008.11.002, 2009.

Niazi, S., Groth, R., Cravigan, L., He, C., Tang, J. W., Spann, K., and Johnson, G. R.: Susceptibility of an airborne common cold virus to relative humidity, *Environ. Sci. Technol.*, 55, 499-508, 10.1021/acs.est.0c06197, 2021a.

Niazi, S., Short, K. R., Groth, R., Cravigan, L., Spann, K., Ristovski, Z., and Johnson, G. R.: Humidity-dependent survival of an airborne influenza A virus: practical implications

for controlling airborne viruses, *Environmental Science & Technology Letters*, 8, 412-418, 10.1021/acs.estlett.1c00253, 2021b.

Nicas, M., Nazaroff, W. W., and Hubbard, A.: Toward understanding the risk of secondary airborne infection: emission of respirable pathogens, *J. Occup. Environ. Hyg.*, 2, 143-154, 10.1080/15459620590918466, 2005.

Nikfar, M., Paul, R., Islam, K., Razizadeh, M., Jagota, A., and Liu, Y.: Respiratory droplet resuspension near surfaces: Modeling and analysis, *Journal of Applied Physics*, 130, 10.1063/5.0050447, 2021.

Nystrom, B., Kjoniksen, A. L., Beheshti, N., Maleki, A., Zhu, K., Knudsen, K. D., Pamies, R., Hernandez Cifre, J. G., and Garcia de la Torre, J.: Characterization of polyelectrolyte features in polysaccharide systems and mucin, *Adv. Colloid Interface Sci.*, 158, 108-118, 10.1016/j.cis.2009.05.003, 2010.

Oswin, H. P., Haddrell, A. E., Otero-Fernandez, M., Mann, J. F. S., Cogan, T. A., Hilditch, T. G., Tian, J., Hardy, D. A., Hill, D. J., Finn, A., Davidson, A. D., and Reid, J. P.: The dynamics of SARS-CoV-2 infectivity with changes in aerosol microenvironment, *Proc. Natl. Acad. Sci. U S A*, 119, e2200109119, 10.1073/pnas.2200109119, 2022.

Ozdemir, O., Karakashev, S. I., Nguyen, A. V., and Miller, J. D.: Adsorption and surface tension analysis of concentrated alkali halide brine solutions, *Minerals Engineering*, 22, 263-271, 10.1016/j.mineng.2008.08.001, 2009.

Pan, J., Duggal, N. K., Lakdawala, S. S., Rockey, N. C., and Marr, L. C.: Mucin colocalizes with influenza virus and preserves infectivity in deposited model respiratory droplets, *Environ. Sci. Technol.*, 59, 2192-2200, 10.1021/acs.est.4c10886, 2025.

Parienta, D., Morawska, L., Johnson, G. R., Ristovski, Z. D., Hargreaves, M., Mengersen, K., Corbett, S., Chao, C. Y. H., Li, Y., and Katoshevski, D.: Theoretical analysis of the motion and evaporation of exhaled respiratory droplets of mixed composition, *Journal of Aerosol Science*, 42, 1-10, 10.1016/j.jaerosci.2010.10.005, 2011.

Pastorino, B., Touret, F., Gilles, M., de Lamballerie, X., and Charrel, R. N.: Prolonged Infectivity of SARS-CoV-2 in Fomites, *Emerg. Infect. Dis.*, 26, 2256-2257, 10.3201/eid2609.201788, 2020.

Peng, C., Chen, L., and Tang, M.: A database for deliquescence and efflorescence relative humidities of compounds with atmospheric relevance, *Fundam. Res.*, 2, 578-587, 10.1016/j.fmre.2021.11.021, 2022.

Pöhlker, M. L., Pöhlker, C., Krüger, O. O., Förster, J. D., Berkemeier, T., Elbert, W., Fröhlich-Nowoisky, J., Pöschl, U., Bagheri, G., Bodenschatz, E., Huffman, J. A., Scheithauer, S., and Mikhailov, E.: Respiratory aerosols and droplets in the transmission of infectious diseases, *Reviews of Modern Physics*, 95, 10.1103/RevModPhys.95.045001, 2023.

Prather, K. A., Wang, C. C., and Schooley, R. T.: Reducing transmission of SARS-CoV-2, *Science*, 368, 1422-1424, 10.1126/science.abc6197, 2020.

Prussin, A. J., Schwake, D. O., Lin, K., Gallagher, D. L., Buttling, L., and Marr, L. C.: Survival of the enveloped virus Phi6 in droplets as a function of relative humidity, absolute humidity, and temperature. *Applied and environmental microbiology*, 84(12), e00551-18, 10.1128/AEM.00551-18, 2018.

Quinn, B., Rodman, N., Jara, E., Fernandez, J. S., Martinez, J., Traglia, G. M., Montana, S., Cantera, V., Place, K., Bonomo, R. A., Iriarte, A., and Ramirez, M. S.: Human serum albumin alters specific genes that can play a role in survival and persistence in Acinetobacter baumannii, *Sci. Rep.*, 8, 14741, 10.1038/s41598-018-33072-z, 2018.

Rahimi, P. and Ward, C.: Kinetics of Evaporation: Statistical Rate Theory Approach, *International Journal of Thermodynamics*, 8, 10.5541/ijot.142, 2005.

Richards, D. S., Trobaugh, K. L., Hajek-Herrera, J., Price, C. L., Sheldon, C. S., Davies, J. F., and Davis, R. D.: Ion-molecule interactions enable unexpected phase transitions in organic-inorganic aerosol. *Science advances*, 6(47), eabb5643, 10.1126/sciadv.abb5643, 2020.

Ridley, C., Kouvatsos, N., Raynal, B. D., Howard, M., Collins, R. F., Desseyn, J. L., Jowitt, T. A., Baldock, C., Davis, C. W., Hardingham, T. E., and Thornton, D. J.: Assembly of the respiratory mucin MUC5B: a new model for a gel-forming mucin, *J. Biol. Chem.*, 289, 16409-16420, 10.1074/jbc.M114.566679, 2014.

Santarpia, J. L., Reid, J. P., Wu, C.-Y., Lednicky, J. A., and Oswin, H. P.: The aerobiological pathway of natural respiratory viral aerosols, *TrAC Trends in Analytical Chemistry*, 172, 10.1016/j.trac.2024.117557, 2024.

Schuit, M., Ratnesar-Shumate, S., Yolitz, J., Williams, G., Weaver, W., Green, B., Miller, D., Krause, M., Beck, K., Wood, S., Holland, B., Bohannon, J., Freeburger, D., Hooper, I., Biryukov, J., Altamura, L. A., Wahl, V., Hevey, M., and Dabisch, P.: Airborne SARS-CoV-2 is rapidly inactivated by simulated sunlight, *J. Infect. Dis.*, 222, 564-571, 10.1093/infdis/jiaa334, 2020.

Selby C, Lobb P.A., and Jeffcoate W.J.: Sex hormone binding globulin in saliva, *Clinical Endocrinology*, 28(1), 19–24, 10.1111/j.1365-2265.1988.tb01198.x, 1988.

Seyfert, C., Rodríguez-Rodríguez, J., Lohse, D., and Marin, A.: Stability of respiratory-like droplets under evaporation, *Physical Review Fluids*, 7, 10.1103/PhysRevFluids.7.023603, 2022.

Smither, S. J., Eastaugh, L. S., Findlay, J. S., and Lever, M. S.: Experimental aerosol survival of SARS-CoV-2 in artificial saliva and tissue culture media at medium and high humidity, *Emerg. Microbes. Infect.*, 9, 1415-1417, 10.1080/22221751.2020.1777906, 2020.

Song, D., Cahn, D., and Duncan, G. A.: Mucin biopolymers and their barrier function at airway surfaces, *Langmuir*, 36, 12773-12783, 10.1021/acs.langmuir.0c02410, 2020.

Spicer, S. S. and Martinez, J. R.: Mucin biosynthesis and secretion in the respiratory tract, *Environ. Health. Perspect.*, 55, 193-204, 10.1289/ehp.8455193, 1984.

Stewart, D. J., Cai, C., Nayler, J., Preston, T. C., Reid, J. P., Krieger, U. K., Marcolli, C., and Zhang, Y. H.: Liquid-liquid phase separation in mixed organic/inorganic single aqueous aerosol droplets, *J. Phys. Chem. A*, 119, 4177-4190, 10.1021/acs.jpca.5b01658, 2015.

Takehara, S., Yanagishita, M., Podyma-Inoue, K. A., and Kawaguchi, Y.: Degradation of MUC7 and MUC5B in human saliva, *PLoS One*, 8, e69059, 10.1371/journal.pone.0069059, 2013.

Tang, I. N. and Munkelwitz, H. R.: Composition and temperature dependence of the deliquescence properties of hygroscopic aerosols, *Atmospheric Environment. Part A. General Topics*, 27, 467-473, https://doi.org/10.1016/0960-1686(93)90204-C, 1993.

Tang, J. W., Bahnfleth, W. P., Bluyssen, P. M., Buonanno, G., Jimenez, J. L., Kurnitski, J., Li, Y., Miller, S., Sekhar, C., Morawska, L., Marr, L. C., Melikov, A. K., Nazaroff, W. W., Nielsen, P. V., Tellier, R., Wargocki, P., and Dancer, S. J.: Dismantling myths on the airborne transmission of severe acute respiratory syndrome coronavirus-2 (SARS-CoV-2), *J. Hosp. Infect.*, 110, 89-96, 10.1016/j.jhin.2020.12.022, 2021.

Tantra, R., Tompkins, J., and Quincey, P.: Characterisation of the de-agglomeration effects of bovine serum albumin on nanoparticles in aqueous suspension, *Colloids Surf. B Biointerfaces*, 75, 275-281, 10.1016/j.colsurfb.2009.08.049, 2010.

Thornton, D. J., Rousseau, K., and McGuckin, M. A.: Structure and function of the polymeric mucins in airways mucus, *Annu. Rev. Physiol.*, 70, 459-486, 10.1146/annurev.physiol.70.113006.100702, 2008.

Tian, J., Alexander, R. W., Hardy, D. A., Hilditch, T. G., Oswin, H. P., Haddrell, A. E., and Reid, J. P.: The microphysics of surrogates of exhaled aerosols from the upper respiratory tract, *Aerosol Sci. Technol.*, 58, 461-474, 10.1080/02786826.2023.2299214, 2024.

Tian, J., Luo, B., Rafferty, A., Haddrell, A. E., Krieger, U. K., and Reid, J. P.; Measurements of surrogate respiratory sessile droplet pH and implications for exhaled respiratory aerosol and airborne disease transmission, *ACS Cent. Sci.*, 11, 6, 1009-1019, 10.1021/acscentsci.5c00284, 2025.

Tillett T.: Don't hold your breath: indoor CO_2 exposure and impaired decision making, *Environmental health perspectives*, 120(12), A475, 10.1289/ehp.120-a475a, 2012.

Ushida, K. and Murata, T.: Chapter 4 - Materials Science and Engineering of Mucin: A New Aspect of Mucin Chemistry, in: Studies in Natural Products Chemistry, edited by: *Atta ur, R., Elsevier*, 115-159, 10.1016/B978-0-444-62615-8.00004-7, 2013.

van Doremalen, N., Bushmaker, T., Morris, D. A.-O. X., Holbrook, M. G., Gamble, A., Williamson, B. N., Tamin, A., Harcourt, J. L., Thornburg, N. J., Gerber, S. I., Lloyd-Smith, J. A.-O. X., de Wit, E., and Munster, V. J.: Aerosol and surface stability of SARS-CoV-2 as compared with SARS-CoV-1, *The New England Journal of Medicine*, 382, 1564–1567, 10.1056/NEJMc2004973, 2020.

Varricchio, R., De Simone, G., Vita, G. M., Nocera Cariola, W., Viscardi, M., Brandi, S., Picazio, G., Zerbato, V., Koncan, R., Segat, L., Di Bella, S., Fusco, G., Ascenzi, P., and di Masi, A.: Human serum albumin binds spike protein and protects cells from SARS-CoV-2 infection by modulating the RAS pathway, *Aspects of Molecular Medicine*, 3, 10.1016/j.amolm.2023.100033, 2024.

Vejerano, E. P. and Marr, L. C.: Physico-chemical characteristics of evaporating respiratory fluid droplets, *J. R. Soc. Interface*, 15, 10.1098/rsif.2017.0939, 2018.

Vu, T. V., Shi, Z., and Harrison, R. M.: Estimation of hygroscopic growth properties of source-related sub-micrometre particle types in a mixed urban aerosol, *npj Climate and Atmospheric Science*, 4, 10.1038/s41612-021-00175-w, 2021.

Wagner, C. E., Wheeler, K. M., and Ribbeck, K.: Mucins and their role in shaping the functions of mucus barriers, *Annu. Rev. Cell Dev. Biol.*, 34, 189-215, 10.1146/annurev-cellbio-100617-062818, 2018.

Walker, J. S., Archer, J., Gregson, F. K. A., Michel, S. E. S., Bzdek, B. R., and Reid, J. P.: Accurate representations of the microphysical processes occurring during the transport of exhaled aerosols and droplets, *ACS Cent. Sci.*, 7, 200-209, 10.1021/acscentsci.0c01522, 2021.

Wang, C. C., Prather, K. A., Sznitman, J., Jimenez, J. L., Lakdawala, S. S., Tufekci, Z., and Marr, L. C.: Airborne transmission of respiratory viruses, *Science*, 373, 10.1126/science.abd9149, 2021.

Wang, J., Zhang, M., Wang, J., and Chen, R.: Coupling effects of human serum albumin and sodium chloride on biological desiccation patterns, *Heliyon*, 9, e19970, 10.1016/j.heliyon.2023.e19970, 2023.

Wang, L., Xu, H., Ren, W., Zhu, L., Chang, Y., Gu, Y., Yan, M., and He, J.: Low serum prealbumin levels in post-stroke depression, *Psychiatry Res.*, 246, 149-153, 10.1016/j.psychres.2016.09.021, 2016.

Wei, Y., Wang, C., Jiang, B., Sun, C. C., and Middaugh, C. R.: Developing biologics tablets: the effects of compression on the structure and stability of bovine serum albumin and lysozyme, *Mol. Pharm.*, 16, 1119-1131, 10.1021/acs.molpharmaceut.8b01118, 2019.

Wells, W. F.: On air-borne infection*: Study II. Droplets and Droplet Nuclei, *American Journal of Epidemiology*, 20, 611-618, 10.1093/oxfordjournals.aje.a118097, 1934.

Weston, A., Vladescu, S. C., Reddyhoff, T., Griffiths, A., Crouzier, T., Fielden, M., Garnett, J. A., and Carpenter, G. H.: The influence of ions on the lubricative abilities of mucin and the role of sialic acids, *Colloids Surf. B Biointerfaces*, 227, 113327, 10.1016/j.colsurfb.2023.113327, 2023.

Wexler, A. S. and Seinfeld, J. H.: Second-generation inorganic aerosol model, *Atmospheric Environment. Part A. General Topics*, 25, 2731-2748, 10.1016/0960-1686(91)90203-J, 1991.

Xie, X., Li, Y., Chwang, A. T., Ho, P. L., and Seto, W. H.: How far droplets can move in indoor environments--revisiting the Wells evaporation-falling curve, *Indoor Air*, 17, 211-225, 10.1111/j.1600-0668.2007.00469.x, 2007.

Yang, W., Elankumaran, S., and Marr, L. C.: Relationship between humidity and influenza A viability in droplets and implications for influenza's seasonality, *PLoS One*, 7, e46789, 10.1371/journal.pone.0046789, 2012.

Zeng, L., Li, J., Lv, M., Li, Z., Yao, L., Gao, J., Wu, Q., Wang, Z., Yang, X., Tang, G., Qu, G., and Jiang, G.: Environmental Stability and Transmissibility of Enveloped Viruses at Varied Animate and Inanimate Interfaces, *Environ. Health. (Washington, D.C.)*, 1, 15-31, 10.1021/envhealth.3c00005, 2023.

Zhang, C. and Carloni, P.: Salt effects on water/hydrophobic liquid interfaces: a molecular dynamics study, *J. Phys. Condens. Matter*, 24, 124109, 10.1088/0953-8984/24/12/124109, 2012.

Zhang, P., Wu, H. M., Shen, Q. Y., Liu, R. Y., and Qi, X. M.: Associations of pulmonary function with serum biomarkers and dialysis adequacy in patients undergoing peritoneal dialysis, *Clin. Exp. Nephrol.*, 20, 951-959, 10.1007/s10157-016-1244-1, 2016.

Zhang, T.: Study on surface tension and evaporation rate of human saliva, saline, and water droplets, Graduate Theses, Dissertations, and Problem Reports. 2271. https://researchrepository.wvu.edu/etd/2271, 2011.

Zieger, P., Vaisanen, O., Corbin, J. C., Partridge, D. G., Bastelberger, S., Mousavi-Fard, M., Rosati, B., Gysel, M., Krieger, U. K., Leck, C., Nenes, A., Riipinen, I., Virtanen, A., and Salter, M. E.: Revising the hygroscopicity of inorganic sea salt particles, *Nat. Commun.*, 8, 15883, 10.1038/ncomms15883, 2017.

Ziegler, G. R. and Foegeding, E. A.: The gelation of proteins, *Advances in Food and Nutrition Research*, 34, 203-298, 10.1016/S1043-4526(08)60008-X, 1990.

Zuend, A., Marcolli, C., Booth, A. M., Lienhard, D. M., Soonsin, V., Krieger, U. K., Topping, D. O., McFiggans, G., Peter, T., and Seinfeld, J. H.: New and extended parameterization of the thermodynamic model AIOMFAC: calculation of activity coefficients for organic-inorganic mixtures containing carboxyl, hydroxyl, carbonyl, ether, ester, alkenyl, alkyl, and aromatic functional groups, *Atmos. Chem. Phys.*, 11, 9155-9206, 10.5194/acp-11-9155-2011, 2011.

Zuo, Z., Kuehn, T. H., Bekele, A. Z., Mor, S. K., Verma, H., Goyal, S. M., Raynor, P. C., and Pui, D. Y.: Survival of airborne MS2 bacteriophage generated from human saliva, artificial saliva, and cell culture medium, *Appl. Environ. Microbiol.*, 80, 2796-2803, 10.1128/AEM.00056-14, 2014.

Publications related to this PhD study

[1] **Meng, Y.**, Kiselev, A., Duft, D., Dresch, T., and Leisner, T.: Role of mucin in controlling evaporation and hygroscopic behavior of human respiratory droplets and potential implications for spreading of pathogens. *Aerosol Science and Technology*, 59(9), 1122–1136. https://doi.org/10.1080/02786826.2025.2505036, 2025.

Close to submission:

[2] **Meng, Y.**, Kiselev, A., Duft, D., and Leisner, T.: Impact of mucin and albumin on the physicochemical behavior of respiratory droplets, in preparation for Atmospheric Chemistry and Physics.

Appendix: Supplement for Results and Discussion

Table S1. Compositions of Pro-clean.

	KATHON^{TM} CG/ICP
Active Ingredients	
5-chloro-2-methyl-4-isothiazolin-3-one	1.15%
2-methyl-4-isothiazolin-3-one	0.35%
Total	1.50%
Inert Ingredients	
Magnesium salts	23.00%
Water	75.50%
Total	98.50%

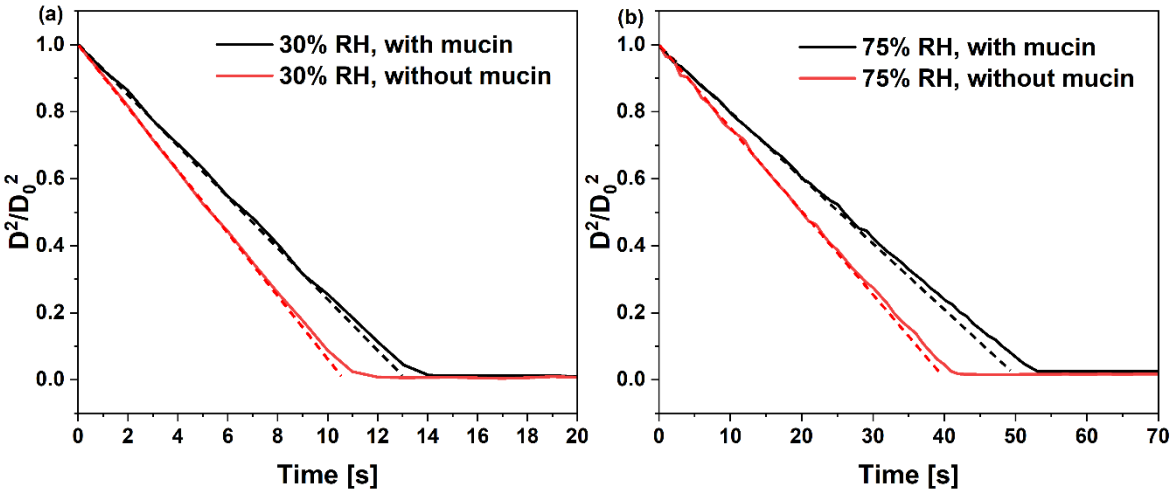

Figure S1. Evolution of normalized surface area of saliva droplets with mucin (ASM) and without mucin (AS) under dry (30% RH) and humid (75% RH) conditions, compared with D^2-law (dashed lines).

Table S2. The densities of ASM and AS droplets before reaching equilibrium, calculated from the SADKAT model (Hardy et al., 2023), except < 5% (Zhang, 2011).

RH [%]	**Density of ASM**	**Density of AS**
< 5	1.380	1.240
15	1.220	1.218
30	1.214	1.213
45	1.208	1.205
60	1.132	1.124
75	1.099	1.096
97	1.034	1.026

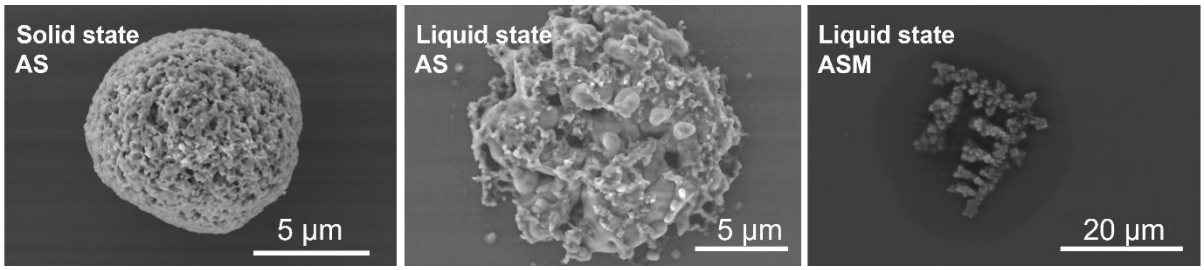

Figure S2. Representative SEM images, illustrating the droplet phase state at the moment of extraction. From left to right: an AS droplet extracted at < 5% RH, an AS droplet extracted at 60% (note the flat pancake shape and the small salt residues around the main particle, which indicate the former existence of a liquid-to-substrate contact line at the moment of deposition), and an ASM droplet extracted at 75% (note the near-circular residue footprint formed by evaporation of a liquid droplet deposited on the substrate).

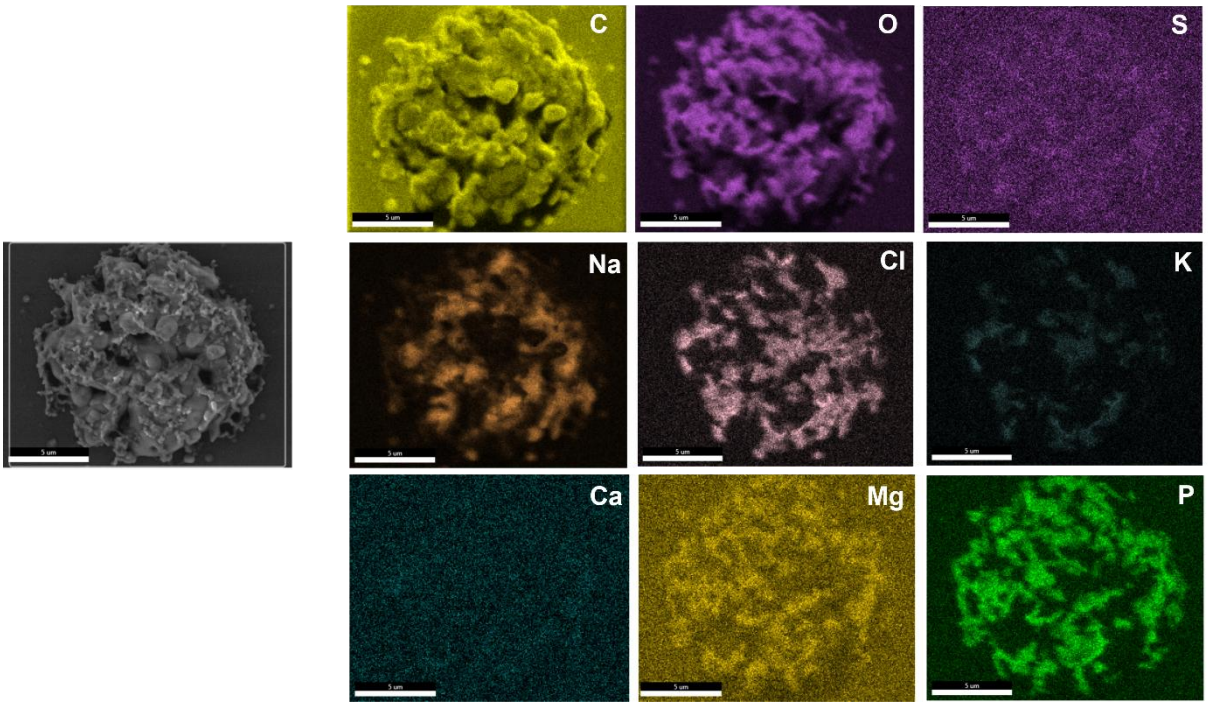

Figure S3. Chemical mapping of a representative AS droplet at a liquid equilibrium state (RH = 60%). Bright and dark colors indicate areas of high and low concentration of the labeled elements.

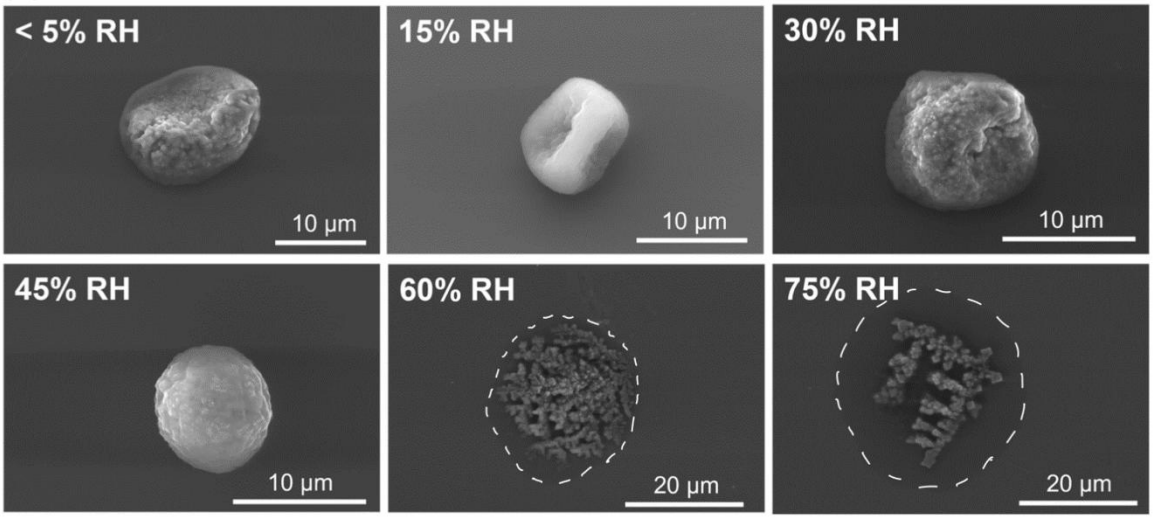

Figure S4. SEM images of ASM droplets collected from EDB when they reached the equilibrium state after evaporation under different RH conditions. The faint footprints of liquid visible in the original images are highlighted by white dashed lines for clarity.

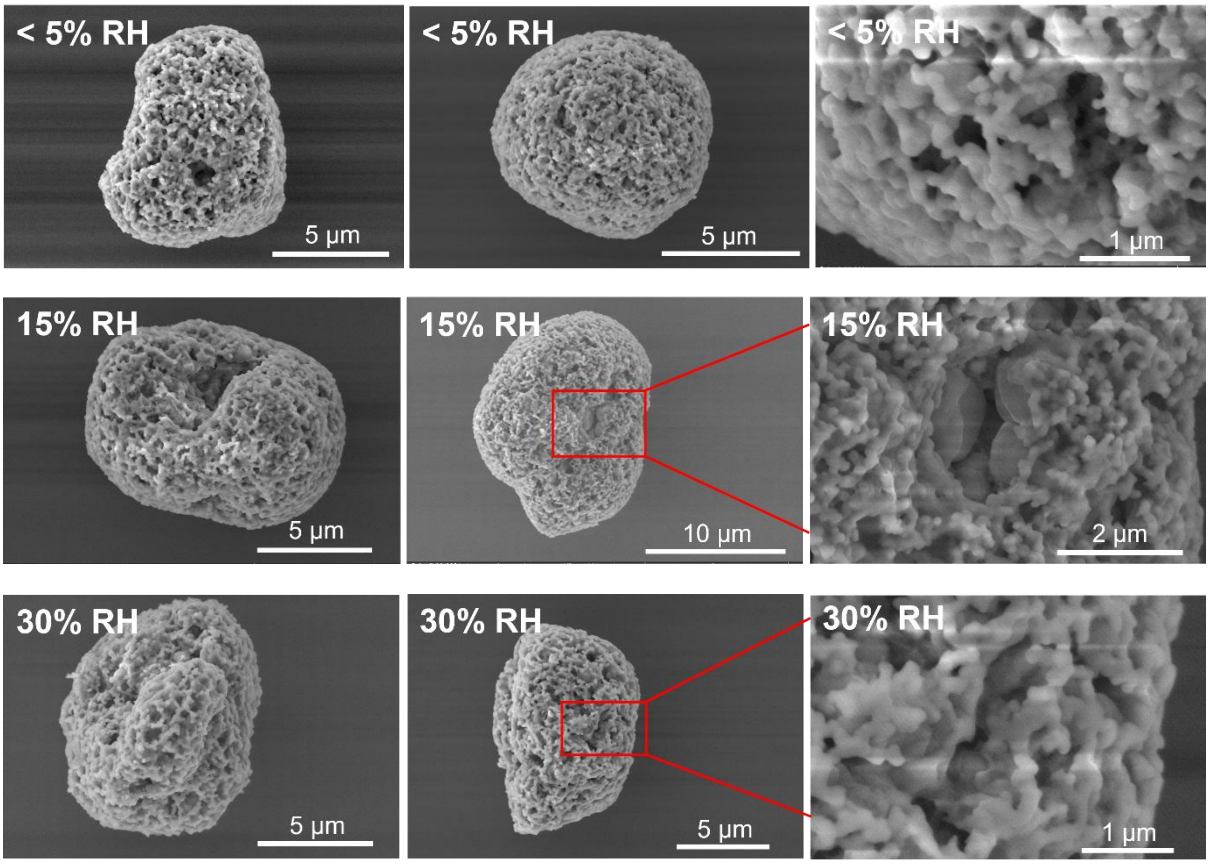

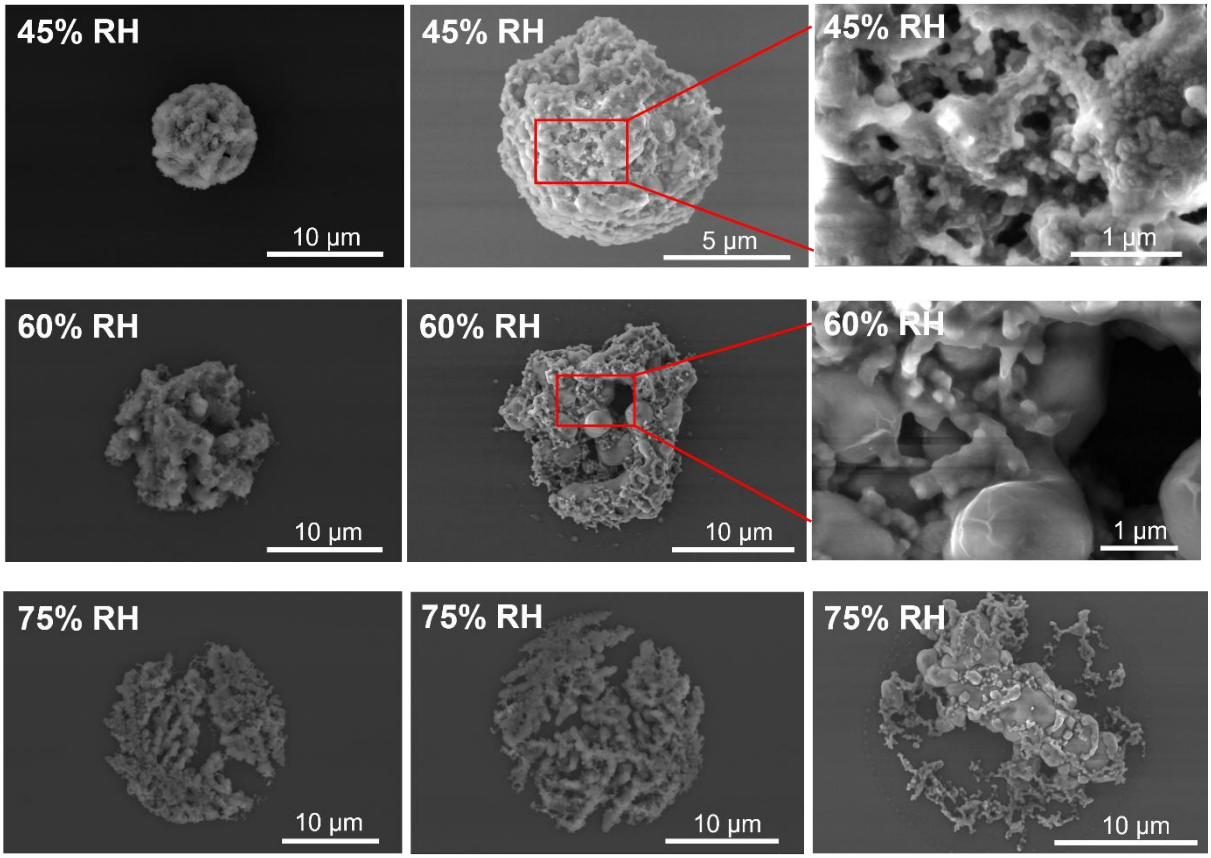

Figure S5. SEM images of AS droplets collected from the EDB at their equilibrium state.

Table S3. Element quantification on the surface of saliva droplet residues at their equilibrium state at 30% RH.

Elements	ASM	AS	ASM	AS
	Weight %		Atomic %	
C	38.01	21.92	57.62	38.09
O	11.00	18.53	12.52	24.16
N	1.65	-	2.15	-
Na	7.71	10.23	6.11	9.28
K	12.10	19.53	5.63	10.43
Cl	16.34	20.23	8.39	11.92
Mg	0.60	0.53	0.45	0.45
Ca	1.90	2.47	0.86	1.29
S	1.24	1.43	0.70	0.93
P	9.46	5.14	5.56	3.46

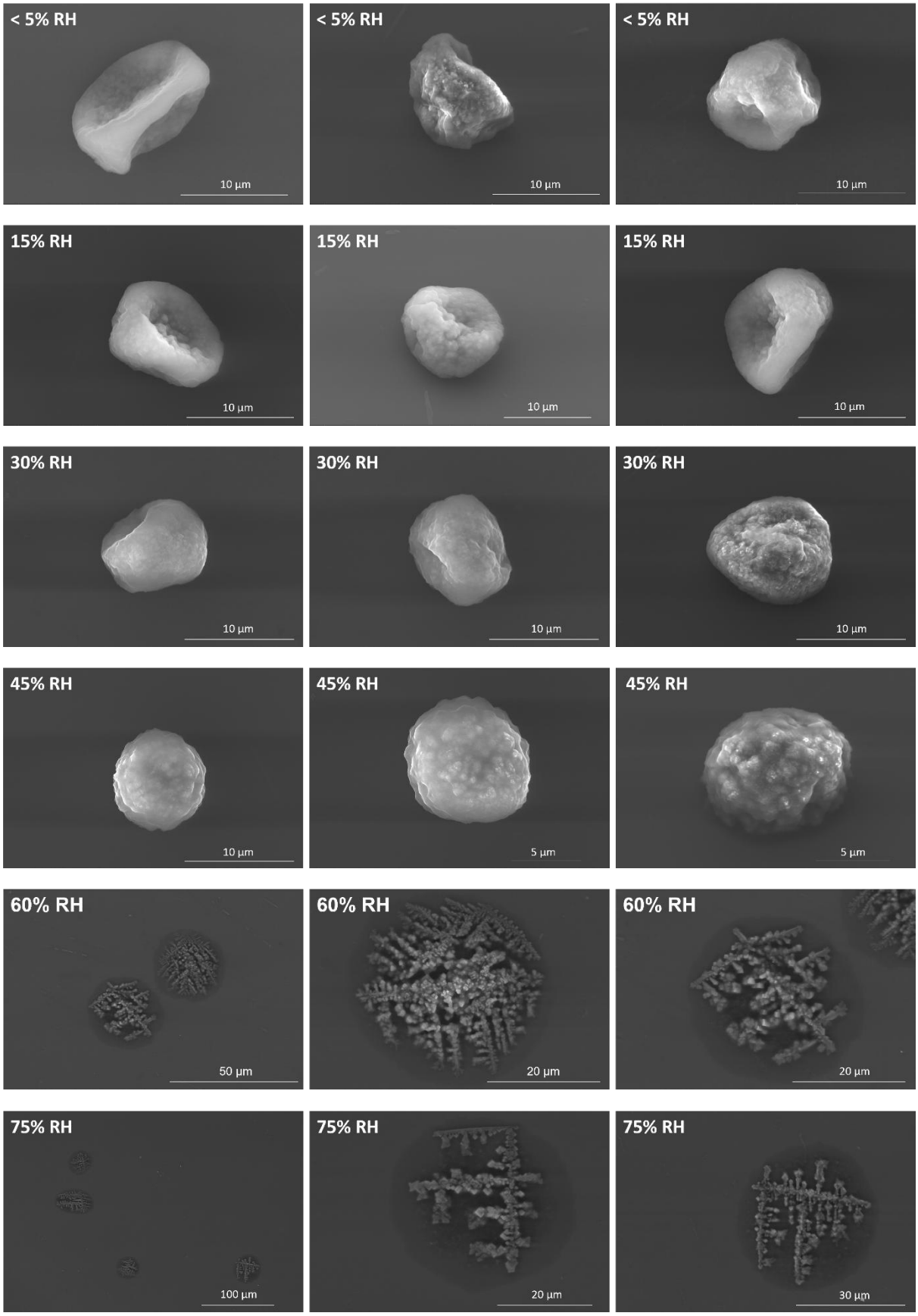

Figure S6. SEM images of ASM droplets collected from EDB at their equilibrium state.

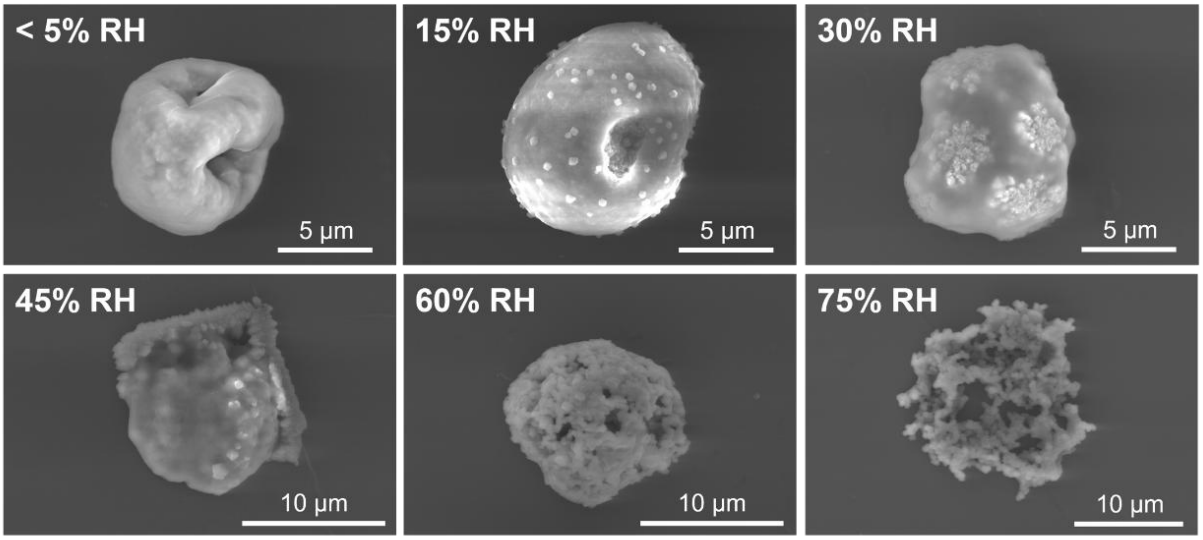

Figure S7. SEM images of saliva droplets without mucin but high in urea (ASU), collected from EDB when they reached the equilibrium state after evaporation under different RH conditions. The droplets contain 1.0 g/L of urea instead of 3.0 g/L of mucin, while maintaining the same weight fraction of all other components in the AS droplets.

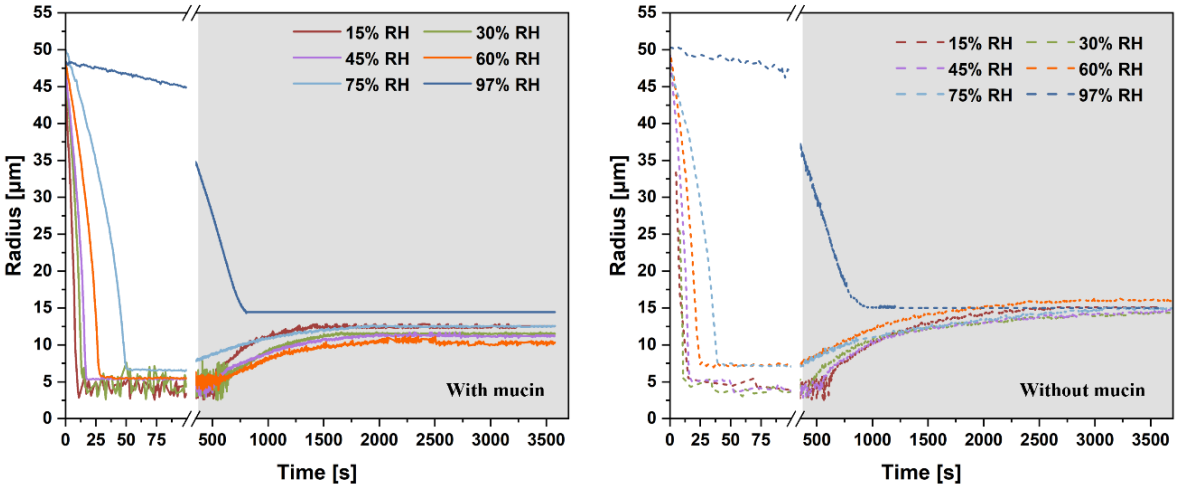

Figure S8. Evaporation and hygroscopic growth of representative saliva droplets with mucin (left) and without mucin (right). The grey area in the figure indicates a rehydration stage after exposure to 97 % RH.

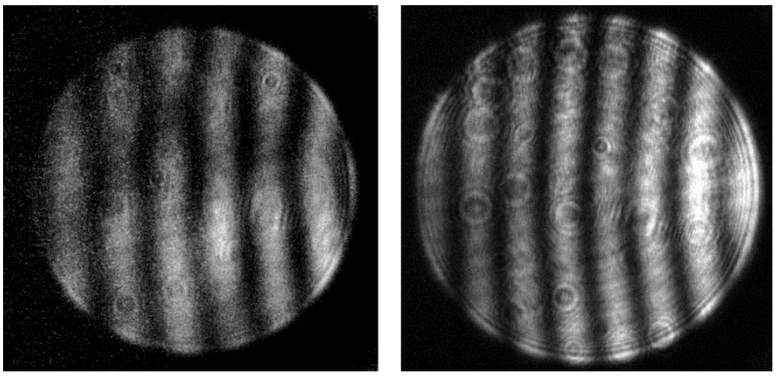

Figure S9. Light scattering patterns of artificial saliva droplet without mucin (left) and with mucin (right) at 70% RH, at equilibrium state. The large vertical fringe pattern is the result of light scattering by the levitated particle, while the small circular fringes are interference patterns caused by the optical imaging system.

Table S4. The densities of NaCl-mucin droplets with different mass fraction of mucin (X_{mucin}) at equilibrium at 30% RH, calculated from the AIOMFAC model.

Mass fraction of mucin	**Density [g/cm^3]**
X(mucin) = 0.1	1.99
X(mucin) = 0.2	1.88
X(mucin) = 0.3	1.79
X(mucin) = 0.362	1.74
X(mucin) = 0.532	1.61
X(mucin) = 0.7	1.5
X(mucin) = 0.85	1.42

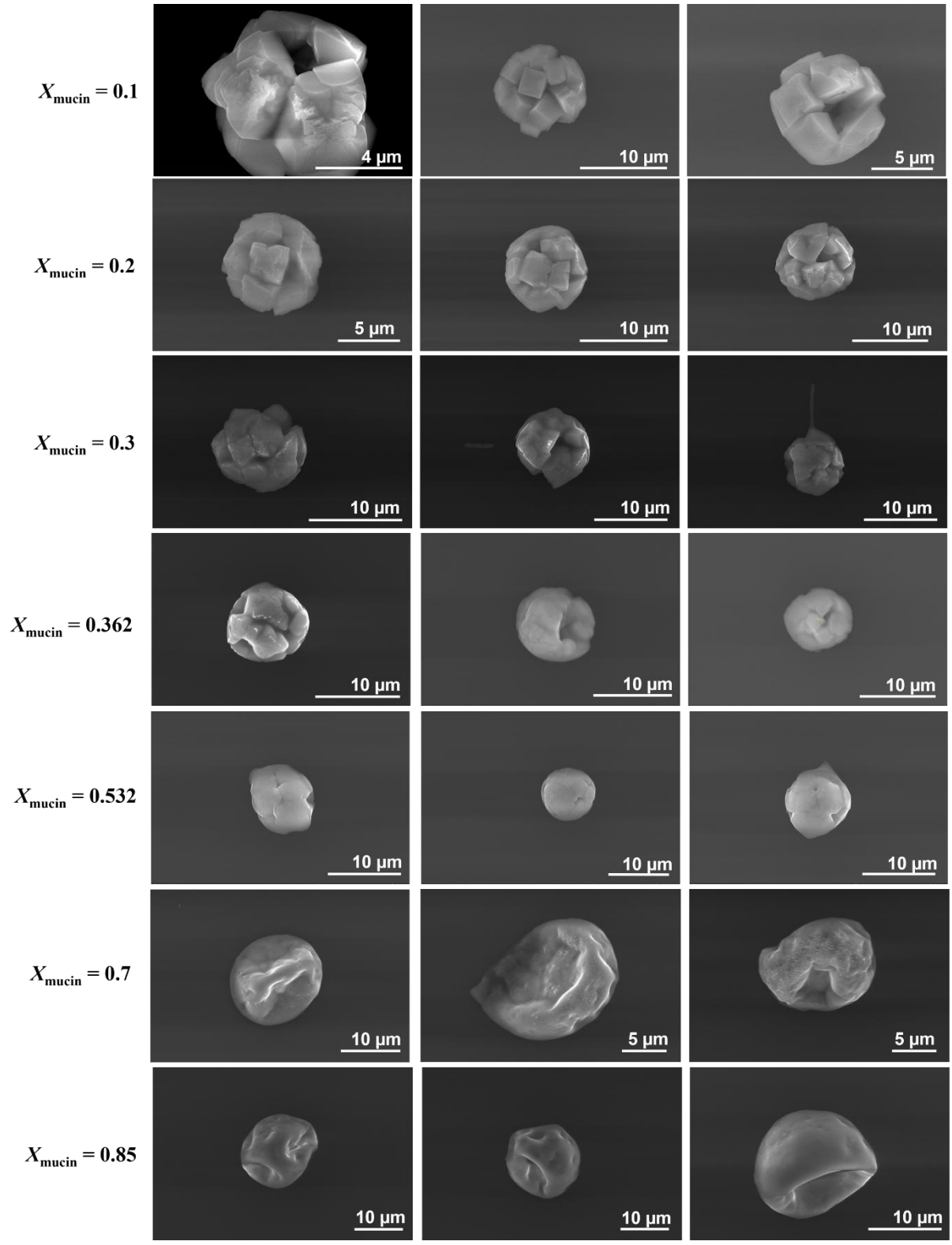

Figure S10. SEM images of NaCl-mucin droplets with mucin mass fraction X_{mucin} = 0.1-0.85, collected from EDB at their equilibrium state under 30% RH conditions.

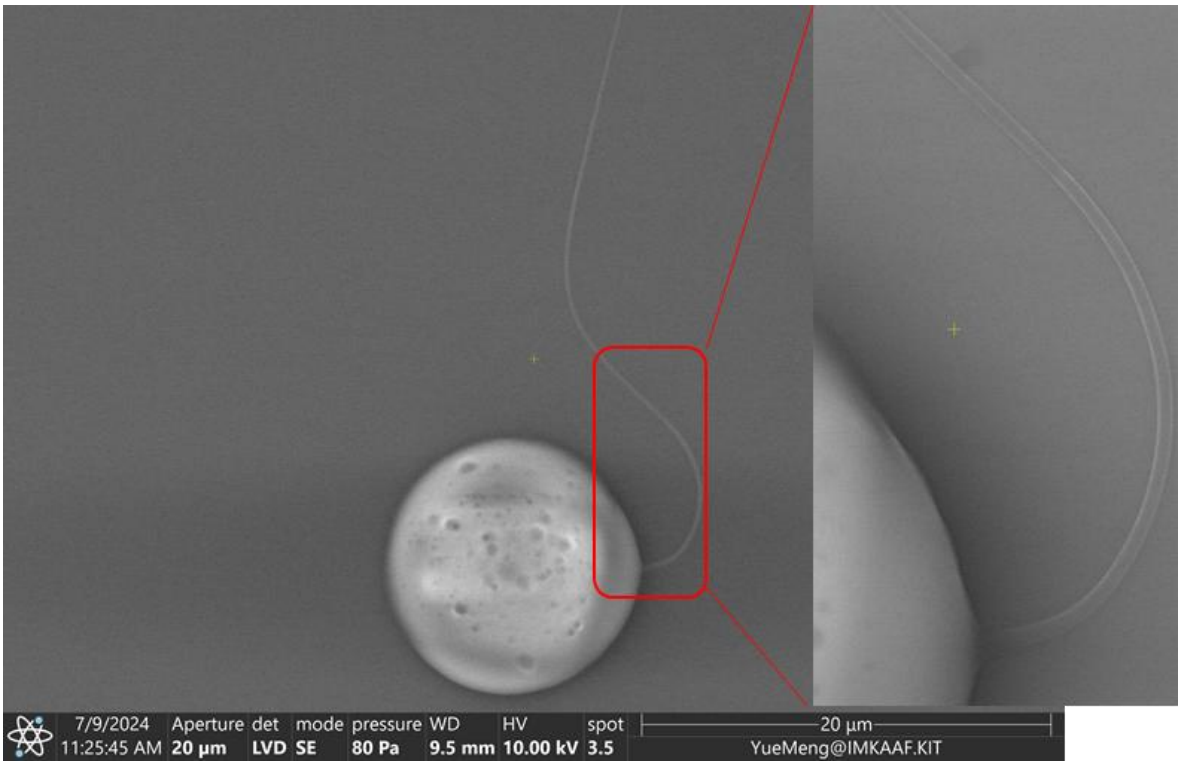

Figure S11. SEM images of a pure mucin droplet, detailing the "tail".

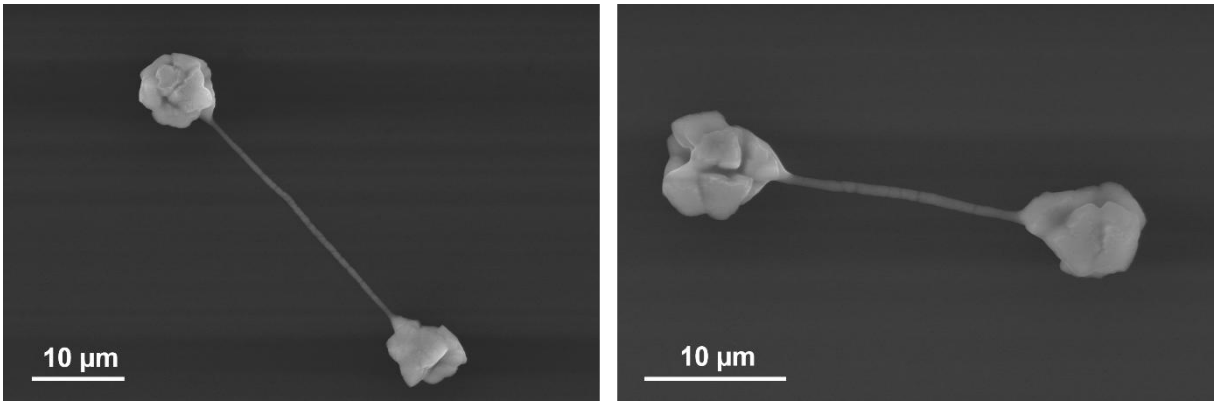

Figure S12. SEM images of NaCl-mucin droplets with X_{mucin} = 0.3, collected from the EDB at 30% RH, illustrating evidence of coulombic instability during evaporation.

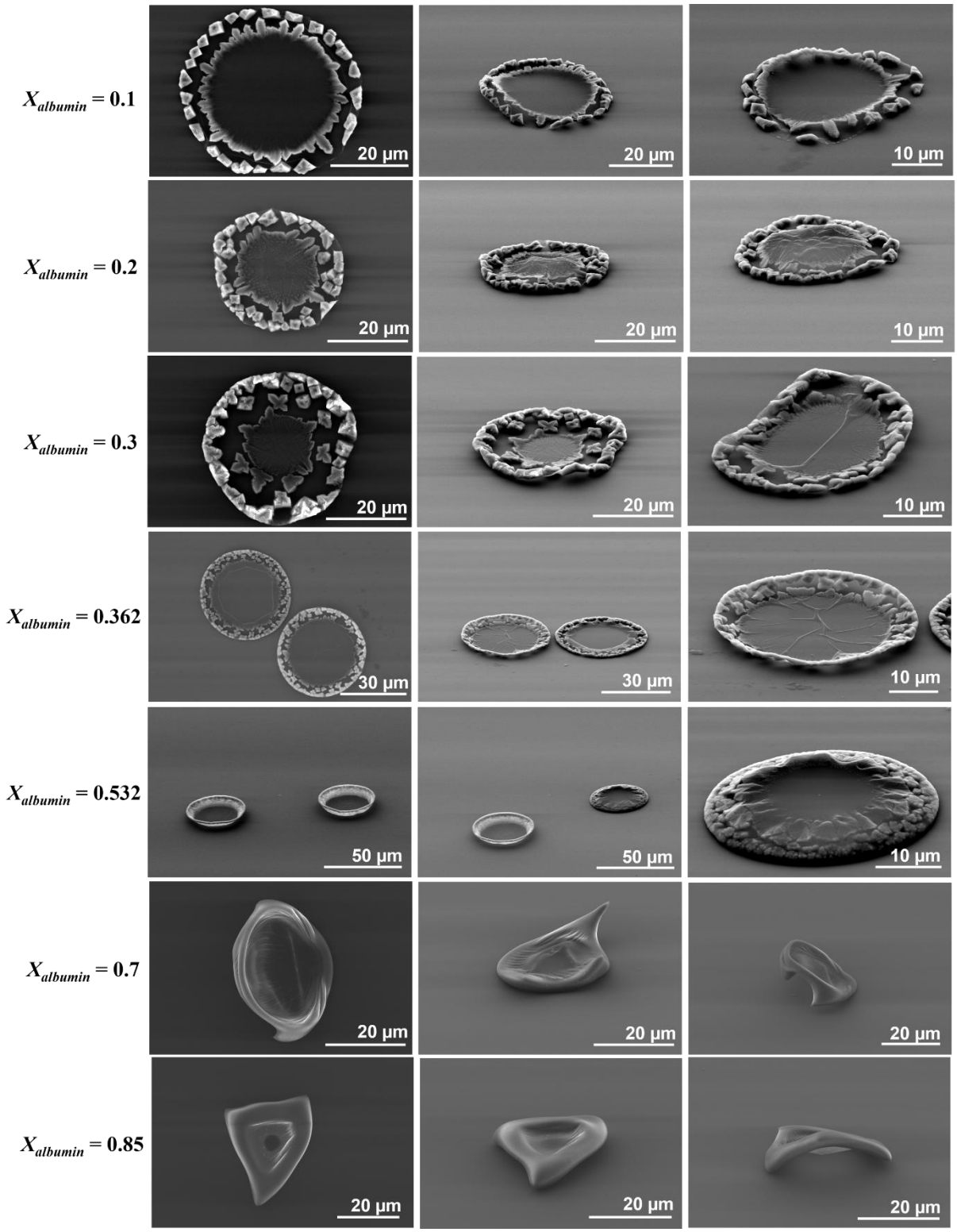

Figure S13. SEM images of NaCl-albumin droplets with albumin mass fraction X_{albumin} = 0.1-0.85, collected from EDB at their equilibrium state under 30% RH conditions.

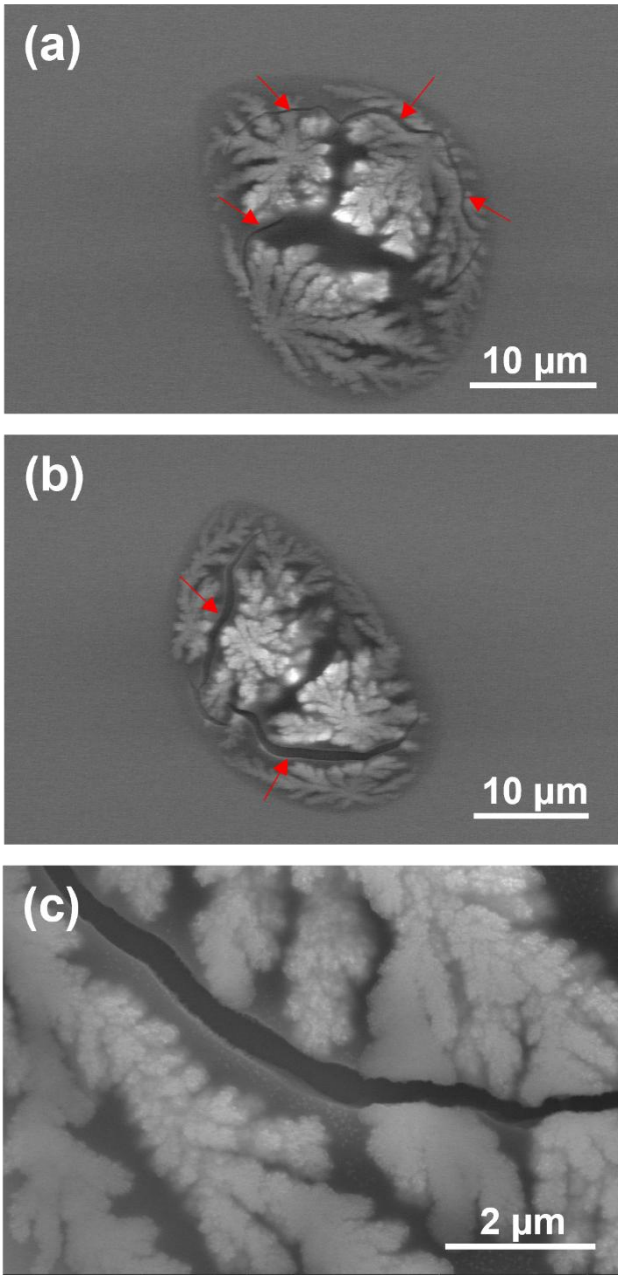

Figure S14. SEM images of NaCl + 0.6 g/L albumin droplets collected after reaching equilibrium at 80% RH. The red arrows point out the crack patterns formed by albumin on the droplet surface. (a) and (b) are showing two different droplets, and (c) shows the magnified mode of the crack.

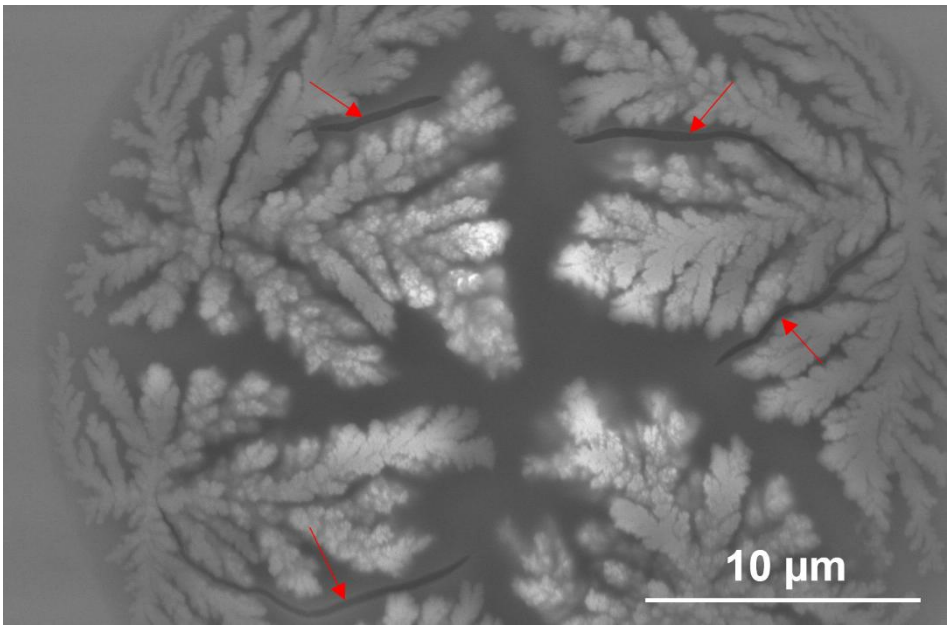

Figure S15. SEM image of NaCl + 0.6 g/L albumin after rehydration to 95% RH. The red arrows point out the crack patterns formed by albumin on the droplet surface.